123p

Report RMD 6028-F
Contract No. NAS-3-2553

INVESTIGATIONS OF SPACE STORABLE PROPELLANTS

Report Period: March 1963-January 1964

Directorate of Propulsion and Power Generation
Office of Advanced Research and Technology
National Aeronautics and Space Administration
Washington, D.C.

Thiokol
CHEMICAL CORPORATION
REACTION MOTORS DIVISION
DENVILLE, NEW JERSEY

INVESTIGATIONS OF SPACE STORABLE PROPELLANTS

THIOKOL CHEMICAL CORPORATION
Reaction Motors Division
Denville, New Jersey

Report RMD 6028-F
on
Tasks I and II

Contract NAS-3-2553

Submitted by: M. Luperi
M. LUPERI
Project Supervisor

Approved by: J. J. Lovingham
J. J. LOVINGHAM
Supervisor,
Thrust Chamber Section

Report Period Covered: March 1963 - January 1964

Directorate of Propulsion and Power Generation
Office of Advanced Research and Technology
National Aeronautics and Space Administration
Washington, D. C.

ABSTRACT

30525

Ablative cooling for high combustion temperature propellants was investigated experimentally in 150 pound thrust chambers using OF_2 and B_2H_6 propellants with a variety of state of the art ablative material combinations. Ablative materials were shown to behave in a predictable manner with OF_2/B_2H_6. Based upon four tests, the durability (erosion rate) of graphite reinforced ablative materials with these propellants was approximately equivalent to that of previous Thiokol-RMD experience[1] with state of the art silica reinforced ablative materials with N_2O_4/50-50.

Sea level injector evaluations conducted at the 2000 pound (space thrust) level demonstrated that OF_2/B_2H_6 delivers high specific impulse (99% of predicted sea level shifting equilibrium) over a wide mixture ratio range. Four types of injectors (mid-diameter vortex, full diameter vortex, coaxial showerhead, and impinging stream) were tested. High performance was obtained with all injectors except for the impinging stream type. Injector optimization was not a program requirement.

Reliable hypergolic ignition of OF_2/B_2H_6 was demonstrated at sea level and altitude conditions over extreme ranges of environment, operating conditions and propellant states.

These investigations conducted with OF_2/B_2H_6 are applicable to other high temperature, high performance propellants; solutions to problems posed by the OF_2/B_2H_6 propellant combination have far-reaching implications for future spacecraft propulsion technology.

Author

---

(1) Thiokol-RMD Project 9037, Second Progress Report, Contract No. AF04(611)-8544, "Ablative Type Thrust Chamber Testing".

SUMMARY

OBJECTIVES

This program investigated a number of behaviorial properties of the high performance space storable propellant combination OF_2/B_2H_6. The program consisted of two major tasks:

Task I investigated the behavior of ablative and heat sink thrust chamber materials both analytically and experimentally at the 150 pound thrust level. Also included in Task I were investigations of the hypergolicity of the propellant combination under a variety of conditions and an investigation of the heat transfer properties of OF_2.

Task II explored the (sea level) combustion performance attainable from the OF_2/B_2H_6 propellant combination at the 2000 pound (space) thrust level, including the acquisition of heat rejection data with four injector types.

TASK I - DESIGN DATA EVALUATION TESTS

Materials Evaluation

The test firings of Task I were in agreement with the prior analytical predictions and showed the graphite-phenolic ablative combination to be the most satsifactory thrust chamber material for the test conditions, followed closely by precharred graphite epoxy. Other chamber material combinations tested (listed in order of decreasing performance) were a graphite cloth-phenolic chamber barrel/silica-phenolic nozzle composite, a silica-phenolic chamber, barrel and nozzle composite and a graphite cloth-phenolic barrel/carbon cloth-phenolic nozzle composite chamber,

A hard-throat configuration, consisting of a USP 5067 silica phenolic barrel with a tungsten-2% molybdenum alloy nozzle insert, was also test fired. This unit experienced no throat erosion after 7.6 seconds of operation. The test was terminated prematurely by an instrumentation failure.

Ignition Tests

Reliable hypergolic ignition was demonstrated for this propellant combination with a variety of injectors at both sea level and simulated altitude conditions. Vortex injection tended to lessen ignition delays at sea level. However, starting transients were smooth in all cases, regardless of injector or chamber configuration. Propellant system variation, such as mixture ratio, temperature, or moderate propellant leads, appeared to have little effect upon ignition delay. Temperatures down to -320F were employed.

TASK II - 2000 POUND SPACE THRUST INJECTOR EVALUATION

Performance Tests

Four injectors, sized for the 2000 pound space thrust level, were designed, fabricated, and test fired with OF_2/B_2H_6 to determine attainable performance levels and to acquire heat rejection data. Two vortex injector configurations, a multiple doublet, and a coasxial showerhead injector were tested at a nominal chamber pressure of 110 psia. Twenty-five firings were accomplished at the 2000 pound space thrust level with O/F's varied from 3.00 to 4.16 at durations from 1.5 to 19.3 seconds.

The mid-diameter and full diameter vortex injectors gave the highest performance (92.5% to 100% c*), the coaxial injector operated at 93 to 94.5% c*, while the multiple doublet ran at a low level of combustion efficiency (78% to 81% c*). In all cases, combustion was uniform and no injector streaking was evident.

These performance figures are baseline values since injector optimization was beyond the scope of the program and was not attempted. The results of these (Task II) investigations confirm the attainable performance levels demonstrated in previous studies at much lower (150 pound) thrust levels.

ACKNOWLEDGMENT

This program was sponsored by the Office of Advanced Research and Technology, NASA Headquarters, under the direction of Mr. Henry Burlage. Technical cognizance was under the Lewis Research Center with Mr. Daniel Bachkin as Technical Manager.

Contributions to the technical content of this report were made by a number of individuals at Thiokol-RMD. Overall Technical Direction was handled by the Thiokol-RMD Thrust Chamber Section, J. J. Lovingham, Section Supervisor. Project Engineer was M. Luperi. The detailed activities were supported by the following:

Ablative Materials	H. Feigel, S. Tick
2000 Pound Injector Studies	R. Fash
Heated Tube OF_2 Heat Transfer	A. Corbett, J. Schaeffer
Vacuum Ignition	A. Corbett, B. Dawson
Test Setup Design	A. Mock, C. Brown
Instrumentation	G. Braddick, H. Mey
Test Operations	R. Axt, C. Breeyear, D. Doney, T. Wilk, W. Ehrenberg, J. Taylor, J. Maciag, F. Ouellette, R. Stark

CONTENTS

ILLUSTRATIONS

ILLUSTRATIONS (cont)

ILLUSTRATIONS (cont)

TABLES

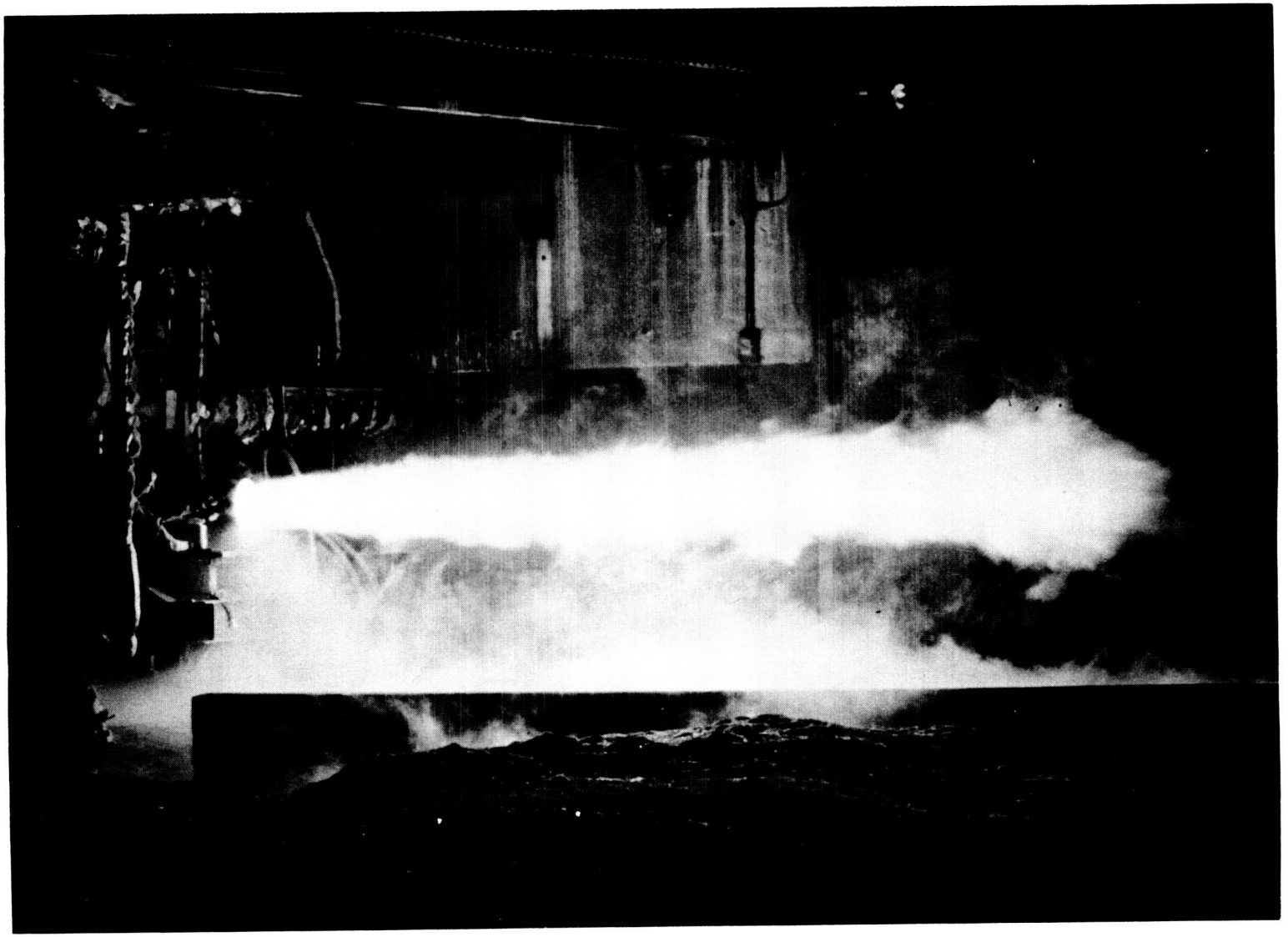

6028-537

Frontispiece - 2K Injector Firing
High Performance Firing With OF_2/B_2H_6
Full Diameter Vortex Injector
c* efficiency = 97.5% Run No. 6CX1464

I. INTRODUCTION

The oxygen difluoride (OF_2)/diborane (B_2H_6) propellant combination has the following characteristics that make it desirable for spacecraft propulsion:

- High performance
- Space storability
- Hypergolicity

The high performance is the result of a high specific impulse and a high bulk density. The high bulk density is important since it permits smaller tankage and reduced vehicle structure weight. Another characteristic contributing to the high performance of OF_2/B_2H_6 is the comparatively low gamma (ratio of specific heats) of the exhaust gases as contrasted to that of such propellant combinations as F_2/H_2, N_2O_4/50-50, etc. This results in a significant continuous increase in space specific impulse as nozzle expansion area ratio is increased. (See Figure 1.) Current theoretical and analytical exploratory investigations of advanced high area ratio nozzle concepts are demonstrating the desirability of low gamma propellants.

OF_2 and B_2H_6 have overlapping liquid temperature ranges without the need for the increased storage pressures required by many other candidate space propellants to obtain the same range of liquid temperature overlap. Furthermore, the liquid temperature ranges of OF_2 and B_2H_6 are favorable with respect to space storage. Consequently, OF_2 and B_2H_6 can be stored in space for long periods of time without insulation or boiloff loss venting operations; for the longer planetary explorations this means greater payloads and high reliability. The reliable, hypergolic ignition of the OF_2/B_2H_6 combination also promotes system simplicity and reliability.

Initial experimental rocket investigations with OF_2/B_2H_6 were conducted by Thiokol with corporate funds. Two experimental rocket firings at the 150 pound thrust level demonstrated hypergolic ignition and indicated the high performance and clean combustion potential of this combination. This work also included the preparation of sufficient OF_2 for the test firings and for

the evaluation of materials. These exploratory investigations were continued and expanded under NASA Contract NAS-w-449. Under the program pertinent OF_2 physical, thermodynamic, and materials compatibility properties were determined. Thrust chamber firings at the 150 pound thrust level demonstrated high performance over a wide range of mixture ratios, demonstrated hypergolic ignition at sea level and simulated space conditions and provided heat transfer data for engine design. These investigations are described in detail in Thiokol-RMD Report 5507-F.

In 1963, the OF_2/B_2H_6 investigations were continued under NASA Contract NAS-3-2553. These investigations, the subject of this report, included:

- A thorough evaluation of the effects of environment, propellant state, and operating conditions on ignition.

- An evaluation of refractory and ablative thrust chamber materials by 150 pound thrust chamber firings.

- Injector evaluations at the 2000 pound thrust level to assess performance, durability, and heat transfer.

The following sections of this report describe in detail the investigations conducted under Contract NAS-3-2553 and the extremely encouraging results.

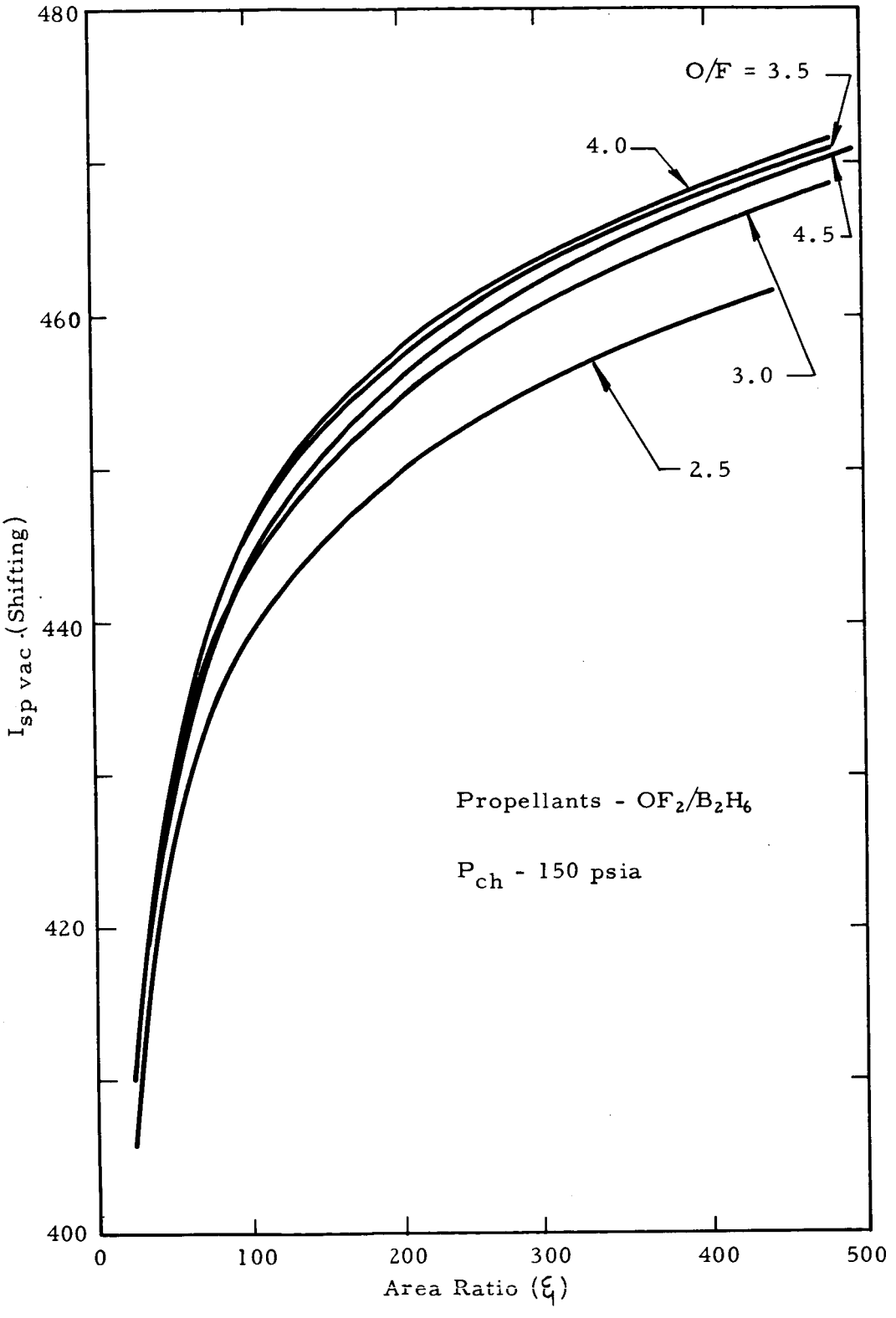

Figure 1. Theoretical Specific Impulse of OF_2/B_2H_6 at High Area Ratios

II. DISCUSSION

A. TASK I - ABLATIVE AND HEAT SINK MATERIALS EVALUATION

1. Objectives of Task I

The objective of this task was the evaluation of thrust chamber materials for use with OF_2/B_2H_6 and the concomitant high temperature (6530F) environment. The materials evaluation program logic was as follows:

a. Preliminary screening and analytical material selection using Thiokol-RMD's proprietary analytical ablative and heat sink models.
b. Testing of the evaluation injectors to assure the attainment of high combustion efficiency and uniformity of combustion.
c. Test firings at the 150 pound thrust level of thrust chambers fabricated from the most promising materials evaluated in Step (a).

Additional investigations planned to develop design data for OF_2/B_2H_6 thrust chambers were:

d. Sea level and vacuum ignition tests.
e. OF_2 heat transfer tests using a heated tube apparatus.

2. Analytical Screening

The preliminary screening of containment materials was accomplished by means of Thiokol-RMD's analytical model* of ablative and nonablating heat sink materials behavior. Since many materials were available and propellant supply limited, this screening was conducted prior to the procurement of the test specimens, thus optimizing the commitment of program funds toward this activity. Briefly, the analytical model determines erosion rates, char depths, and temperature profiles by means of a radial, one dimensional

---

*S.J. Tick, G.R. Huson, and R. Griese, Design of Ablative Thrust Chambers and Their Materials, AIAA Paper No. 64-261, Presented at the First AIAA Annual Meeting, Washington, D.C., June 29 - July 2, 1964.

transient heat transfer analysis solved numerically by finite difference techniques on a high speed digital computer. The ablative materials considered included silica, graphite, carbon, zirconia, magnesium oxide, and Refrasil reinforcements, impregnated with phenolic, epoxy, nylon, and Buna-N resins (and modified resins) and fillers; the nonablating, gas side, heat sink materials considered included tungsten, tantalum carbide, zirconium carbide, pyrolytic graphite, and high density graphite.

These materials were evaluated for the conditions to be established during the Task I firings: P_{ch} = 150 psia, O/F = 3.0, F = 150 pounds (nominal) and, conservatively, at 100% c*. Material property data (density, specific heat, heat of ablation, etc.) were obtained from previous test firings at RMD, reported test firings by other investigators, and from the vendors.

The results of the analytical screening suggested that the graphite reinforced-ablative materials would prove to be the most durable ablating material combination and that tungsten would be the most satisfactory nonablating heat sink material. Figure 2 depicts the generalized results of the screening program for ablative materials. The superior durability of the graphite reinforced ablatives over the silica reinforced materials is immediately apparent.

The predicted performances of the nonablating throat configurations are summarized in Table I. On the basis of these predictions, three combinations appeared promising: (1) a tungsten-2% molybdenum insert retained in a high density graphite substrate; (2) a tantalum-coated high density graphite insert; and (3) a pyrolytic graphite washer-type insert. The high thermal conductivity of these materials, however, leads to problems at the insert substrate interface, necessitating backup insulation to protect the structural component from overheating. In these predictions it was assumed that adequate substrate insulation was available although in reality development effort in this area is indeed necessary.

Prior test experience at Thiokol-RMD with N_2O_4/hydrazine base fuels had shown that a tungsten-molybdenum throat insert was more durable and reliable than either a tantalum carbide coated graphite or a pyrolytic graphite washer type throat insert. Consequently, a tungsten-2% molybdenum throat insert was selected (rather than either of the other two designs) for evaluation in this program. Since the fabrication of a durable 1/2 inch thick pyrolytic graphite sleeve for backup insulation was foreseen to be a development beyond the scope of this program, alternate approaches were sought. Thus, analyses of a tungsten-2% molybdenum throat insert utilizing ceramic insulation showed that a design utilizing zirconia insulation on a steel sleeve assembled about the graphite heat sink is feasible for short durations of up to 40 seconds.

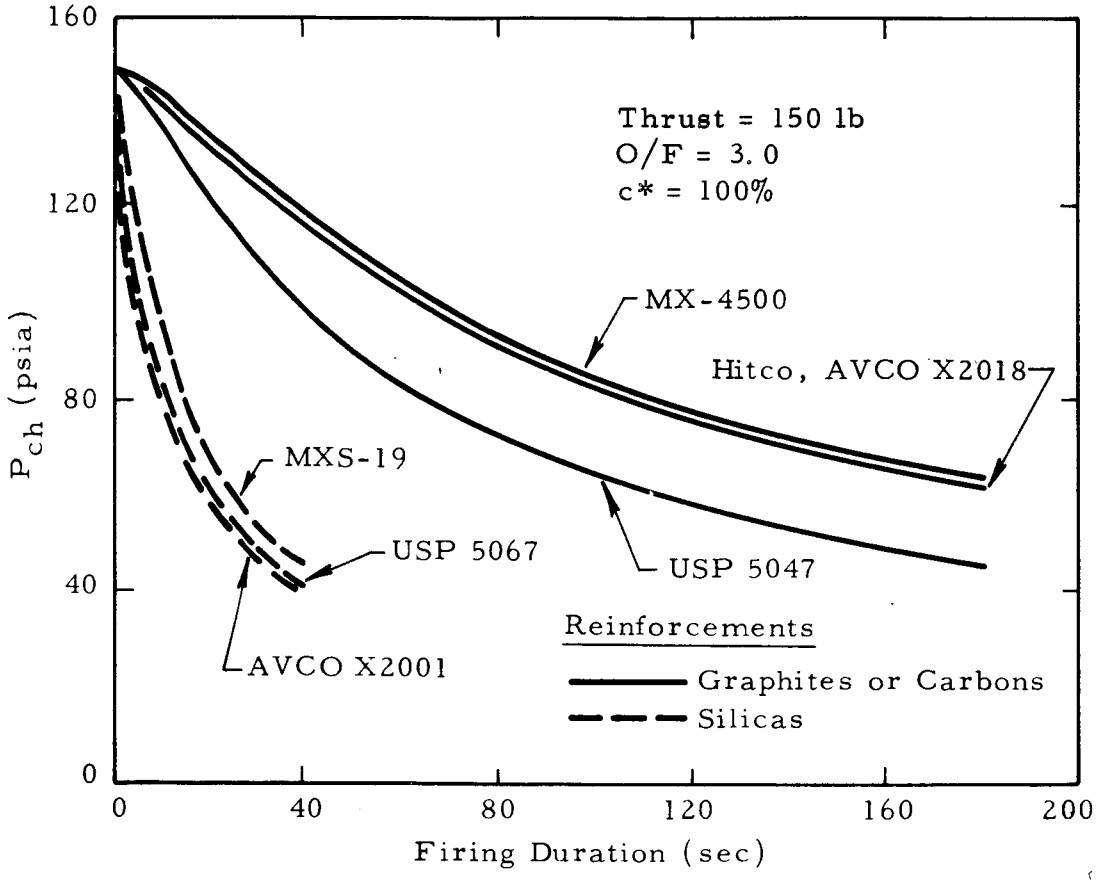

Figure 2. Predicted Ablative Behavior - OF_2/B_2H_6

TABLE I

SUMMARY OF NONABLATIVE MATERIAL ANALYSIS

Assy. Item No.	Material and Thickness		Temp at Inside Dia (°F) 20 sec	180 sec	Nominal Max Run Duration (sec)	Run Conditions Temp.(°F)	Heat Soak Conditions Run plus Soak Duration (sec)	Temp.(°F)
1	Tungsten - 2% Molybdenum	(.317)	3571	6000	10	2776	(Not calculated)	
	Graphite (ATJ)	(.675)	2669	5878		1696		
	Silica Phenolic	(.342)	1486	5337		856		
	Stainless Steel Shell	(.188)	80	284		80		
2	Tungsten - 2% Molybdenum	(.317)	3493	5886	90	5034	(Not calculated)	
	Graphite (ATJ)	(.675)	2578	5745		4761		
	Pyrolytic Graphite ("C")	(.32)	1271	5087		3663		
	Silica Phenolic	(.022)	169	1828		945		
	Ablatalite	(.268)	126	1704		843		
	Stainless Steel Shell	(.188)	80	120		85		
3	Tungsten - 2% Molybdenum	(.317)	3492	5883	180	5883	360	4850
	Graphite (ATJ)	(.175)	2576	5742		5742		4847
	Pyrolytic Graphite ("C")	(.542)	1267	5080		5080		4770
	Ablatalite	(.068)	89	846		846		1529
	Stainless Steel Shell	(.188)				211		620
4	Tantalum Carbide	(.015)	4451	6084	10	3893	(Not calculated)	
	Graphite (ATJ)	(.977)	4450	6083		3890		
	Silica Phenolic	(.342)	1563	5000		930		
	Stainless Steel Shell		80	276		80		
5	Tantalum Carbide	(.015)	4411	5981	180	5981	360	4533
	Graphite (ATJ)	(.977)	4411	5981		5981		4533
	Pyrolytic Graphite ("C")	(.542)	1316	4712		4712		4557
	Ablatalite	(.068)	91	820		820		1472
	Stainless Steel Shell	(.188)	80	209		209		602
6	Zirconium Carbide	(.015)	4460	6084	10	3909	(Not calculated)	
	Graphite (ATJ)	(.977)	4460	6084		3909		
	Silica phenolic	(.342)	1568	5000		943		
	Stainless Steel Shell		80	276		80		
7	Pyrolytic Graphite ("C")	(.992)	6403	6524	180	6524	(Not calculated)	
	Silica Phenolic	(.342)	80	300		300		
	Stainless Steel Shell	(.188)	80	83		83		
8	High Density Graphite	(.992)	4385	6010	10	3870	(Not calculated)	
	Silica Phenolic	(.342)	1501	4720		880		
	Ablatalite	(.268)	81	300		80		
	Stainless Steel Shell	(.188)	80	80		80		
9	High Density Graphite	(.992)	4360	5925	180	5925	360	4440
	Pyrolytic Graphite ("C")	(.542)	1289	4615		4615		4367
	Ablatalite	(.068)	91	808		808		1454
	Stainless Steel Shell		81	212		212		596
			(25 sec)					
10	Tungsten - 2% Molybdenum	(.317)	3816		25	3816	(Not calculated)	
	Graphite (ATJ)	(.675)	2961			2961		
	Rokide	(.075)	1608			1608		
	Silica Phenolic	(.64)	1000			1000		
			(25 sec)					
11	Tungsten -2% Molybdenum	(.317)	3811		40	4241	(Not calculated)	
	Graphite	(.675)	2954			3606		
	Rokide	(.15)	1560			2125		
	Silica Phenolic	(.64)	488			1018		

The predicted erosions, char depths, and temperatures generated by the screening program for the individual test chambers are presented graphically on the Task I performance summary sheets which appear in paragraph 4d of this section.

These predictions were published in the first quarterly report prior to completion of the test firing program. Comparison of the actual and predicted performances in the summary plots shows remarkable agreement during the run and in the subsequent heat soak period. The successful scaling of the predictive program to the higher temperature OF_2/B_2H_6 propellant combination is a significant accomplishment of this project in light of the early uncertainty concerning the design and specification of containment for high combustion temperature propellants.

3. Test Injector Evaluation

a. Design

The vortex injector designs chosen for use in the materials evaluation test firings were essentially water cooled versions of the two highest performing heat sink injectors used with these propellants in an earlier feasibility program (NAS-w-449). Water cooling was adopted for the small injectors to permit accomplishment of the ablative firings at the earliest moment.

Both a full diameter vortex (diameter of fuel injector = diameter of chamber) and a mid-diameter vortex (diameter of fuel injector < diameter of chamber) were considered. Modifications necessary to insure durability over the planned long duration materials evaluation firings could be accomplished only on the full diameter vortex due to program schedule limitations. Consequently, the full diameter vortex design (shown in Figure 3) was used in the materials evaluation firings. A summary of injector configurations used in the Task I effort is shown in Table II.

b. Performance and Streaking Tests

Nine test runs were made to establish the performance level and combustion uniformity of the evaluation design. This verification of the expected high performance was essential; combustion temperatures and heat transfer rates are implicitly related to performance level.

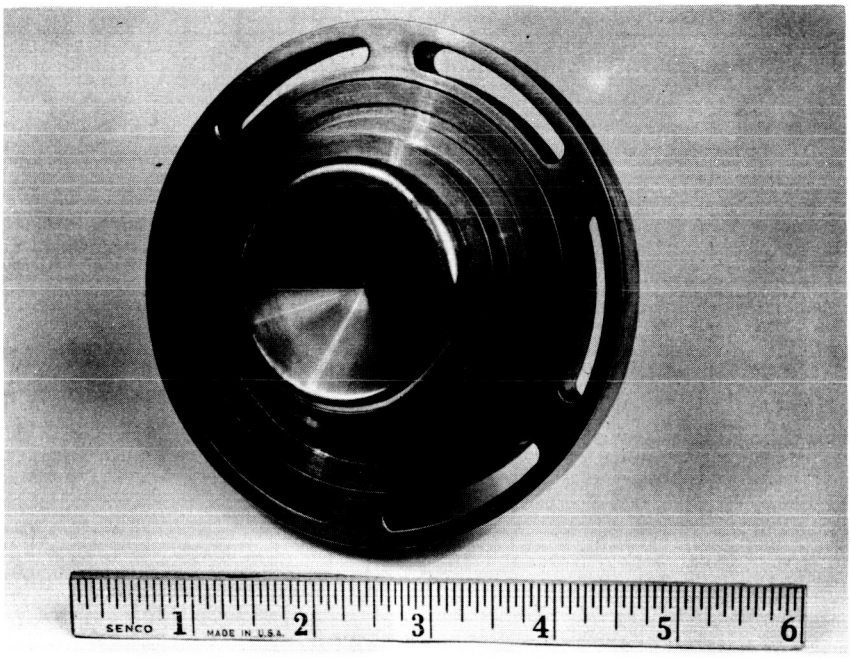

6028-522

Oxidizer Injector

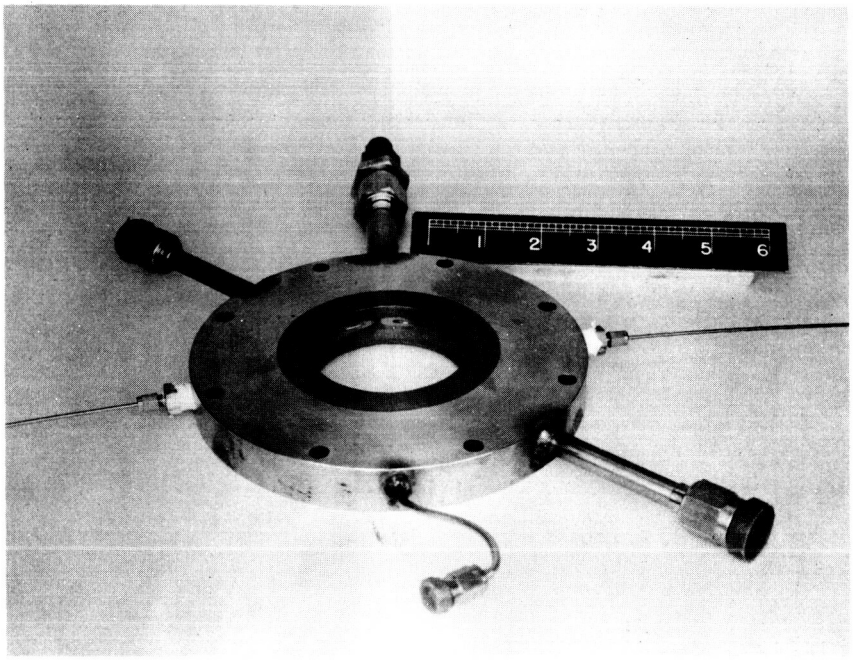

Fuel Injector 6028-334

Figure 3. Materials Evaluation Full Diameter Vortex Injector

TABLE II

TASK I - INJECTOR CONFIGURATIONS

Injector Designation	S/N	Combustion-Side Materials	Method of Assembly	Run No.	Accumulated Exposure Time (sec)	Total	Remarks
Full Diameter Vortex (Heat Sink)	1	Copper	Press Fit - Braze	2AX3734	1.50	1.50	Injector in excellent condition.
Mid-Diameter Vortex	1			2AX3743	3.37		
				2AX3744	3.28	6.65	Oxidizer injector burnout.
Full Diameter Vortex Fuel	1			2AX3742	2.90		Slight localized erosion of injector due to combustion gas seal leaks.
				2AX3745	2.80		
				2AX3746	2.86		
				2AX3747	15.35	23.91	
	2			2AX3748	10.28		
				2AX3749	20.85		Injector face erosion due to oxidizer injector burnout.
				2AX3840	2.60		
				2AX3841	30.30	64.03	
	3			2AX3838	2.70		
				2AX3839	0.70	3.40	Injector flange damaged on disassembly.
	4			2AX3842	2.50		
				2AX3843	43.60		Injector in excellent condition.
				2AX3844	34.70		
				2AX3845	7.60	88.40	
Oxidizer	1			2AX3742	2.90	2.90	Injector burnout.
	2			2AX3745	2.80		Injector in excellent condition
				2AX3746	2.86		
				2AX3747	15.35		
				2AX3748	10.28		
				2AX3749	20.85	52.14	
	3			2AX3838	2.70	2.70	Cooling passage failure.
	4			2AX3839	0.70		Coolant passage failure.
				2AX3840	2.60		
				2AX3841	30.30	33.60	
	5			2AX3842	2.50		Injector in excellent condition.
				2AX3843	43.60		
				2AX3844	34.70		
				2AX3845	7.60	88.40	

The performance tests were conducted with the copper heat sink chamber shown in Figure 4. Propellant flow was maintained at a constant rate by cavitating venturis. The test chamber included low grade ablative insert rings used to assess uniformity of combustion. Since the ablation of these inserts does not change the chamber geometry significantly and a noneroding condition is maintained, it is possible to acquire both performance and streaking data simultaneously.

The test data for the injector performance verification runs are shown in Table III. High combustion efficiency, calculated on the basis of theoretical shifting equilibrium (Appendix C), was attained. Combustion was uniform and there was no evidence of streaking or hot spots. The injector was judged to be entirely satisfactory for use in the subsequent materials evaluation tests.

4. Materials Evaluation

a. Description of Chambers

Three types of ablative chamber assemblies were tested to evaluate chamber materials:

1. Composite ablative with dissimilar nozzle and chamber materials

2. Monolithic ablative assembly

3. Ablative chamber with refractory insert.

The composite ablative chambers used barrel liners previously procured under Contract NAS-w-449 combined with nozzle inserts procured under this program. The chamber barrel liners were flat (shingle) wrapped, while the nozzle insert reinforcement was oriented at a 90° angle to the thrust chamber axis. The nozzle inserts were cemented to the barrel liner; both the barrel liners and the nozzle inserts were bonded to a stainless steel structural shell by a layer of Thiokol-RMD Ablatalite Type 1-A passive insulation.

The monlithic ablative chambers were fabricated with a nominal 60° lay-up angle in both the barrel and throat.

An ablative chamber with a refractory throat insert was also evaluated. The refractory insert, tungsten alloyed with 2% molybdenum, was assembled

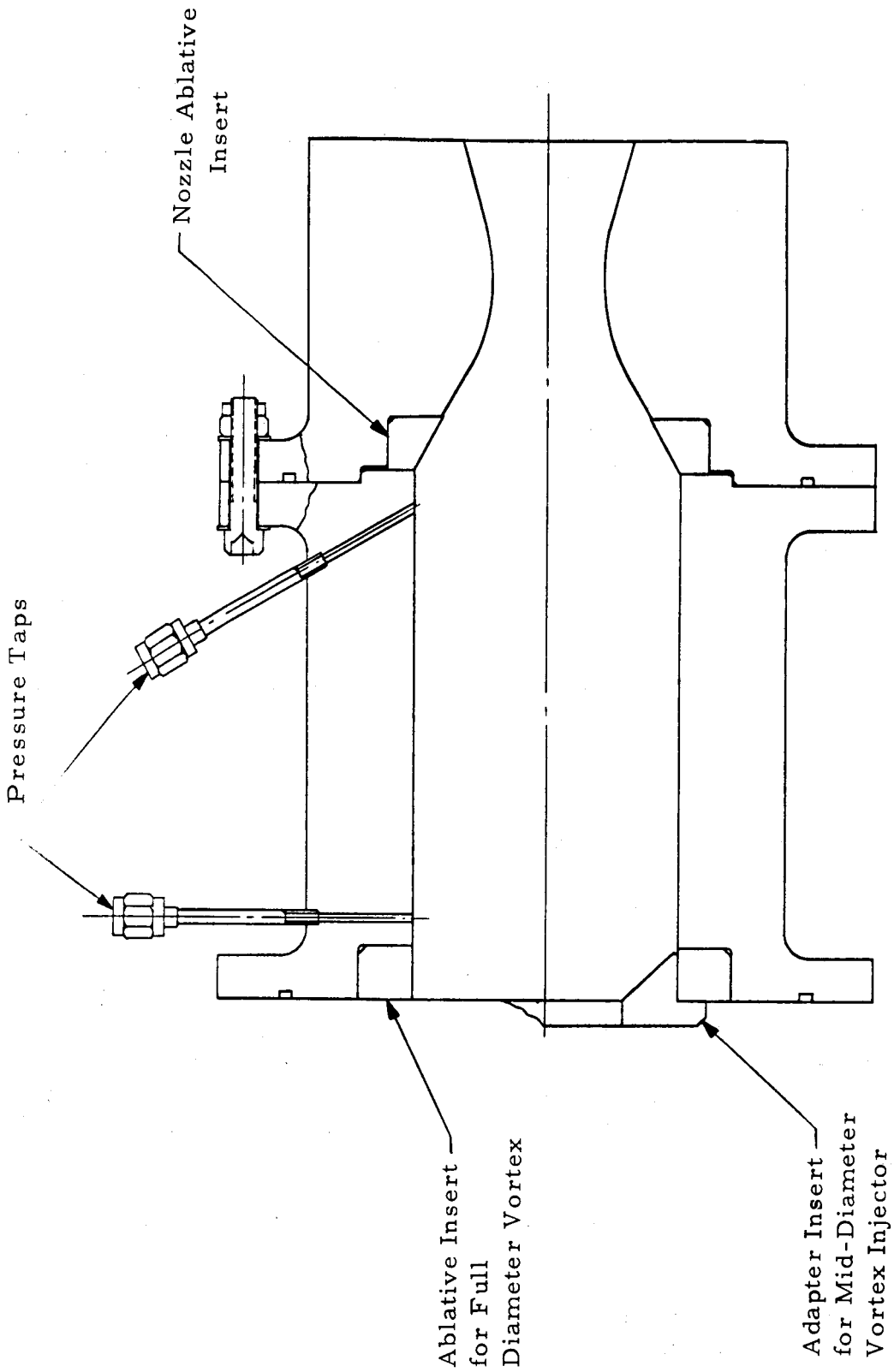

Figure 4. Performance and Streaking Evaluation Thrust Chamber

TABLE III

SUMMARY OF TASK I INJECTOR PERFORMANCE AND STREAKING TEST DATA

Run No.	Injector	F lb	Pc psia	$\dot{w}$ lb/sec	Mixture Ratio	Duration secs	C* fps	C* %	I_{sp} S.L. (sec)(1)	Remarks
2AX3734	Full Dia. Vortex	147	147.5	.586	3.15	1.50	6675	96.3	250	Heat sink injector. No apparent streaking-hardware in good condition.
2AX3742	Full Dia. Vortex	124	122.7	.511	2.90	2.90	6725	97.0	243	Ox Inj. burnout. Streaking at burnout location.
2AX3743	Mid-Dia. Vortex	- -	74	---	---	3.37	---	---	---	Test stand leak. Hardware in good condition. No apparent streaking.
2AX3744	Mid-Dia. Vortex	- -	136.7	---	---	3.28	---	---	---	Ox Inj. burnout. Streaking at burnout location.
2AX3745	Full-Dia. Vortex	133	140.	.550	2.82	2.80	6650	96.1	242	Pre-cool cycle and injector modification. Hardware in good condition.
2AX3838	Full Dia. Vortex	127(2)	137	.533	3.50	2.70	6680	96.5	239(2)	Satisfactory run to 2.4 sec. (Injector cooling passage failure).
2AX3839	Full Dia. Vortex	- -	---	---	2.82	0.70	---	---	---	Premature Automatic shutdown hardware in good condition.
2AX3840	Full Dia. Vortex	127(2)	139	.558	3.08	2.60	6480	93.4	228(2)	Satisfactory run. Hardware in good condition.
2AX3842	Full Dia. Vortex	134(2)	142	.585	3.00	2.50	6320	91.0	229(2)	Satisfactory run. Hardware in good condition.

Note: All Task I injector performance tests conducted with copper heat sink chambers.

(1) $\varepsilon = 2.44$

(2) Thrust Zero Shift

in a graphite substrate. This assembly was backed by a steel sleeve insulated with zirconia (Rokide Z). The entire assembly was bonded to the barrel liner and assembled into a steel structural shell.

The details of construction of the chambers evaluated during the test program are discussed in paragraph 4d.

b. Chamber Material Quality Control

Ablative materials vendors were required to attest to compliance with an RMD prepared certification list which required the inspection and reporting of some 20 critical parameters describing the ablative materials supplied and the fabrication of ablative components. These requirements included such detailed information as the warp and woof spacing of the reinforcement, orientation angle during layup, radiographic inspection of the finished components, etc.

The objective of the certification program was to insure the repeatability of ablative materials performance. The success of this control is exemplified by the similarity of performance exhibited by chambers fabricated at Haveg from separate lots of Fiberite MX4500.

c. Chamber Instrumentation

Thermocouple instrumentation consisted of tungsten/rhenium, platinum/rhodium, chromel/alumel, and copper/constantan junctions located in the throat plane, the nozzle entrance plane, and the 50% chamber coordinate plane. Depths ranged from within 0.060 in. of the initial gas side wall to the outer diameter of the steel shell, with the thermocouple distribution determined by the analytical predications.

To examine the uniformity of the combustion process in the three instrumented thrust chamber planes and to provide the redundancy necessary for one-shot firings, secondary thermocouples were oriented at 90 degrees to the primary group. All assemblies were x-rayed before and after the test run to determine the thermocouple locations precisely.

d. Test Results

A total of eight tests were run to evaluate the performance of ablative or refractory materials at the 150 pound thrust level. The results of these

tests are summarized in Table IV and Figures 5 to 16. The ablative test data are presented in order of decreasing performance. Five silica phenolic components, four graphite phenolic components, two precharred graphite epoxy components, one carbon phenolic, and a tungsten molybdenum alloy refractory were tested.

The performance data for all of the materials evaluation tests were taken one second after start. The c* data were obtained by using the following equation:

$$c^*_{test} = \frac{P_{ch} \cdot A_t \cdot g}{\dot{w}_t},$$

where: P_{ch} = measured chamber pressure,

A_t = initial throat area,

$\dot{w}_t$ = total propellant flow, and

g = gravitational constant, 32.2 ft/sec^2.

The c* data at shutdown (utilizing measured post-run throat area) were within $\pm 1.5\%$ of the initial c* level.

Test results indicate that the graphite phenolic material has the lowest erosion rate of the four types of ablative materials evaluated, although both the silica phenolics and the graphite phenolics performed satisfactorily in the thrust chamber barrel. However, the superior durability of the graphite phenolic systems is evident when performance in the critical throat region is considered. Run 2AX3843, a test of a monolithic Fiberite MX4500 graphite phenolic chamber fabricated by Haveg, ran continuously for 43.6 seconds at a combustion efficiency of 96% of theoretical, corresponding to a theoretical flame temperature of 6020F. During this time, chamber pressure decayed from an initial value of 146 psia to 106 psia.

Figure 5 shows both actual and predicted chamber pressure for this run as a function of time. The figure also shows both the predicted and measured post-run char depths in bar chart form and a photo of the sectioned chamber in the post-run condition. The drop in the measured pressure value at 30 seconds corresponds to an equivalent fluctuation in total propellant flow. It should be noted that no throat erosion occurred until approximately 12 seconds.

TABLE IV

TEST DATA - ABLATIVE CHAMBER EVALUATION

Performance Rank	Run No.	Configuration	Injector	F (lb)	P_c Initial (psia)	P_c Final (psia)	$\dot{w}$ (lb/sec)	Mixture Ratio	Duration (sec)	c* (fps)	c* (%)	S.L. I_{sp} (sec)(1)	ΔA_t (%)	Remarks
1	2AX3843	Nozzle and Chamber (Monolithic) MX4500	Full Dia Vortex	138(2)	146	106	.571	3.00	43.6	6650	96.0	242(2)	40	Satisfactory run. Hardware in good condition. Auto shutdown at preset chamber pressure.
2	2AX3749	Nozzle and Chamber (Monolithic) MX4500	Full Dia Vortex	154	152	126	.563	2.78	20.85	7000	101.0	274	21	Full duration run.
3	2AX3841	Nozzle and Chamber (Monolithic) AVCO X2018	Full Dia Vortex	135(2)	142	115(3)	.566	2.95	30.3	6520	94.0	239(2)	29	Ox Venturi Pressure fluctuates after 1.3 sec. Injector cooling passage failure at 2 sec.
4	2AX3844	Nozzle and Chamber (Monolithic) AVCO X2018	Full Dia Vortex	137(2)	144	112(3)	.574	2.85	34.7	6530	94.2	239(2)	30	Hardware in good condition. Auto shutdown from clogged chamber pressure tap.
5	2AX3747	Nozzle - RAP 3002 Silica Cloth-Phenolic Chamber - USP 5064 Graphite Cloth Phenolic	Full Dia Vortex	154	144	81	.553	2.76	15.35	6720	97.5	278	75	Shutdown at approach to predetermined chamber pressure.
6	2AX3748	Nozzle - USP 5067 Silica Cloth-Phenolic Chamber - USP 5067 Silica Cloth-Phenolic	Full Dia Vortex	155	151	101	.566	2.68	10.28	6990	100.9	274	52	Gradual Seal leak. Started at 6.0 sec.
7	2AX3746	Nozzle - RAP 2002 Carbon Cloth-Phenolic Chamber - USP 5064 Graphite Cloth Phenolic	Full Dia. Vortex	155	147	105	.561	2.82	2.86	6850	98.9	276	81	Shutdown because of test stand diborane leak.
8	2AX3845	Nozzle - Tungsten 2% Moly Chamber - USP 5067 Silica Cloth-Phenolic	Full Dia. Vortex	130(2)	142	---	.547	2.97	7.6	6750	97.4	238(2)	0	Injector, nozzle and liner in good condition. Chamber pressure tap failed.

(1) $\bar{\eta}$ = 2.44
(2) Thrust Zero Shift
(3) Extrapolated (see text)

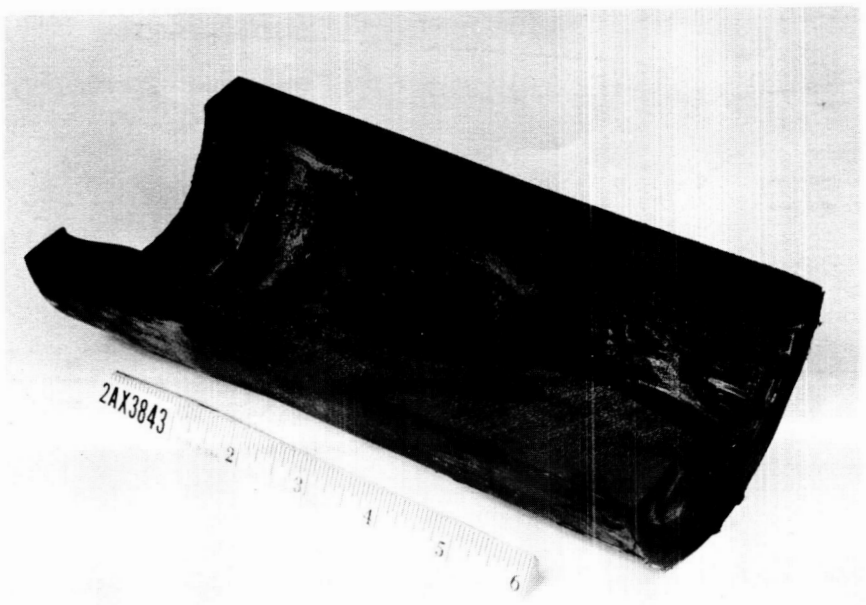

6028-507

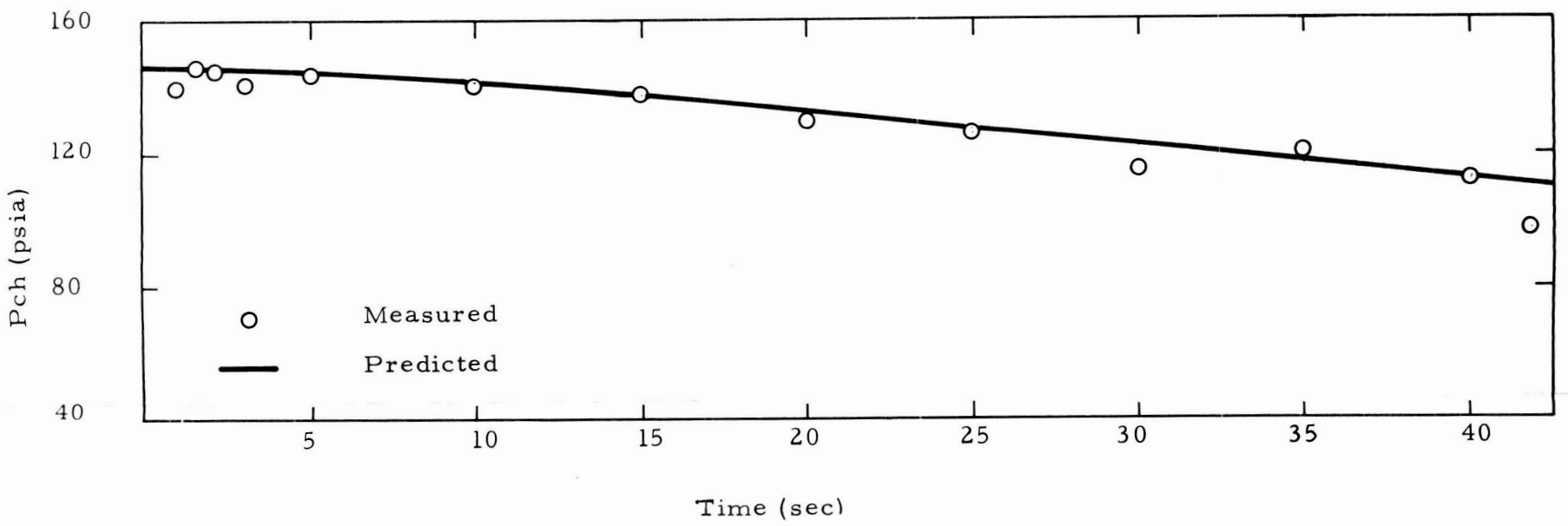

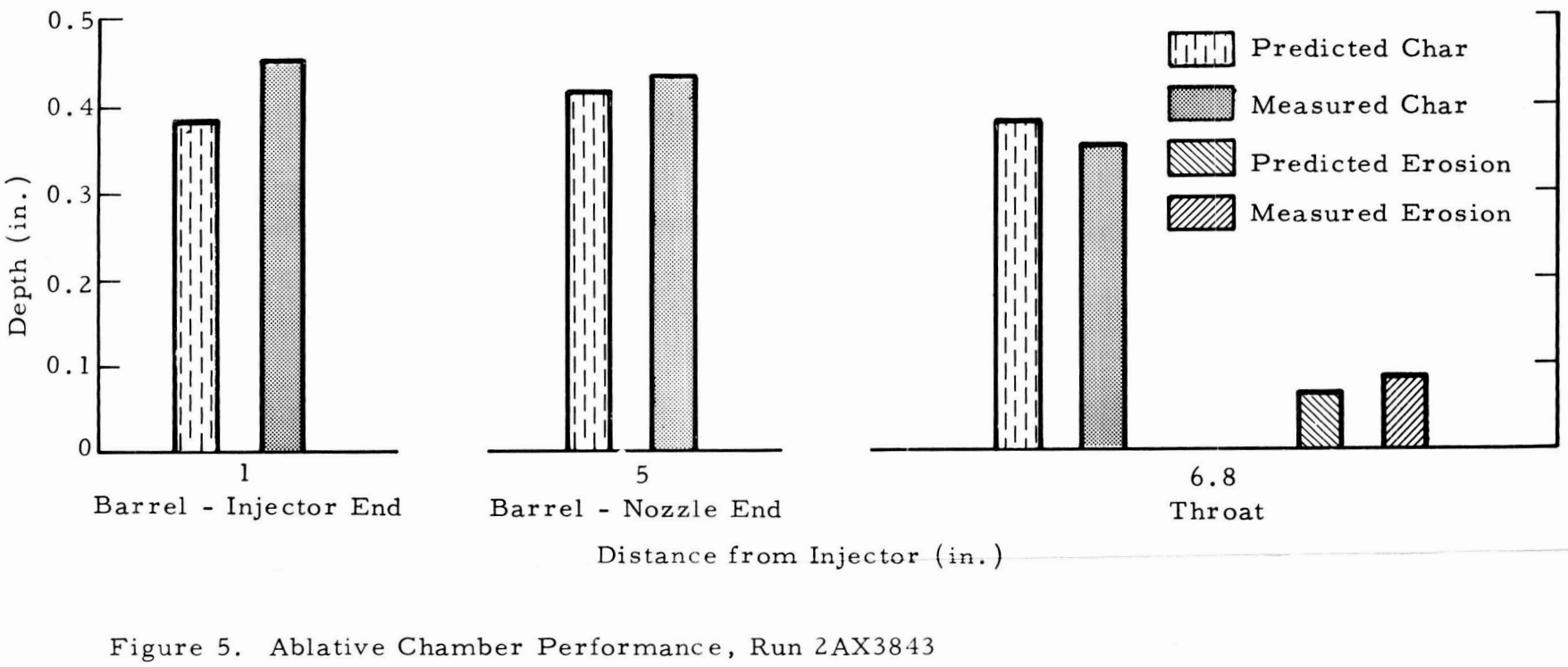

Figure 5. Ablative Chamber Performance, Run 2AX3843

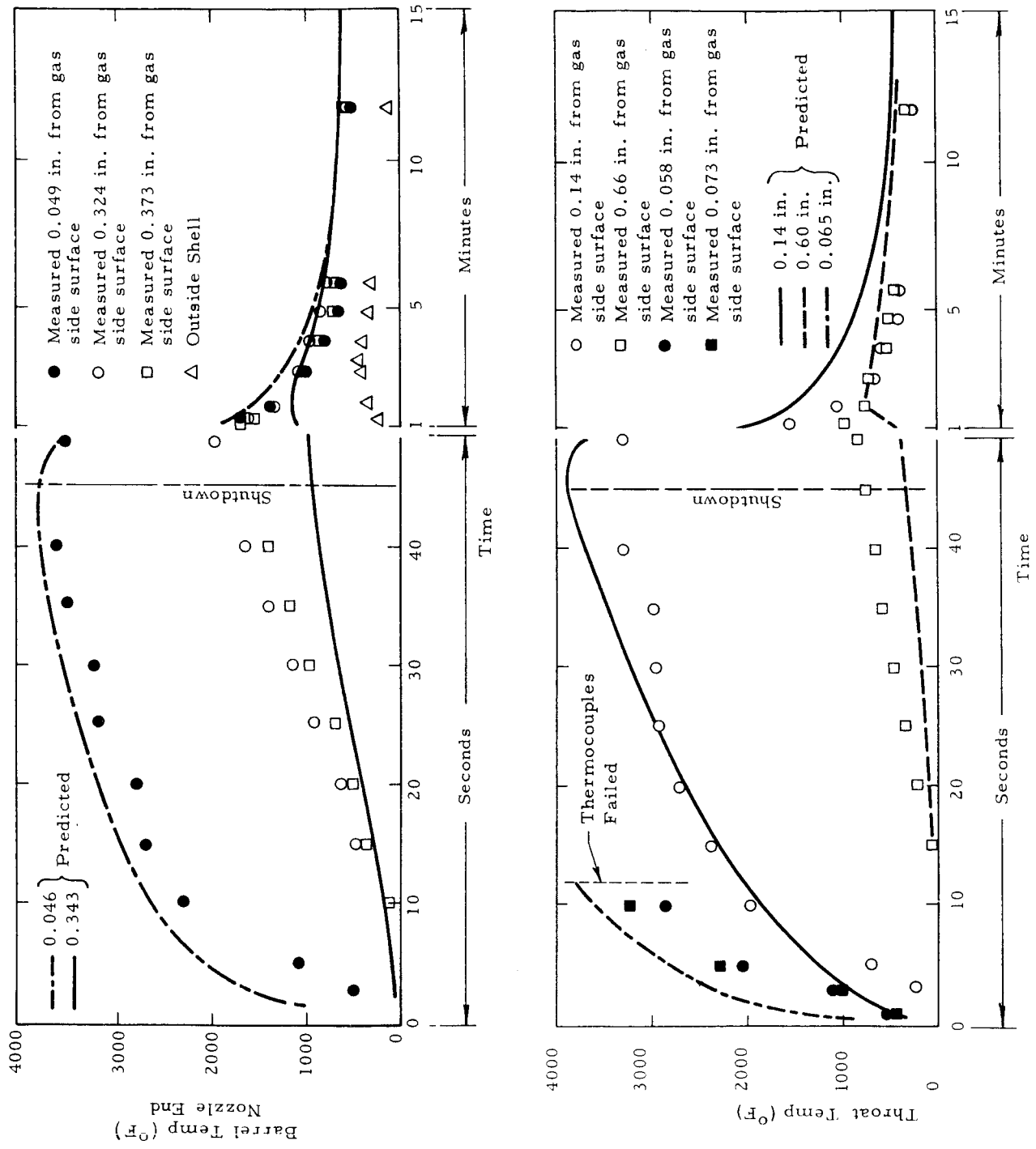

Figure 6. Thermocouple Data, Run 2AX3843

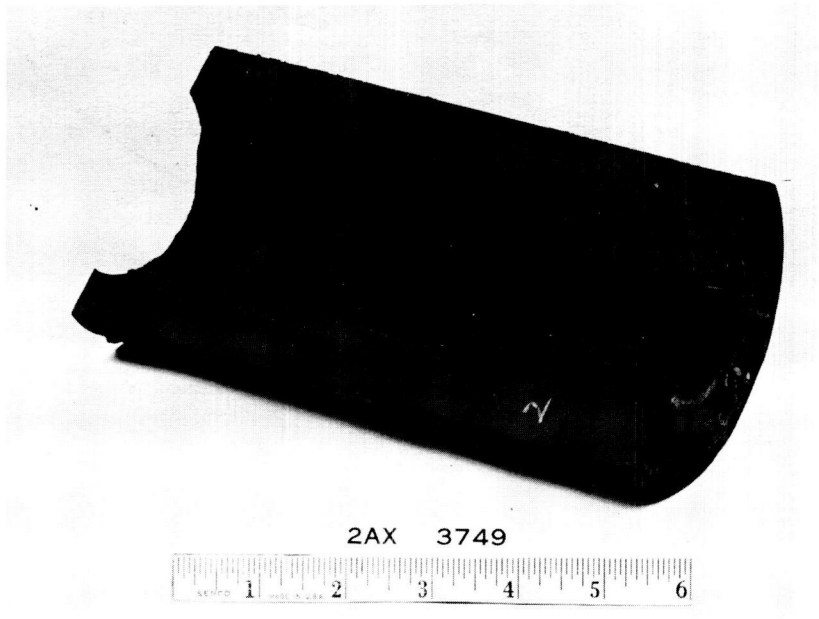

6028-200

Figure 7. Ablative Chamber Performance, Run 2AX3749

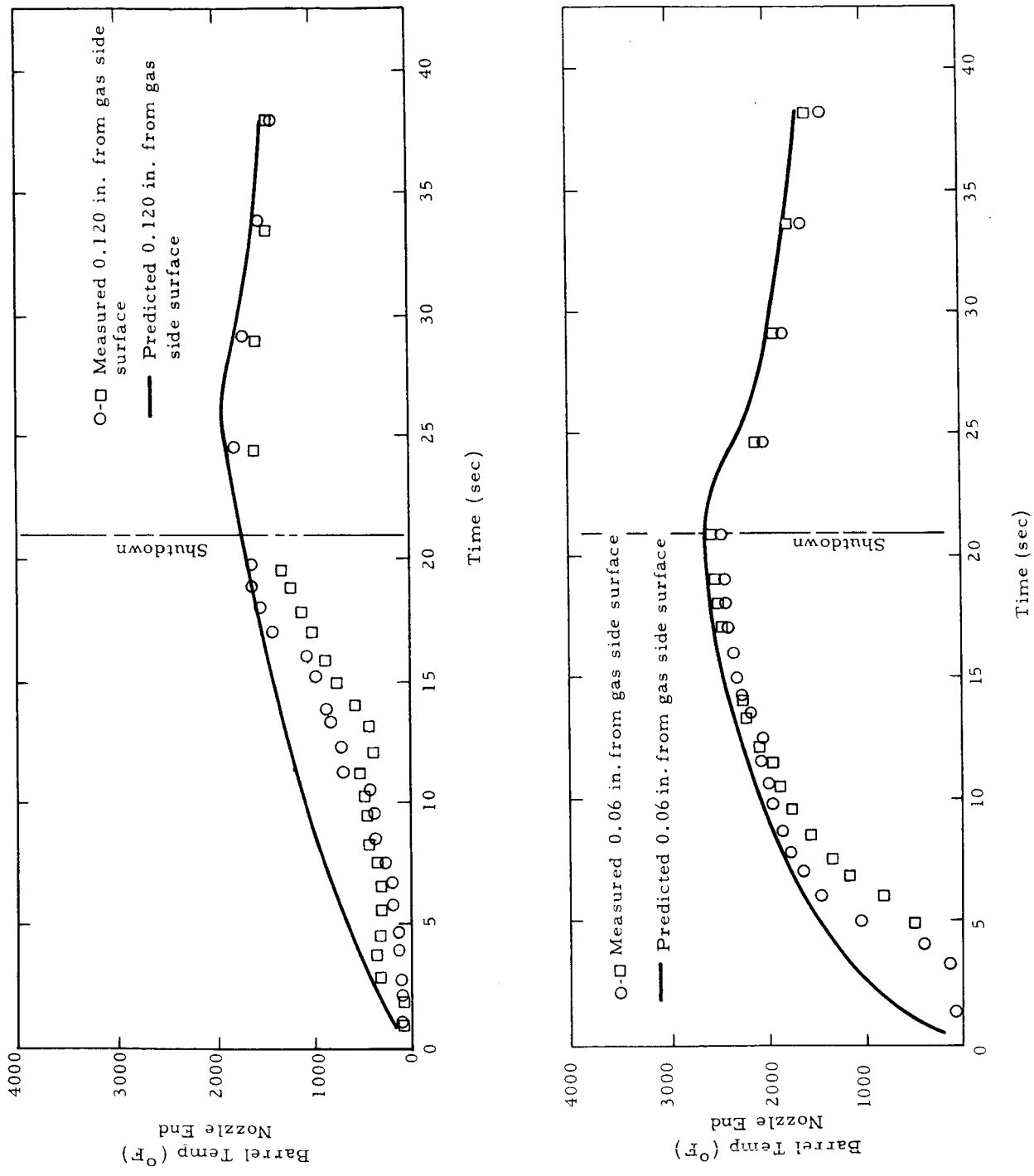

Figure 8. Thermocouple Data, Run 2AX3749

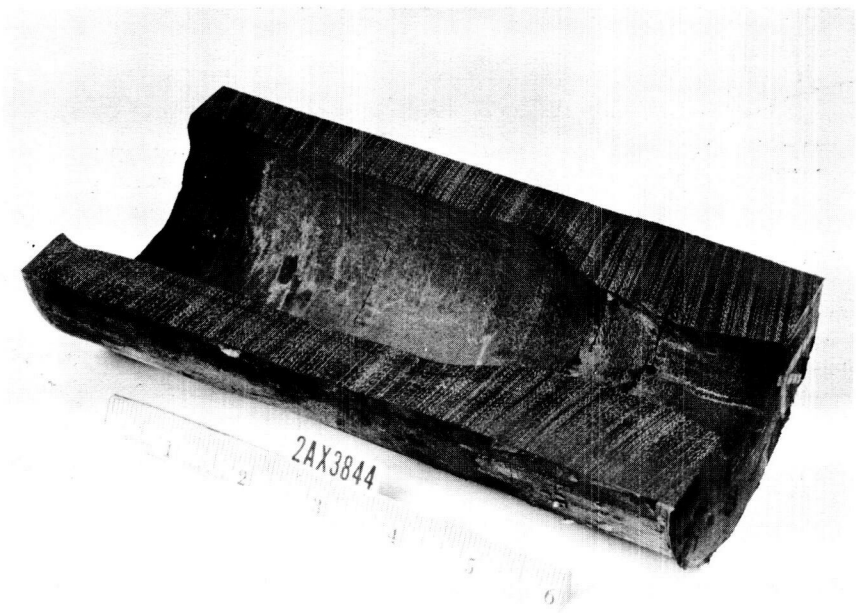

6028-500

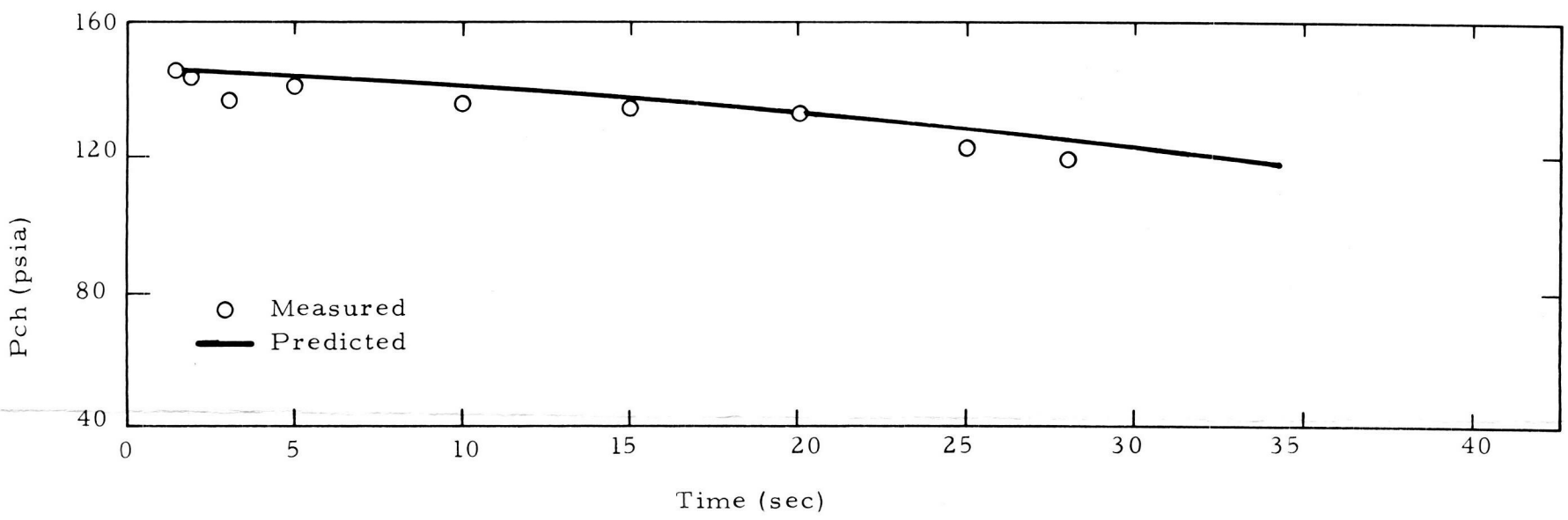

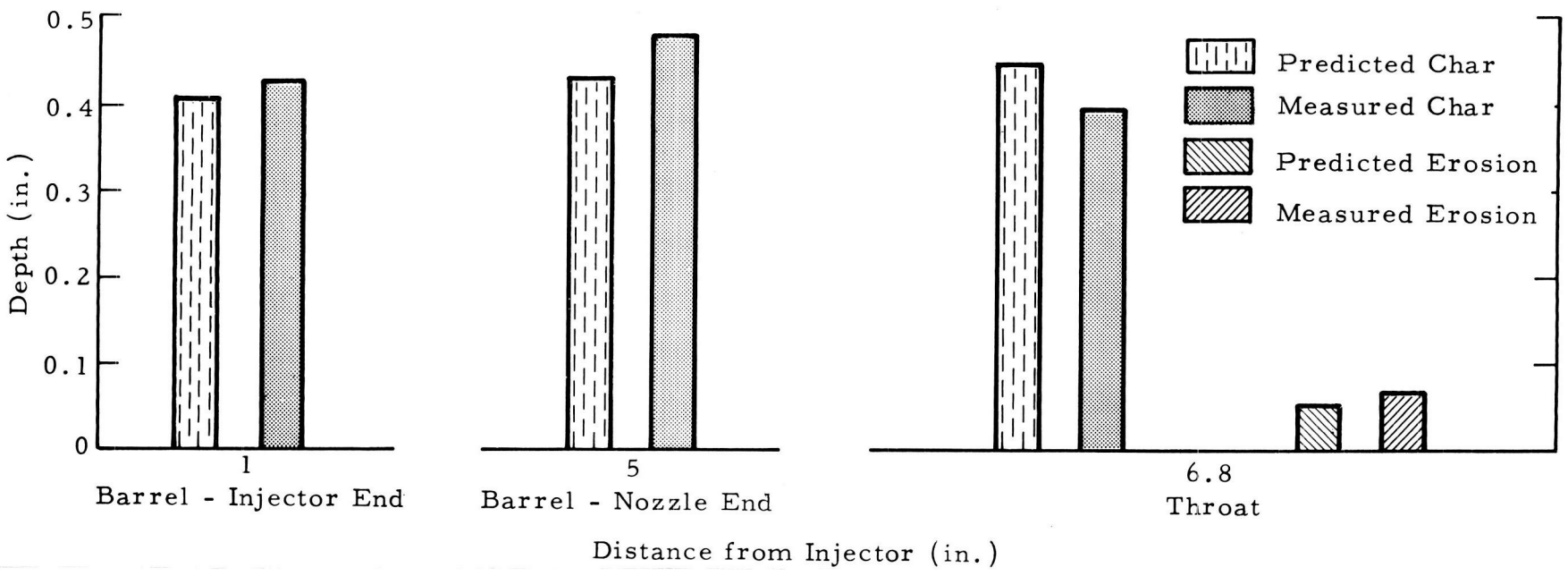

Figure 9. Ablative Chamber Performance, Run 2AX3844

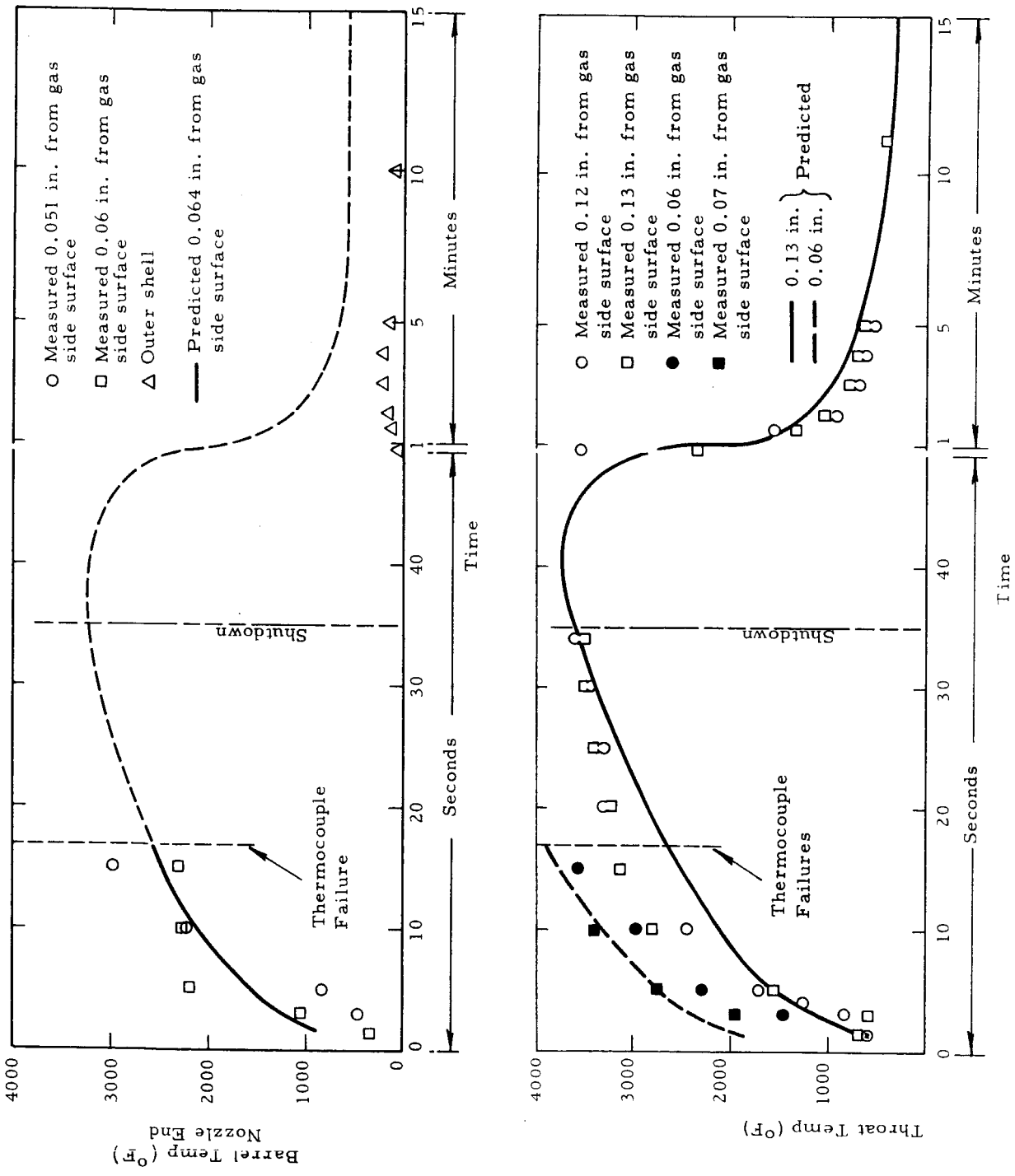

Figure 10. Thermocouple Data, Run 2AX3844

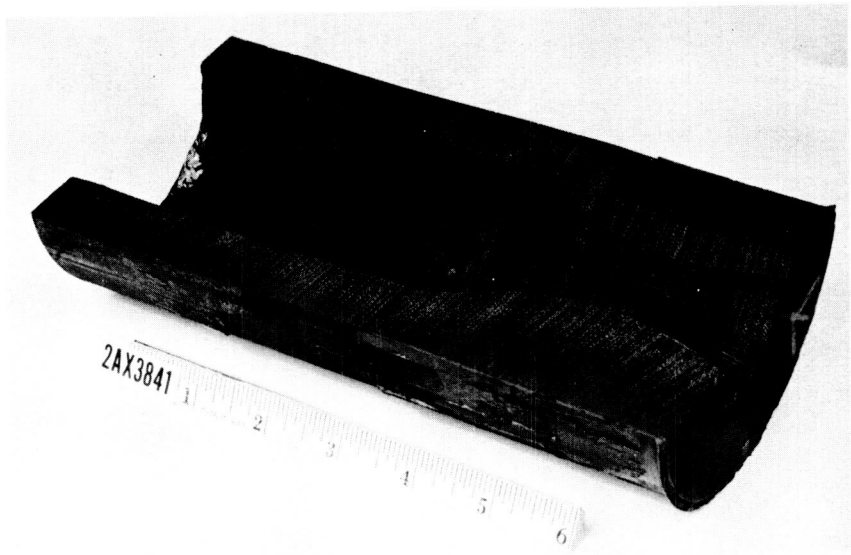

6028-505

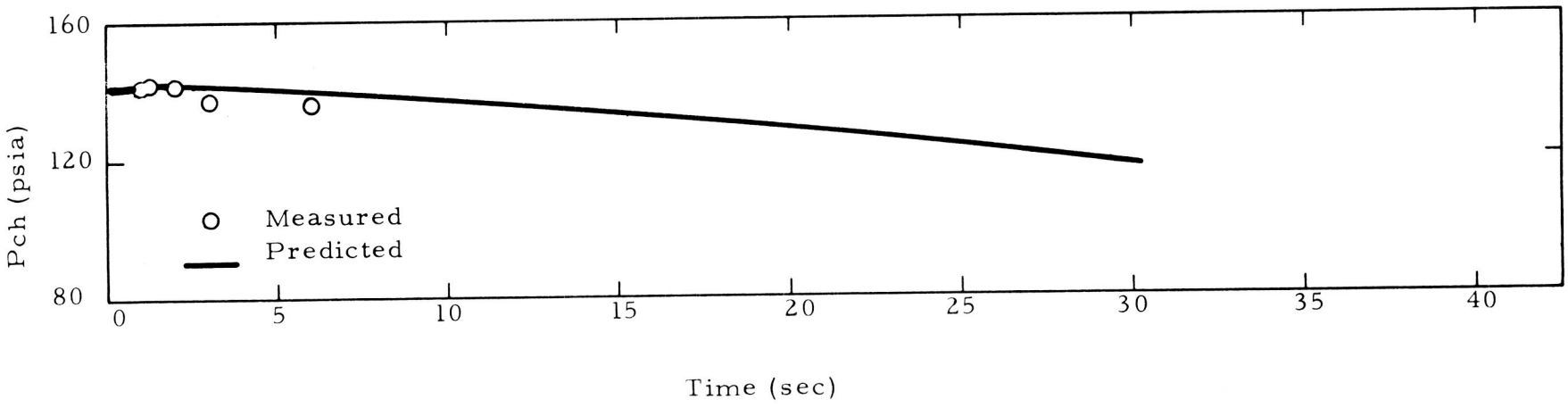

Figure 11. Ablative Chamber Performance, Run 2AX3841

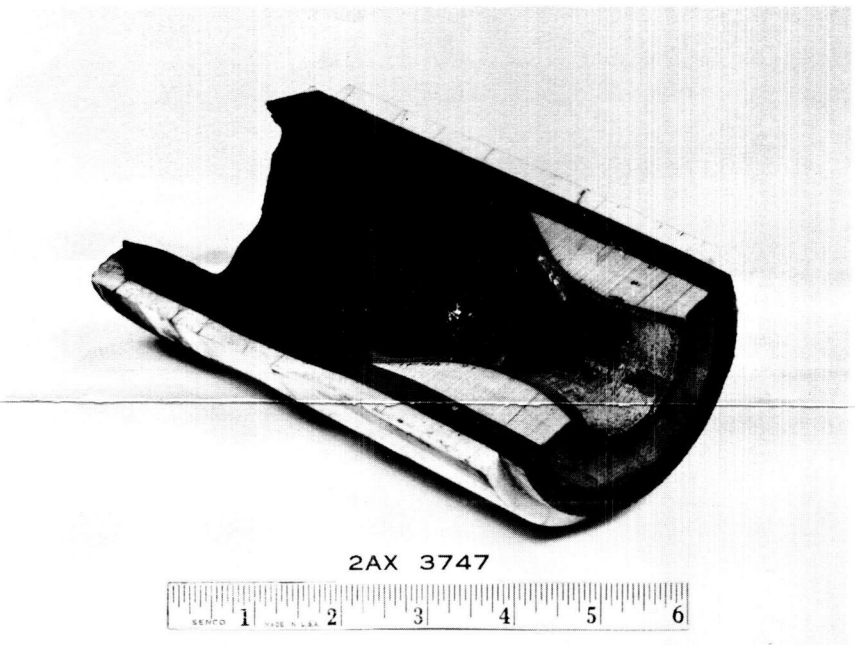

6028-215

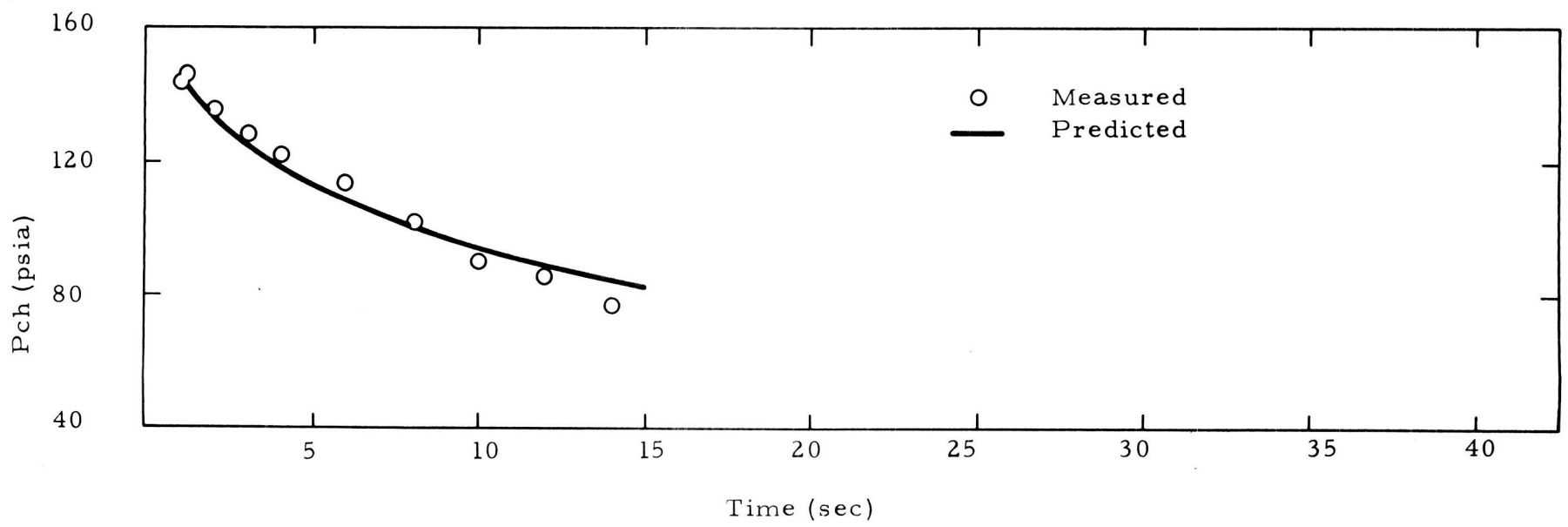

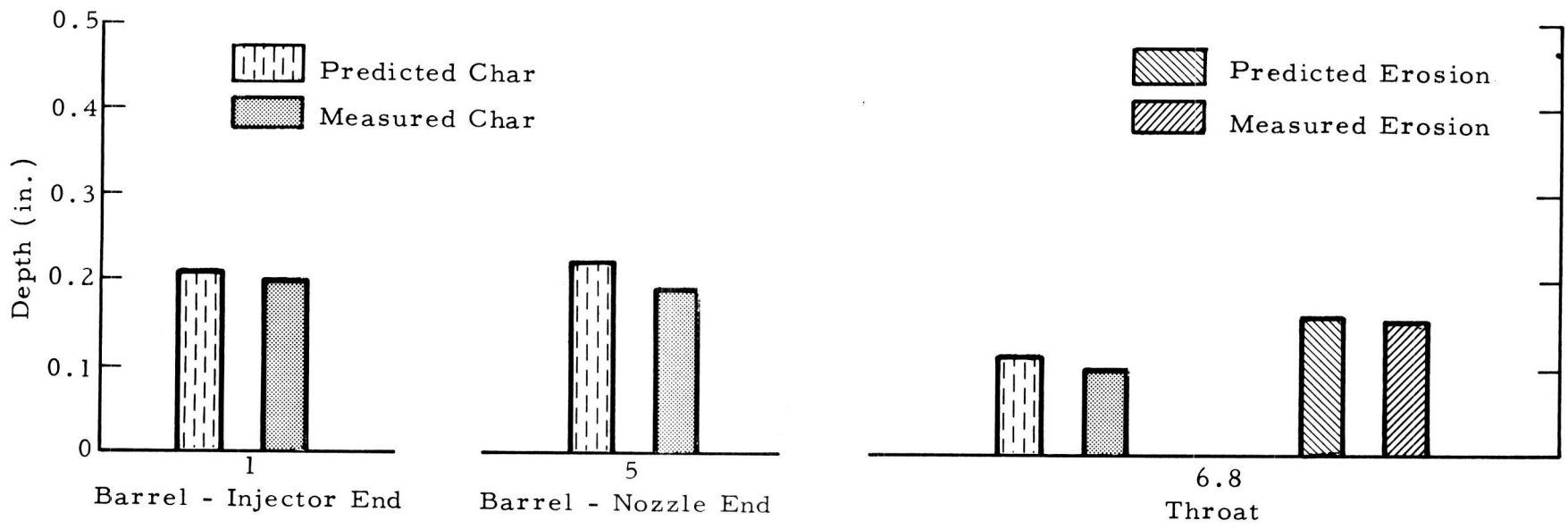

Figure 12. Ablative Chamber Performance, Run 2AX3747

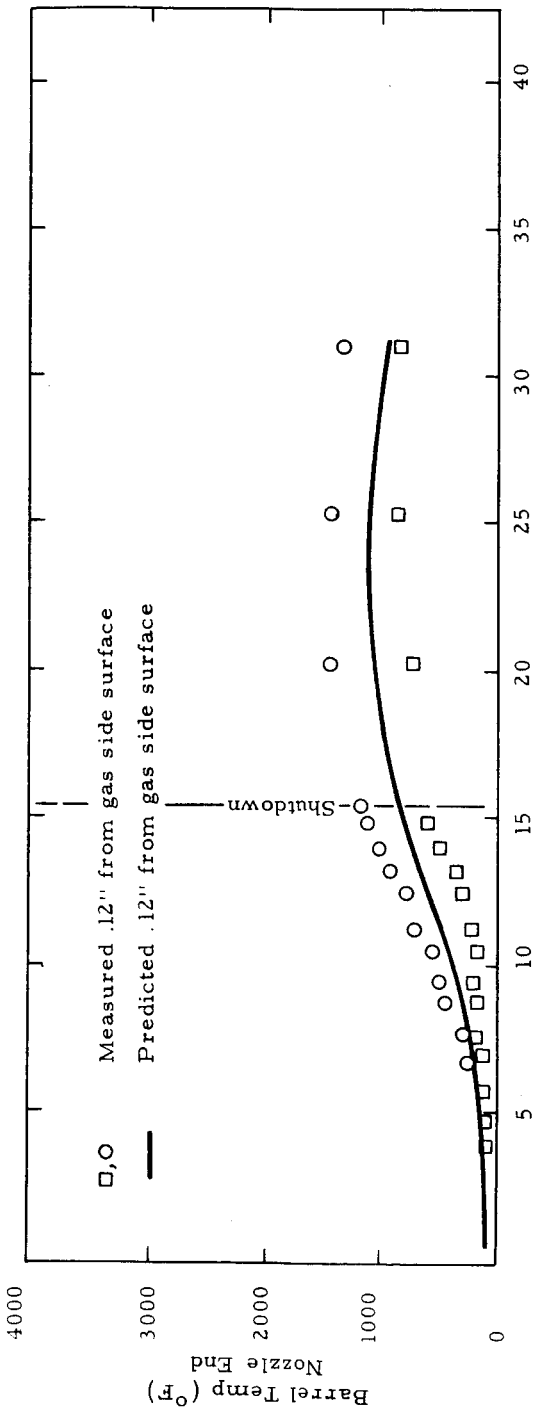

Figure 13. Thermocouple Data, Run 2AX3747

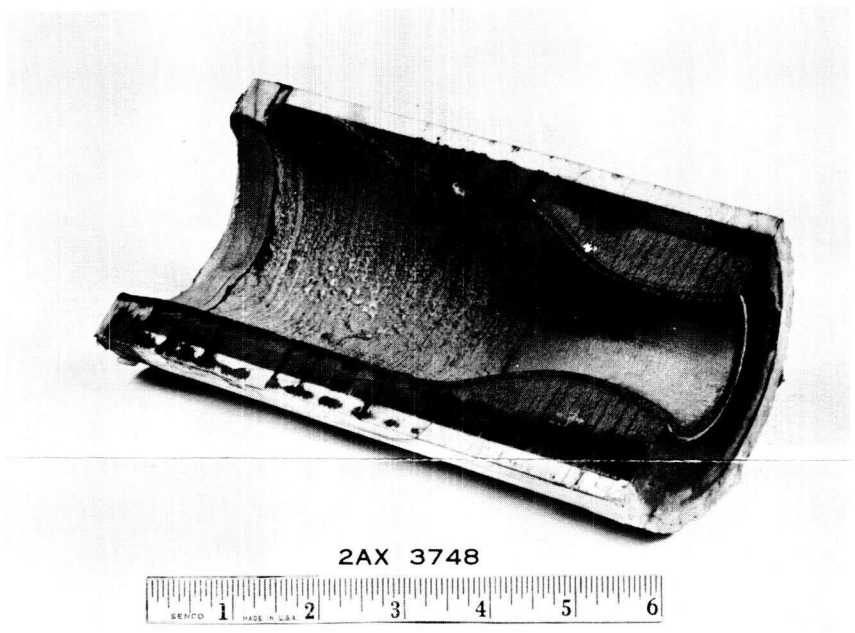

6028-207

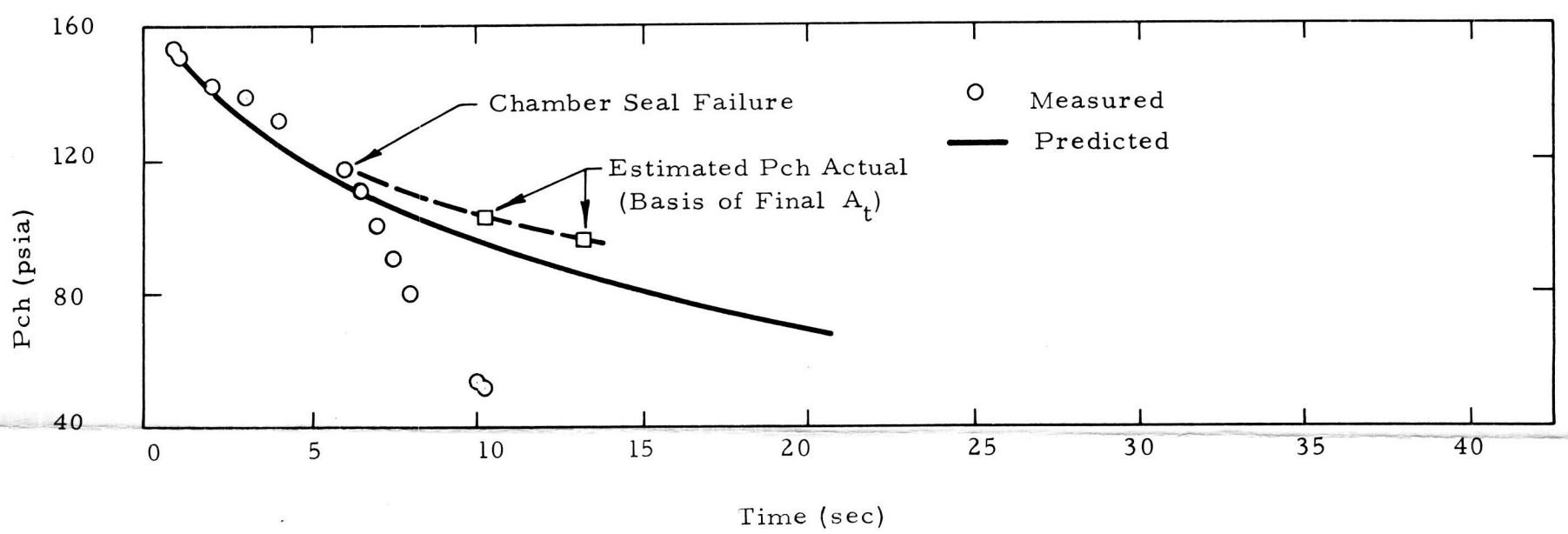

Thiokol
REACTION MOTORS DIVISION

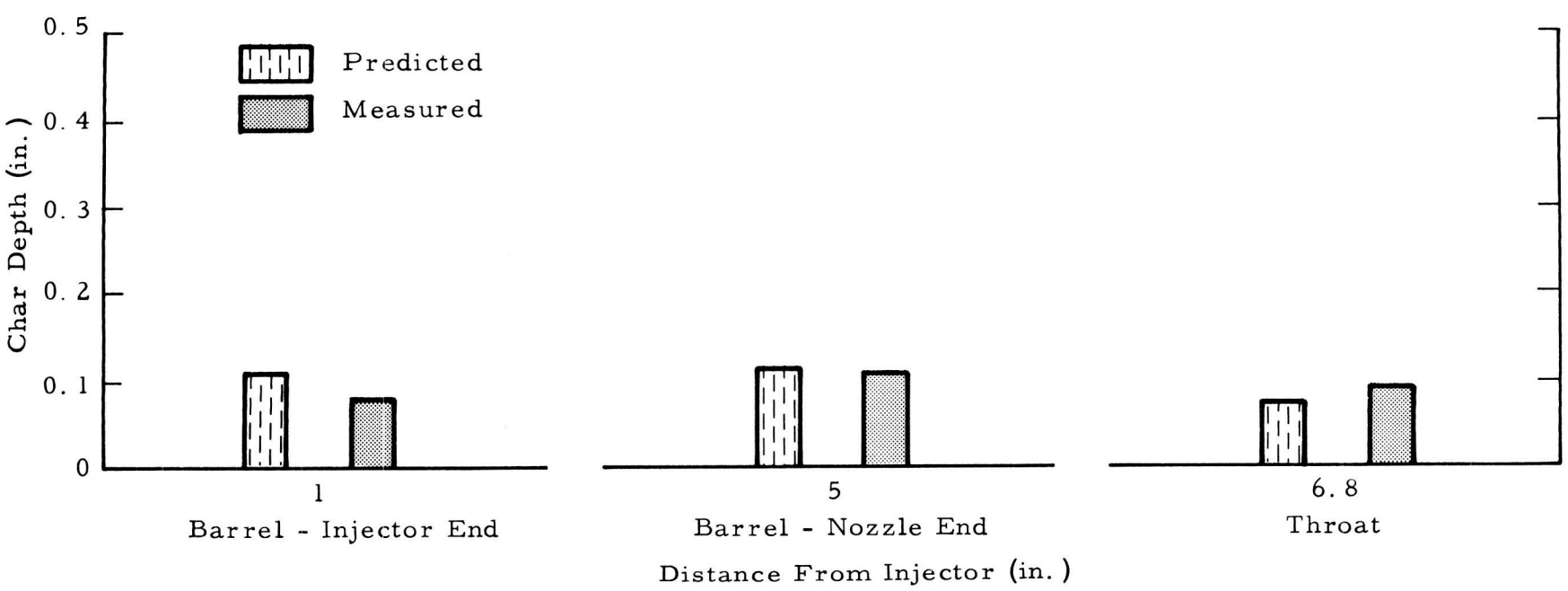

Figure 14. Ablative Chamber Performance, Run 2AX3748

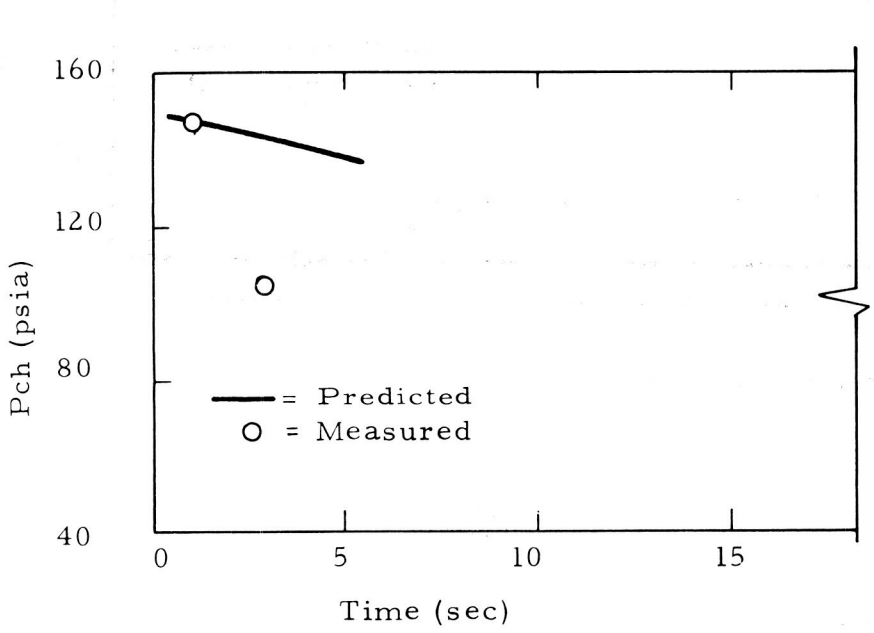

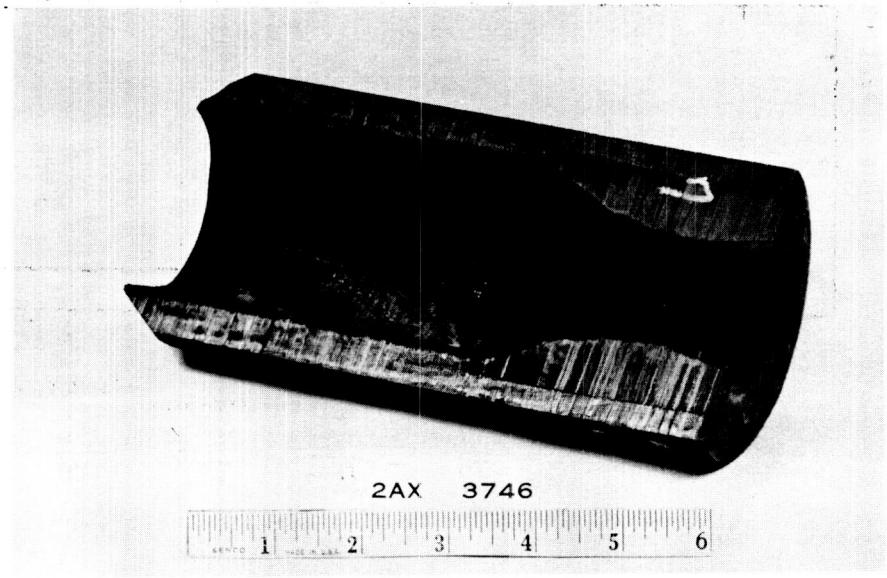

6028-209

Figure 15. Ablative Chamber Performance, Run 2AX3746

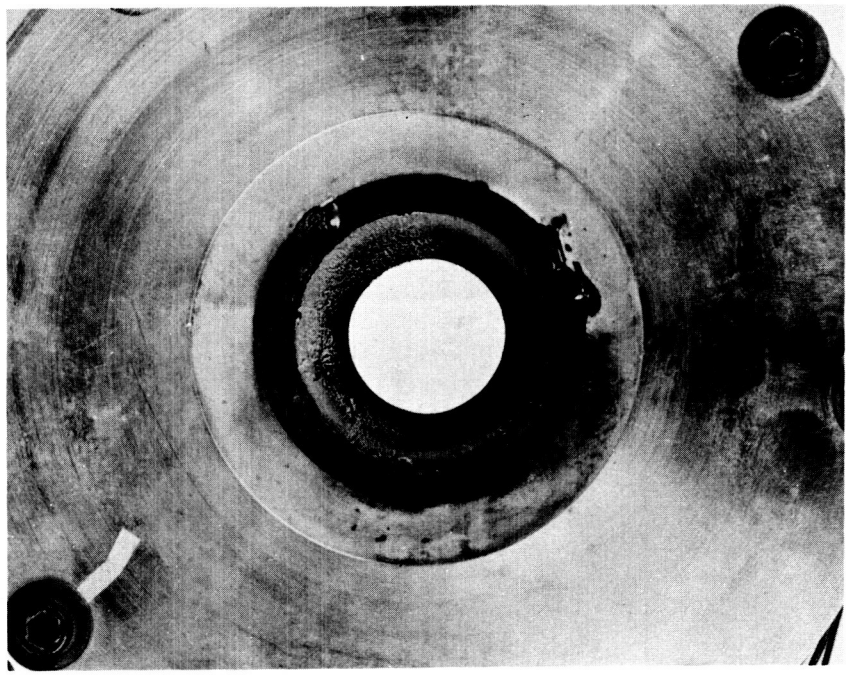

View From Nozzle Exit 6028-529

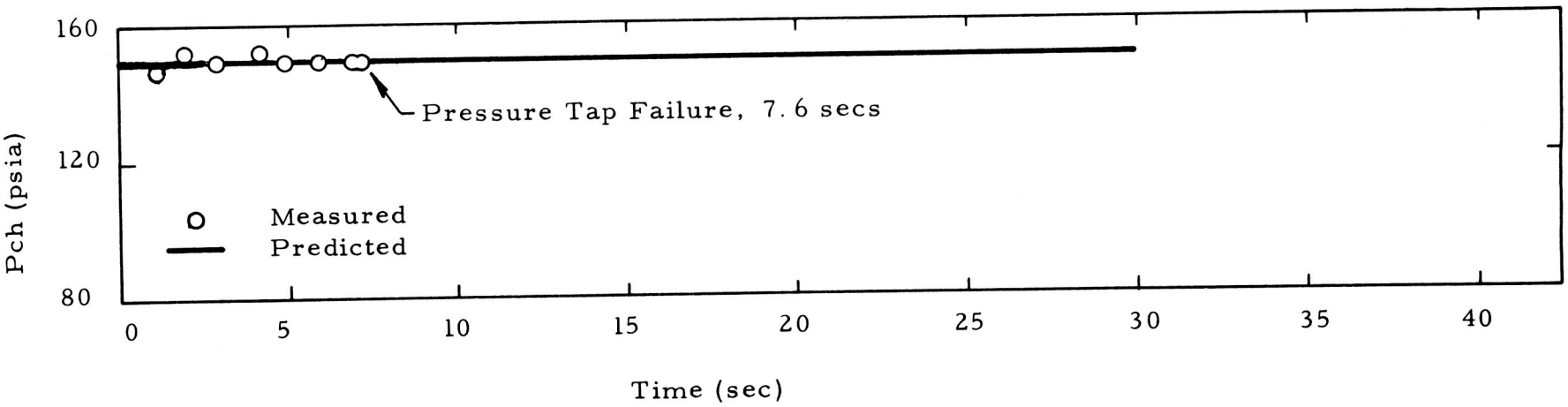

Figure 16. Ablative Chamber (Heat Sink Throat) Performance, Run 2AX3845

Examination of the throat revealed uniform erosion. The predictions of char depth include the char growth that continues after shutdown and into the soak period. Following the actual run, however, injector purge gas was flowing through the chamber, providing some cooling which probably explained the lower values of measured char depth in the throat. Similarly, chamber wall temperature decayed faster than predicted because of purge gas cooling. Temperature vs time in the throat plane for typical thermocouples is shown in Figure 6 along with predicted values for similar depths.

The data for a second specimen of the same graphite phenolic, MX4500, are shown in Figure 7 for run 2AX3749 and barrel temperature data in Figure 8. This chamber ran for the programmed 20 seconds. The analytical predictions for this run were similar to those of 2AX3843, but not identical since the initial chamber pressure and mixture ratio were slightly different. Superior performance is again evident. No useful temperature data were obtained for the throat due to a thermocouple malfunction.

Based on property data supplied by the vendor, a precharred graphite epoxy material, AVCO X2018, showed the lowest predicted erosion rate of all the materials analytically screened at the beginning of the program. Analysis of the test data, however, indicated a slightly higher erosion rate than for MX 4500. The data for two monolithic assemblies of this material are shown in Figures 9 and 10 (run 2AX3844), and Figure 11 (run 2AX3841.) The predictions shown are based on more recent property data acquired during the course of the program. Chamber pressure for run 2AX3844 decayed from 144 psia to 112 psia after 34.7 seconds of running at 94.2% of theoretical c*. Chamber pressure data for run 2AX3844 had to be extrapolated from 28 seconds to the end of the run because of clogging of both the upstream and downstream pressure taps. Test run 2AX3841 resulted in an injector cooling passage failure at two seconds and water was injected into the chamber. An automatic high pressure shutdown terminated the run (due to increased mass flow) at 30.3 seconds. As a result of the cooling water leak into the chamber no correlations are attempted.

A graphite cloth-phenolic barrel and silica-phenolic nozzle composite chamber ranked next in performance. Test data (run 2AX3747) for this chamber are presented in Figures 12 and 13. Phenolic impregnated, shingle-wrapped USP 5064 graphite cloth was used for the chamber barrel, and a laminated 90 degree orientation Thiokol-Panelyte RAP 3002 silica cloth-phenolic was used in the nozzle. Erosion was uniform, but was greater than in the monolithic graphite-phenolic chambers. The run was

terminated at 15.4 seconds by the automatic pressure cutoff when the chamber pressure decayed to 75 psia. Instrumentation difficulties precluded the acquisition of useful temperature data in the throat plane.

A laminated silica-phenolic nozzle (90 degree orientation) of USP 5067 was also run with a shingle-wrap chamber liner of USP 5067 silica cloth-phenolic (test run 2AX3748). The run was terminated at 10.3 seconds due to a combustion gas seal leak. Behavior was predictable (Figure 14) up to the time of the seal leak. Throat erosion was uniform and correlation with the predicted char depth was good. Interestingly, the char depth in the barrel and nozzle was much lower than that of the graphite cloth-phenolics, but erosion was high. This thin char layer is the result of higher pseudo-steady state dimensional ablation and the lower conductivity of the silica phenolic as compared to the graphite cloth phenolic material. Unfortunately, a stepper switch malfunction resulted in the loss of temperature data for this run.

Additional composite ablative chamber data were obtained from a barrel liner of shingle-wrap USP 5064 silica cloth-phenolic and a 90 degree laminated nozzle insert of Thiokol-Panelyte RAP 2002 carbon cloth-phenolic (Figure 15, run 2AX3746). The run was terminated at 2.9 seconds due to a diborane leak in the test stand manifold. The throat eroded appreciably faster than predicted. This is attributed to abnormally high (54%) resin content, which was probably contributory to the apparent spalling of the carbon cloth. No correlation with the predicted char depth temperature gradients in the ablative wall was attempted since the fuel leak resulted in an off-mixture ratio operation.

Analytical predictions showed that the graphite reinforced materials would have the lowest erosion rates and that silica reinforced materials would erode at a much higher rate. The better theoretical and subsequently confirmed test behavior of the graphite materials can be attributed to their higher thermal conductivity and resultant lower gas side wall temperature. The graphitic reinforcement materials also have higher melting temperatures (sublimation in the case of graphite) than the silica or glass reinforcement materials. The past performance of graphitic materials with earth storable propellants has not been as good as that of silica at combustion temperatures of approximately 5600F and is attributed primarily to the strong oxidizing atmosphere and water content of earth storable propellant combustion products. However, this disadvantage was not apparent at the 6530F combustion temperature with OF_2/B_2H_6 propellants.

The tungsten/molybdenum alloy nonablative throat (run 2AX3845, Figure 16) was run with a silica phenolic chamber liner fabricated by Thiokol-Panelyte.

The insert was in excellent condition after a 7.6 second run that was terminated by a pressure tap failure near the injector end of the chamber. However, chamber pressure was constant according to a second pressure tap as shown in Figure 16. Since the run duration represented only 25% of the hardware capability, the effects of temperature were not manifested at the thermocouples until after shutdown and consequently are not shown. Sectioning of the chamber was not considered, since the chamber is still in good condition and might be useful in further studies.

e. Materials Evaluation Summary

Briefly, the results of the Task I ablative materials tests are as follows:

Chamber Materials	Test Duration (sec)	ΔA Throat (%)
1. Monolithic Fiberite MX4500 (Graphite Phenolic)	43.6	40
2. Monolithic Fiberite MX 4500 (Graphite Phenolic)	20.85	21
3. Monolithic AVCO X2018 (Precharred Graphite Epoxy)	34.7	30
4. Monolithic AVCO X2018 (Precharred Graphite Epoxy)	30.3	29
5. USP 5064 Barrel (Graphite Cloth Phenolic) RAP 3002 Nozzle (Silica Phenolic)	15.35	75
6. USP 5057 Barrel and Nozzle (Silica Phenolic)	10.28	52
7. USP 5064 Barrel (Graphite Cloth Phenolic) RAP 2002 Nozzle (Carbon Cloth Phenolic)	2.86	81

The hard throat (tungsten-2% molybdenum alloy insert) configuration experienced no erosion after 7.6 seconds of operation in a test prematurely terminated as a result of an instrumentation failure.

f. Materials Evaluation Conclusions

The following conclusions have been drawn regarding the 150 pound thrust chamber materials evaluation program:

- Based on both the analytical predictions and the test data obtained in this program, present state of the art ablative materials are found to behave in a predictable manner with OF_2/B_2H_6. The data from four test firings indicate that the durability (erosion rate) of graphite cloth reinforcement materials with these propellants is approximately equivalent to that of the state of the art silica-phenolic materials with N_2O_4/50-50.

- The graphite reinforced ablative materials demonstrate the lowest erosion rates.

- Analytical studies show that nonablating throat configurations (i.e., refractory, ceramic, or refractory composites) hold promise for limited duty cycles. The application of such configurations is limited primarily by the heat sink capacity of the insert and substrate and back-up insulation effectiveness within reasonable envelope and weight requirements. Unfortunately, an instrumentation failure on a chamber assembly utilizing a tungsten-molybdenum throat insert precluded full evaluation of this configuration.

5. Design Data Tests

a. Objectives

Two other test programs were conducted with the OF_2/B_2H_6 propellant system under Task I. The first was a study of the ignition behavior of the OF_2/B_2H_6 combination; the second was an investigation of the heat transfer properties of OF_2 by heated tube techniques. Each of these investigations, programmed to generate factual design data for high temperature combustion containment, is discussed separately and in detail in the following sections.

b. Ignition Studies

(1) Introduction - The hypergolicity of the OF_2/B_2H_6 combination, at both sea level and space conditions, was established by RMD under Contract

NAS-w-449. However, the test setup employed in that series of experiments employed uncooled, unjacketed lines between the propellant valves and the injector. Consequently, it was not possible to investigate liquid phase, sea level injection or altitude ignition characteristics.

A definitive investigation of the ignition properties of OF_2/B_2H_6 was conducted under Contract NAS-3-2553 at a nominal 150 pound thrust level. Both the injector and the propellant lines were jacketed in variable temperature baths. The test program was statistically designed to permit the isolation and identification of significant variables in the ignition process and also to generate pertinent design information. The variables examined included ambient pressure level, oxidizer vs fuel leads, propellant inlet temperatures, chamber temperature, mixture ratio, chamber geometry, and injector type.

(2) Test Hardware - Three different injector types were used in the ignition studies: the full diameter vortex, the mid-diameter vortex, and a doublet configuration injector. These injectors were mated to transparent plastic chambers equipped with copper or steel nozzles.

A stainless steel tube replaced the plastic chamber for three tests to permit cooling the entire engine to -320F; the plastic tube would shatter upon ignition if precooled to this temperature. The steel tube was fitted with a nozzle orifice in the side of the chamber and a plastic end plate replaced the nozzle to permit photographing the ignition sequence.

(3) Test Setup - The ignition test engines were mounted vertically (to preclude propellant holdup or puddling in the chamber) as shown in Figure 17. Both the injector and the propellant lines were placed in cooling baths to prevent propellant vaporization (Figures 18 and 19). The volume of each propellant line from the propellant valve to the injector was approximately 3 $in.^3$, including the pressure transducer line and the purge line back to the check valve.

The injector was mounted on the bottom of the propellant bath (Figure 19) with the chamber and nozzle mounted vertically below. The nozzle was connected to a 40 gallon vacuum tank by a two inch pipe and elbow. A blow-off disc relieved the pressure in the tank after ignition.

(4) Data Acquisition - The entrance of the lagging propellant into the thrust chamber and the ignition of the propellant mixture are the end points of the ignition delay period. The determination of these two points was

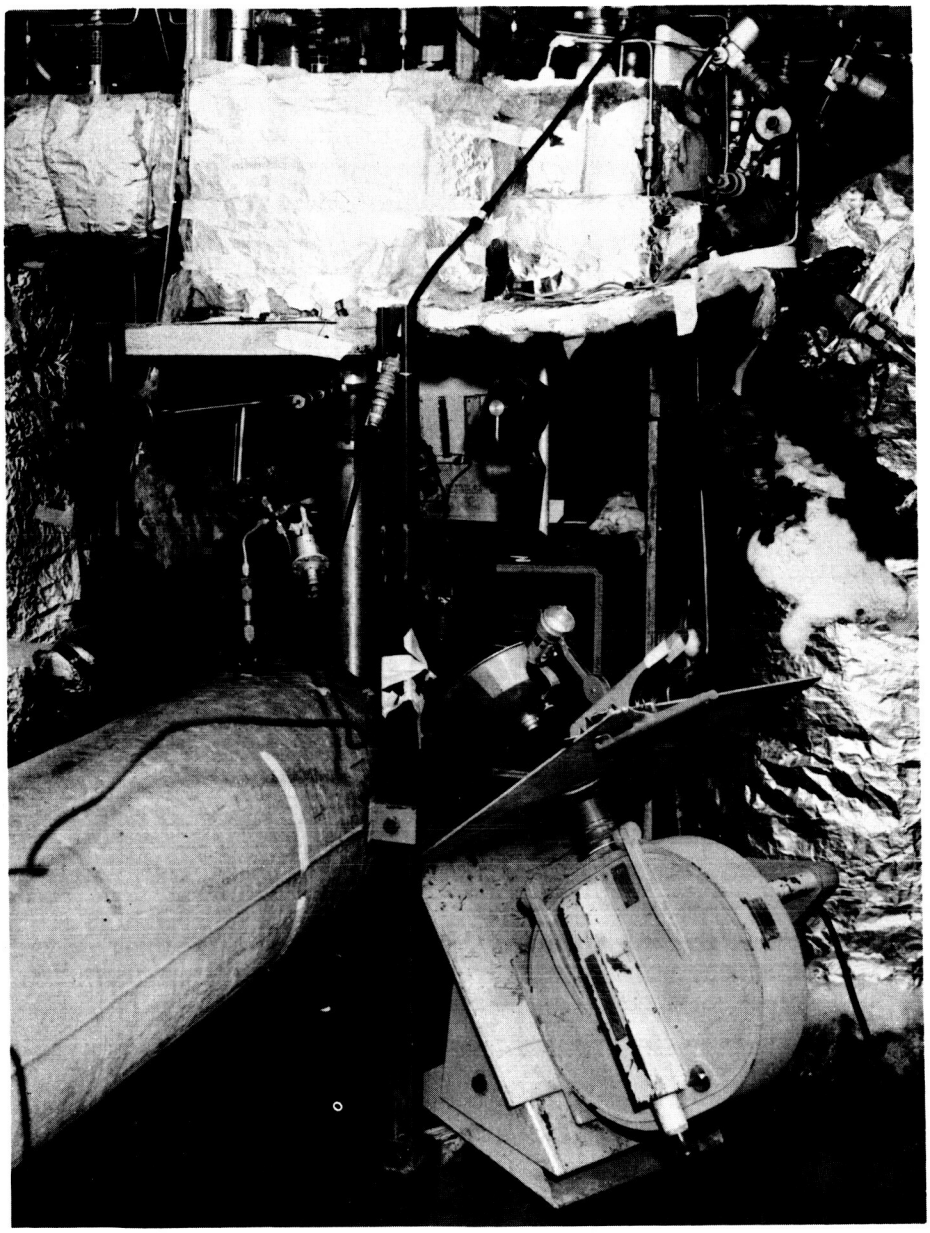

6028-187

Figure 17. Ignition Test Setup

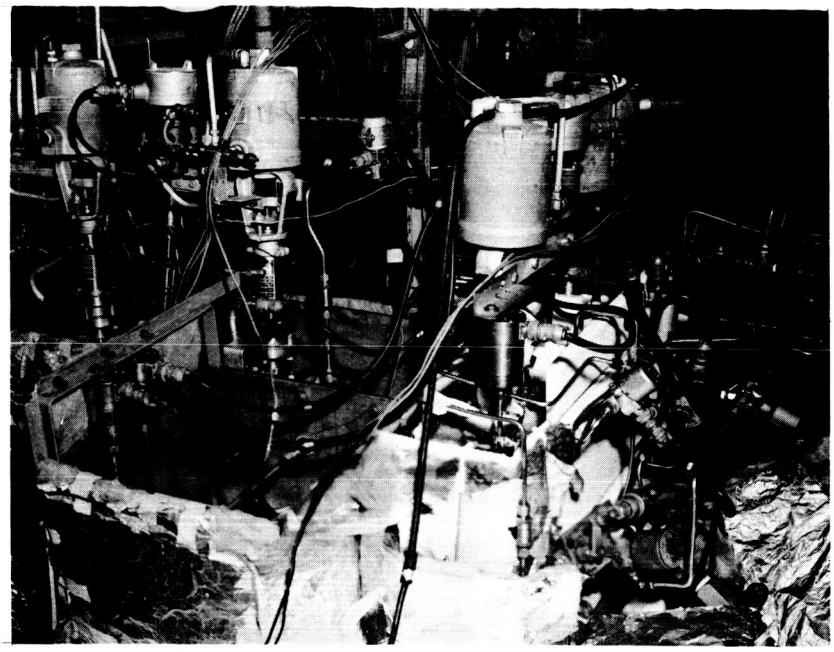

6028-188

Figure 18. Propellant Valves and Cooling Baths

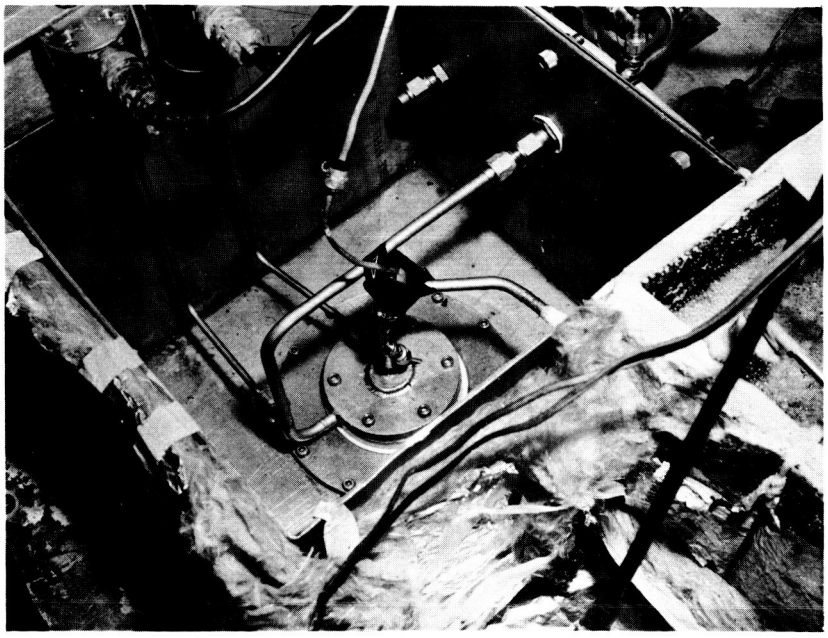

6028-189

Figure 19. Doublet Injector in Cooling Bath

somewhat complicated due to the cryogenic nature of the propellants and the nature of the test apparatus.

For example, the entrance of the propellant could not be determined precisely simply by using the valve timing and a flowrate, since the propellant changed density (or even state) while flowing. Thus, alternate means (such as photographic data, injector pressure data, chamber pressure data or temperature measurements at the injection orifices) were used to detect the presence of propellant whenever possible.

Consequently, although the same definition of ignition delay (time elapsed between entry of the second propellant and ignition) is used in all cases, the techniques used to determine these two events varies from case to case, depending on the conditions imposed by the experiment.

A variety of techniques were employed to insure the acquisition of meaningful data. These included high speed cinematography, high response pressure transducers, low mass thermocouples, and light intensity (photo-electric cell) instrumentation. The data were recorded simultaneously on oscillographic recorders and magnetic tape. A playback of taped ignition test data for a typical run is shown in Figure 20.

(5) Test Results - Analysis of the ignition data for the various configurations and conditions discussed in the previous sections indicates that they can be classified in four general groups within which the characteristics are similar. These groups are shown in Table V.

TABLE V

IGNITION TEST DATA GROUPS		
Propellant State	Pressure Environment	Injector
Liquid	S.L.	Vortex
Liquid	S.L.	Doublet
Liquid	Altitude	Vortex or Doublet
Gaseous	S. L. or Altitude	Vortex or Doublet, For Either Environment

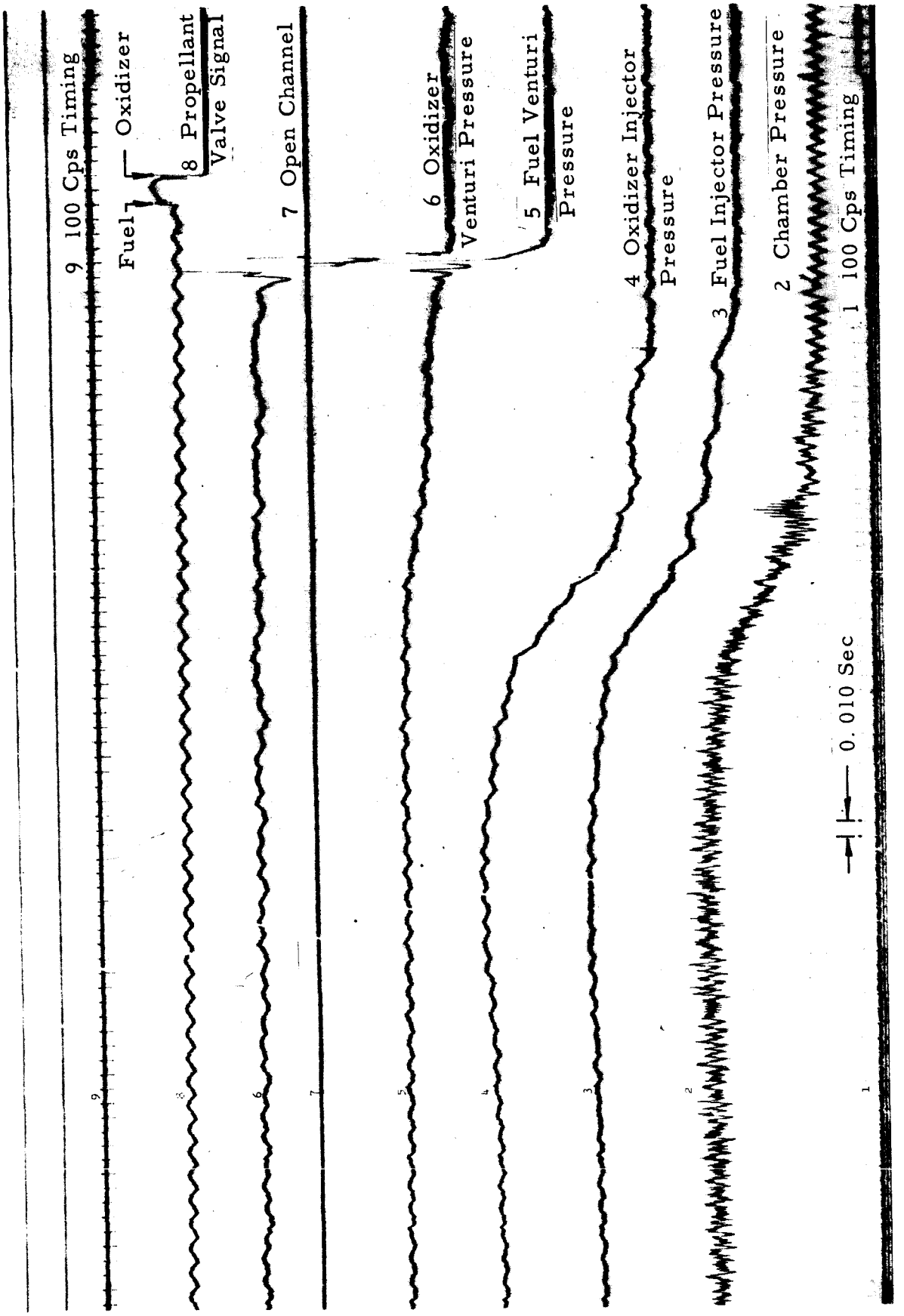

Figure 20. Typical Ignition Test Record

Variation of the other test parameters, such as chamber configuration,temperature, mixture ratio, and propellant leads and lags within these groupings, had little or no effect on ignition characteristics. The test conditions are summarized in Table VI; the test results are given in Tables VII and VIII.

Run duration was established by a preset timer rather than chamber pressure. Consequently, steady state chamber pressure was not attained in every run. However, combustion was continuous from time of ignition in all cases; no flameouts occurred.

- Gaseous Propellants (Tests 25, 26, 27; see Tables VII and VIII)

Gaseous injection of diborane and OF_2 produced reliably hypergolic ignition both at sea level and at simulated altitudes. Ignition delays of 9 to 16 msec were recorded for the two tests made at altitude and 14 msec for the one test made at sea level. These times are based on the initial rise of injection inlet pressures and chamber pressures since gaseous propellant entry into the chamber could not be observed visually or be otherwise reliably detected with the various instrumentation methods used.

When both propellants were injected almost simultaneously at altitude (Test 25), ignition was rapid (9 msec) and smooth. A diborane lead of 10 msec (Test 26) at altitude resulted in a slightly longer delay (16 msec) with a short pressure spike on ignition. A long OF_2 lead at sea level (Test 27) resulted in a small pressure peak at ignition followed by a smooth rise to steady state.

Although all three tests were made with the mid-diameter injector, it is not expected that the injector type would have a significant effect on ignition when the propellants were injected in the gaseous state, based on the many altitude tests in which liquid propellants vaporized before initial injection.

- Vortex Injector at Sea Level (Tests 21, 23, 24, 29; see Table VII)

The results of all sea level tests with liquid propellants are summarized in Table VII. Propellant entry times for all sea level tests are based on the initial injector pressure rises since this was the only measurement available in these tests. The camera could not observe the propellant injected last and the thermocouples could not always distinguish between propellants because of the size of the hardware. Ignition time is based on solar battery (photocell), camera, or chamber pressure data, in that order of preference when all indicators are not available or one is questionable.

The four liquid propellant tests with vortex injection had oxidizer leads of 40 to 50 msec. Reference to Table VII shows that in Test 21 with the full diameter vortex injector submerged in a liquid nitrogen bath and in Test 23 with the mid-diameter vortex injector submerged in a water bath, the ignition delays were essentially zero. In Tests 24 and 29 with the mid-diameter vortex injector in a dry ice bath, the ignition delays were only 23 to 24 msec.

Comparison of these four tests (vortex injectors) with the doublet injector tests in Table VII shows the significant effect of the injector type on ignition delays at sea level conditions. Ignition delays with the vortex injectors were less than 25 msec in ever case, while the delays with the doublet injector were well over 100 msec in every test but one.

The effects of the other variables, such as propellant lead, mixture ratio, temperature, etc., were of secondary nature over the rather wide range of conditions investigated. As might be expected, it would appear that good liquid-phase mixing of the propellants is required for good ignition characteristics when the propellants are injected primarily as liquids. The impingement

TABLE VI. IGNITION TEST CONDITIONS

Test No.	Run No. 2AX37	Injector Type	Chamber Material	Chamber Diameter in.	Leading Propellant	Equivalent Attitude ft	Mixture Ratio O/F	Injector Temp. °F	Chamber Temp. °F	Propellant State
1	50	Doublet	Plastic	2.5	Fuel	0	3	-150	ambient	liquid
2	51	Doublet	Plastic	2.5	Fuel	0	3	-100	ambient	liquid
3	52	Doublet	Plastic	2.5	Fuel	0	3	-150	ambient	liquid
4	53	Doublet	Plastic	2.5	Ox	0	3	-140	ambient	liquid
5	54	Doublet	Plastic	2.5	Ox	75,000*	3	-160	ambient	liquid
6	55	Doublet	Plastic	2.5	Ox	55,000*	3	-80	ambient	liquid
7	56	Doublet	Plastic	2.5	Ox	0	4	-140	ambient	liquid
8	57	Doublet	Plastic	2.5	Ox	0	3	+60	ambient	liquid
9	58	Doublet	Plastic	2.5	Ox	0	3	-320	ambient	liquid
10	59	Doublet	Plastic	2.0	Ox	56,000*	3	+65	ambient	liquid
11	60	Doublet	Plastic	2.0	Ox	59,000*	4	+67	ambient	liquid
12	61	Doublet	Plastic	2.0	Ox	55,000*	2	+60	ambient	liquid
13	62	Doublet	Steel	2.5	Ox	0	2	-320	ambient	liquid
14	63	Doublet	Steel	2.5	Fuel	75,000	2	-320	ambient	liquid
15	64	Doublet	Steel	2.5	Fuel	0	2	-320	ambient	liquid
16	65	Full Dia	Plastic	2.5	Fuel	84,000	3	+60	ambient	liquid
17	66	Full Dia	Plastic	2.5	Ox	87,000	3	0	ambient	liquid
18	67	Full Dia	Plastic	2.5	Ox	60,000*	-	-15	ambient	liquid
19	68	Full Dia	Steel	2.5	Ox	50,000*	3	-320	-320	liquid
20	69	Full Dia	Steel	2.5	Ox	80,000	3	-320	-320	liquid
21	70	Full Dia	Steel	2.5	Ox	0	3	-320	-320	liquid
22	71	Mid Dia	Plastic	1.6	Fuel	67,000	3	+60	ambient	liquid
23	72	Mid Dia	Plastic	1.6	Ox	0	4	+50	ambient	liquid
24	73	Mid Dia	Plastic	1.6	Ox	0	4	-110	ambient	liquid
25	74	Mid Dia	Plastic	1.6	Fuel	59,000*	-	ambient	ambient	gas
26	75	Mid Dia	Plastic	2.5	Fuel	74,000	-	ambient	ambient	gas
27	76	Mid Dia	Plastic	2.5	Ox	0	-	ambient	ambient	gas
28	77	Mid Dia	Plastic	2.5	Ox	60,000*	-	-110	ambient	liquid
29	78	Mid Dia	Plastic	2.5	Fuel	0	-	-110	ambient	liquid
30	79	Mid Dia	Plastic	2.5	Fuel	73,000	-	-100	ambient	liquid

* estimated from manometer

TABLE VII

IGNITION DELAYS FOR SEA LEVEL TESTS

Test No.	Injector Type	Leading Propellant	Lead Time (msec)	Ignition Delay Time (msec)	Ignition Delay Method
1	Doublet	Fuel	21	133	(1)
2	Doublet	Fuel	30	107	(2)
3	Doublet	Fuel	7	124	(1)
4	Doublet	Ox	22	135	(1)
7	Doublet	Ox	29	126	(2)
8	Doublet	Ox	81	107	(1)
9	Doublet	Ox	75	90	(2)
13	Doublet	Ox	110	216	(2)
15	Doublet	Ox	19	135	(2)
21	Full Dia Vortex	Ox	51	1	(2)
23	Mid-Dia Vortex	Ox	45	1	(2)
24	Mid-Dia Vortex	Ox	43	23	(1)
27	Mid-Dia Vortex	Ox (gaseous)	55	14	(2)
29	Mid-Dia Vortex	Ox	43	24	(3)

Notes: Time reference: t = O at initiation of electrical signal to open oxidizer propellant valve.

(1) IPF or IPO rise to photographed ignition
(2) IPF or IPO rise to P_{ch} rise
(3) IPF or IPO and photocell

TABLE VIII

IGNITION DELAYS FOR ALTITUDE TESTS

Test No.	Injector Type	Leading Propellant	Lead Time (msec)	Ignition Delay Time (msec)	Altitude (ft)
5	Doublet	Ox	19	20	75,000
6	Doublet	Ox	15	22	55,000
10	Doublet	Ox	63	4	56,000
11	Doublet	Ox	52	8	59,000
12	Doublet	Ox	87	--	55,000
14	Doublet	--	0	--	75,000
16	Full Dia Vortex	--	0	33	84,000
17	Full Dia Vortex	Ox	49	1	87,000
18	Full Dia Vortex	Ox	8	43	60,000
19	Full Dia Vortex	Ox	4	38	50,000
20	Full Dia Vortex	Ox	91	19	80,000
22	Mid-Dia Vortex	--	0	42	67,000
25	Mid-Dia Vortex	Fuel (gaseous)	2	9(1)	59,000
26	Mid-Dia Vortex	Fuel (gaseous)	10	16(1)	74,000
28	Mid-Dia Vortex	Ox	7	44	60,000
30	Mid-Dia Vortex	Fuel	21	51	73,000

Note: Propellant lead determined by difference in propellant valve opening indication ignition delay for these tests is determined by the time difference between ignition as seen by the camera and the lagging propellant valve opening indication.

(1) Ignition delay determined by IPO rise to P_{ch} rise

of the liquid oxidizer streams upon the fuel streams confined by the tangential injector in the vortex design insures proper mixing under these conditions.

- Doublet Injector at Sea Level (Tests 1, 2, 3, 4, 7, 8, 9, 13, 15)

The results of these tests are also summarized in Table VII; propellant entry and ignition times are defined as in the previous section .

In general, the tests with the doublet injector conducted under conditions similar to the vortex injector tests resulted in significantly longer ignition delays. These delays are probably due to the poorer mixing of the liquid propellants in the doublet injector.

In the doublet injector, the fuel is injected axially and the oxidizer injected at a 45° angle toward the fuel from a larger diameter. Although the stream lengths were the same as in the vortex injector, physical mixing was not assured by mechanical means, such as the splash-plate effect of the tangential fuel injector inherent in the vortex design.

Comparing Tests 1 and 4 (made under identical conditions except that fuel was injected first in Test 1) there was no significant difference in ignition delay between a moderate ($\sim$ 20 msec) oxidizer or fuel lead. In Test 15, with approximately the same oxidizer lead, the delay was also about the same when the injector and propellant manifolds were conditioned to -320F in the liquid nitrogen bath.

Although relatively long oxidizer leads (81 and 75 msec, respectively) were employed in Test 8 at ambient temperatures and

Test 9 at -320F, the ignition delays were somewhat shorter than the corresponding tests with more moderate propellant leads. However, when the oxidizer lead was increased to 110 msec in Test 13 with the injector at -320F, the greatest delay (216 msec) was experienced with a pressure peak greater than steady-state chamber pressure. Although sufficient runs were not made to determine the envelope of lead times which can be used without affecting ignition delay, it appears that moderate leads of either propellant are satisfactory.

- Simulated Altitude Tests (Tests 5, 6, 10, 11, 12, 14, 16, 17, 18, 19, 20, 22, 25, 26, 28, 30; see Table VIII)

In the simulated altitude tests with both the vortex and the doublet injectors, the propellants initially entered the combustion chamber as gases and ignition took place rapidly in the gas phase. The ignition delays could not be measured directly because there was no visible indication or satisfactory means of determining when each propellant first entered the chamber.

The ignition delays shown in Table VIII, therefore, are based on the time between the opening signal from the lagging propellant valve and the first indication of ignition on the high speed film. It should be noted, therefore, that the delay times shown also include the time necessary for the propellants to reach the chamber after the valves start to open. The start of injection pressure rise could not be used as an indication of when propellants had entered the chamber under altitude conditions. This was because in all cases ignition was observed well before the oxidizer injector pressure began to rise and in some cases before the fuel injector pressure began to rise with both the doublet and the vortex injectors.

Although both propellants were stored in the test system in low temperature baths to insure liquid condition and low vapor pressure, both propellants vaporized in the manifolds when the propellant valves were opened during simulated altitude tests. Vaporization occurred even when the injector and manifolds were submerged in low temperature baths.

To some extent the degree of vaporization is undoubtedly affected by the propellant feed system design. In this test setup there was approximately 18 inches of tubing between the propellant valves and the injector in order to accommodate the various temperature baths, venturis, and instrumentation lines. This length could be reduced, of course, for a specific application.

In these altitude tests, ignition occurred at discrete points corresponding to the injector orifices, indicating relatively small initial gas flowrates. Combustion was confined to the annulus of the vortex injector or to the injector end of the chamber for a period of 20 to 40 msec before flowrates were high enough to fill the chamber. When liquid propellants did enter the chamber, the transition to steady state was smooth with no chamber pressure peaks. In the three tests (25, 26, 27) in which the propellants were intentionally injected as gases, the entire chamber became illuminated within 0.17 msec — the time between frames of the Fastax camera at 6000 frames/sec.

In summary, altitude ignitions occurred in the gas phase due to low ambient pressure regardless of system temperatures. Although exact ignition delays could not be ascertained because the entry of the gases into the chamber could not be detected, ignition delays were small. Contrary to the sea level tests, the type of injector had no significant effect on ignition characteristics under altitude conditions.

(6) Conclusions - Based on the results of the ignition test program, the following conclusions can be drawn:

- The propellant combination oxygen difluoride/diborane is reliably hypergolic over the simulated altitude range investigated from sea level to 87,000 ft.

- Ignition occurred in the gas phase in simulated altitude tests. Ignition delays were short and chamber pressure rise smooth.

- Chamber and injector configurations had little effect on ignition characteristics at altitude. Propellant system variations, such as temperature, moderate propellant leads and lags, mixture ratio, etc., also had little effect on ignition characteristics. However, the length of the propellant manifolds between the valves and the injector should be minimized to minimize vaporization and the time required to fill the manifolds.

- The injector design has a significant effect on ignition delay at sea level. The delays with the vortex injectors were significantly less than with the doublet injector. Good liquid phase mixing is required for minimum ignition delay.

c. OF_2 Heat Transfer

(1) Objectives - The objective of this effort was the determination of the liquid side heat transfer coefficients and upper limit of nucleate boiling of OF_2. A sharp change in the coefficient occurs when the upper limit of nucleate boiling is reached since the state of the boundary film changes from liquid phase to two phase (liquid with nucleation) to gaseous. This point, therefore, represents the useful upper limit of the propellant as a coolant and defines the burnout flux.

(2) Test Apparatus - The apparatus used to conduct this investigation was assembled and tested with liquid N_2 under Contract NAS-w-449. It is shown schematically in Figure 21. Essentially, it consists of a storage and receiving tank connected by a piping system containing the necessary valving and instrumentation (Figure 22). The storage and receiving tanks are immersed in a bath of liquid nitrogen to keep the OF_2 in the liquid state. Inserted in the flow line is a section of electrically heated thin-walled tubing.

The heat flux rejected to the OF_2 in this section can be calculated from the known output of the electrical power source. The outer wall temperature of the tube is measured by thermocouples and the inner wall temperature is obtained by subtracting the temperature drop through the wall, calculated from the known tube geometry and material properties and the heat input. The bulk temperature of the OF_2 is obtained by averaging the OF_2 inlet and outlet temperatures. The heat transfer coefficient of the film can then be calculated from the difference in temperatures and the heat input.

(3) Test Procedure - Propellant was flowed through the test section while simultaneously applying heat. The heat, supplied as electrical energy from a DC welder, was applied to the test section after propellant temperature at the inlet to the test section had stabilized. Tank size limited run durations to a maximum of 45 seconds at a velocity of 30 ft/sec. Several heat input levels were attempted in each run (by changing welder output) on the initial tests; however, because of the short run duration, only one level of heat input per run was made on subsequent tests to insure stable operating conditions and equilibrium temperatures.

(4) Test Results - Seven heat transfer tests were made with OF_2. These tests were made with the OF_2 flowing through the test section at a nominal velocity of 30 ft/sec at approximately 150 psia outlet pressure.

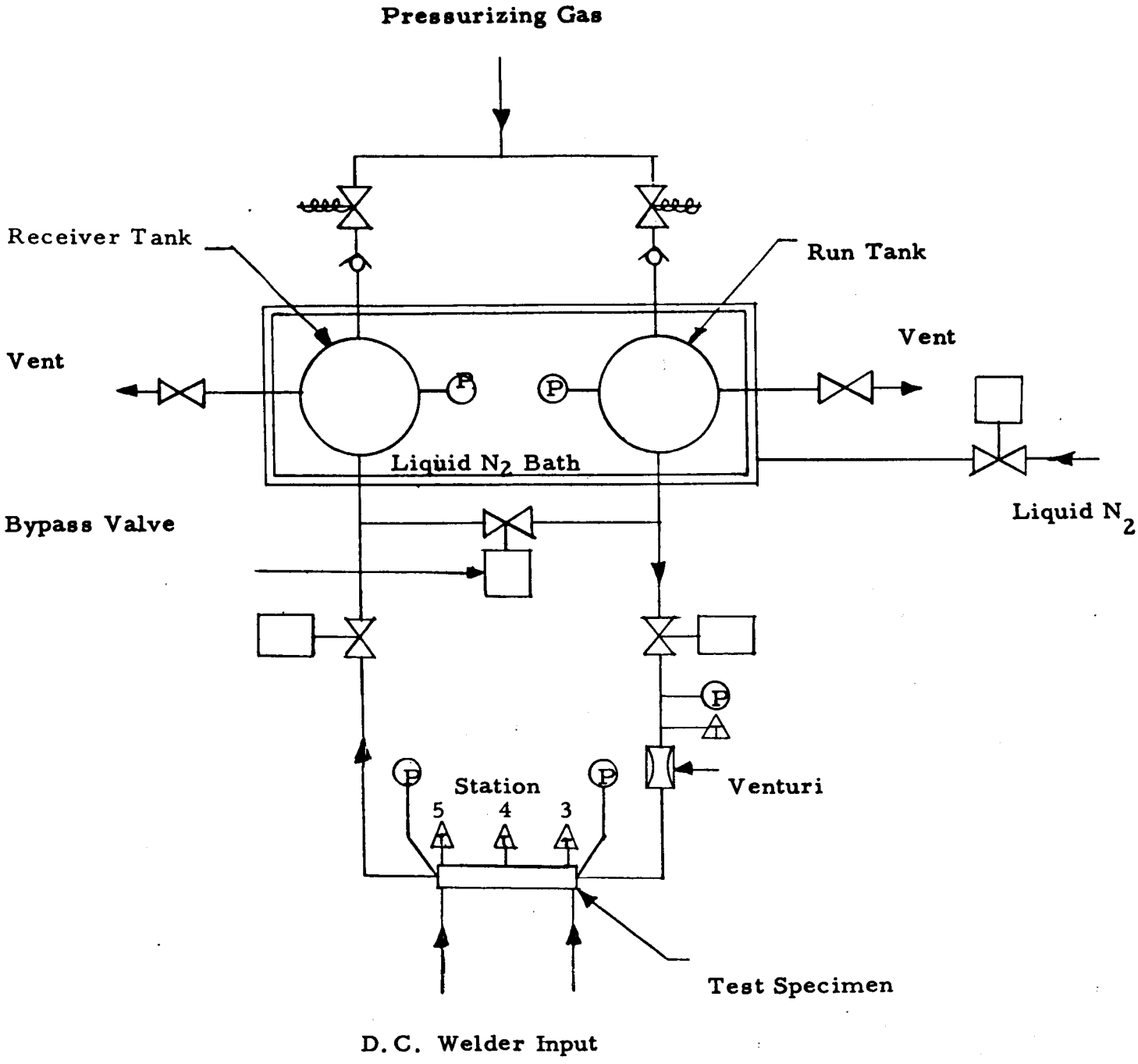

Figure 21. Schematic Heated Tube Test Apparatus

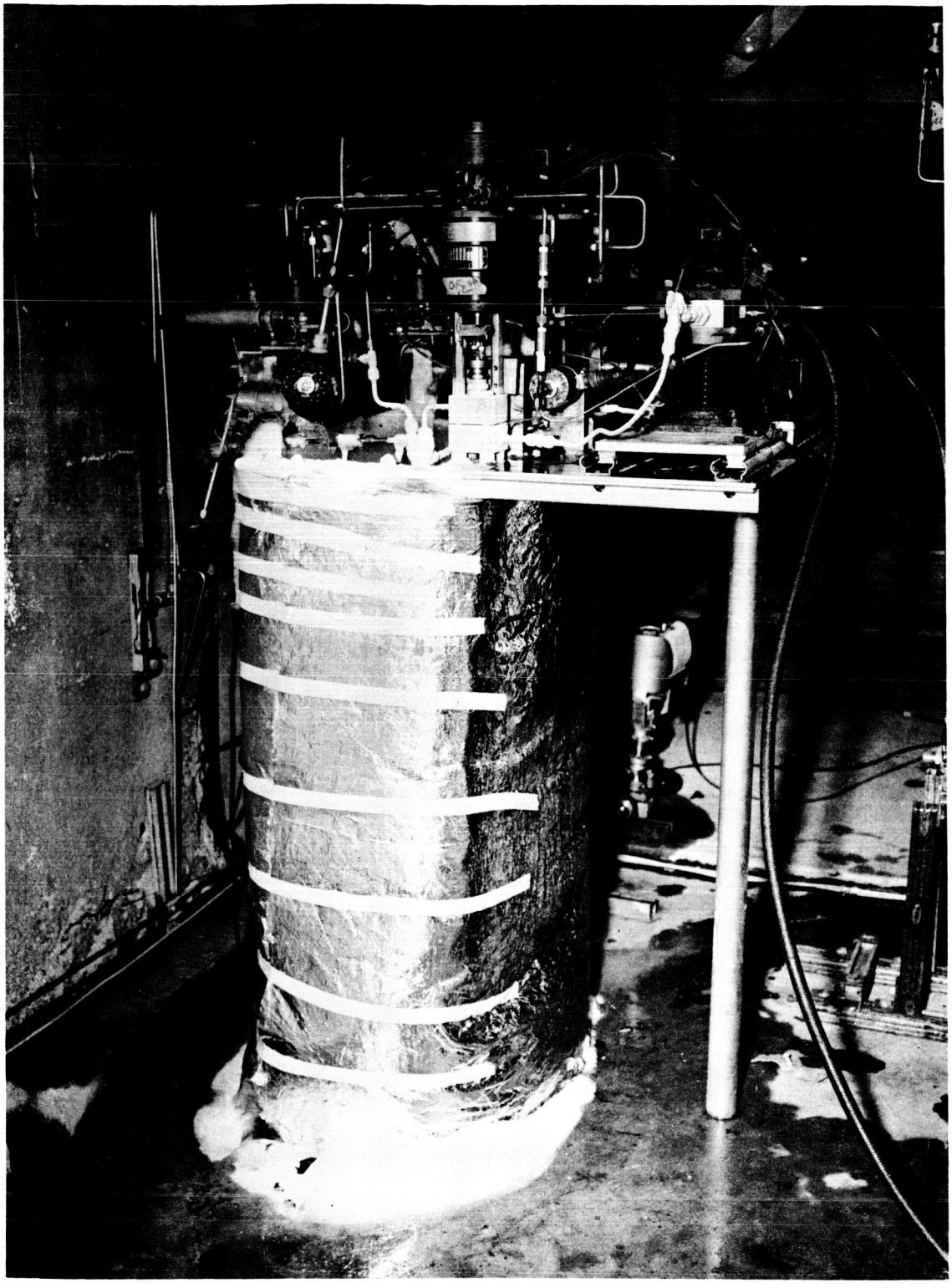

Figure 22. Heated Tube Heat Transfer Test Setup

5507-4

Review and analysis of the test data indicated an imbalance in the test section energy input and output. Voltage-current data consistently indicated higher energy inputs than the OF_2 bulk temperature rise would confirm. Further analysis indicated that the apparent test data error was caused by a parallel current path not uncovered, although specifically checked for, during test stand checkout and operation. This inconsistency is substantiated by a comparison of the test section measured resistance with that calculated from the voltage-amperage data. Using the measured resistance of the test section, it appears that the maximum power passed into the test section during the OF_2 tests was only 60 percent of that based on welder output (volts x amps). Unfortunately, the limited scope of the heat transfer effort on this contract precluded rerunning the test under more closely controlled conditions.

The maximum heat flux that could have been obtained during these tests (based on the measured resistance of the test section) is 1.11 Btu/sec-in^2. Theoretical calculations predict a burnout flux of 1.6 Btu/sec-in^2 for the test conditions.

Additional experimentation under more closely controlled test conditions and more reliable data measurements are necessary to determine OF_2 burnout flux levels.

B. TASK II - INJECTOR EVALUATION, 2000 LB - SPACE THRUST LEVEL

1. Objectives

The objective of Task II was the evaluation of four injector configurations, three of which were previously evaluated at the 150 lb thrust level, in order to provide comparisons of performance, durability and heat transfer at the 2000 pound space thrust level. Injector evaluations were made on the basis of characteristic velocity, sea level thrust coefficient and specific impulse, and also included investigations of streaking.

2. Test Program

Twenty-five test firings were conducted to obtain the data required to meet the Task II objectives. These were divided as follows:

Injector	Firings
Mid-Diameter Vortex	6
Modified Mid-Diameter Vortex	5
Full Diameter Vortex	5
Coaxial Showerhead	6
Multiple Doublet	3

As originally planned, each injector was to be subjected to five performance tests (over a selected O/F range) followed by a 20 second duration firing to generate heat transfer data.

Primary emphasis was placed on the performance evaluations since injector fabrication and durability problems were encountered early in the program. The heat transfer tests were rescheduled for the end of the program; satisfactory injector fabrication techniques were developed and a 19.3 second duration firing was accomplished with the mid-diameter vortex injector.

Performance and streaking data were obtained for all four injector configurations. Water cooled heat transfer data were obtained only with the mid-diameter vortex injector. One test conducted with the full diameter vortex injector was terminated by an injector braze joint failure and no useful heat transfer data were obtained. No heat transfer firings were attempted with the doublet injector, since the poor performance ($\leq$80% c*) of this configuration would not have yielded useful data; modifications to incorporate a dual oxidizer

inlet manifold in the coaxial showerhead injector could not be completed in sufficient time to allow running heat transfer firings within the limits of this program.

3. Test Hardware

a. Injectors

Four injector types designed for the 2000 lb space thrust level were tested at sea level to determine the attainable level of performance: a coaxial showerhead, an impinging stream doublet, a mid-diameter vortex, and a full diameter vortex. The designs of the vortex injectors and the doublet injector were based on those evaluated on the prior contract (NAS-w-449). These injectors were designed on the basis of previously established parameters. No attempt to optimize 2K injector performance was made. It is expected that a three or four percent increase in performance could be attained through injector optimization, particularly with vortex injectors. The coaxial showerhead injector configuration (the only injector design not evaluated previously) was selected after an extensive survey of injector types. A summary of the injector hardware used in Task II is given in Table IX.

(1) Mid-Diameter Vortex Injector - The mid-diameter vortex (Figure 23) is so named because the fuel injector is smaller than the chamber barrel. Fuel is injected tangentially in a characteristic swirling pattern and oxidizer is injected radially into the fuel. As in the case of the doublet, the design was a scaled-up propellant-cooled version of the heat sink hardware used in the feasibility demonstrations.

During the course of the program, the original oxidizer spud design was changed to shorten the axial length of the spud, thus reducing the exposed gas side area (Figure 24) to enhance durability. Because of this shortening, it was necessary to use a single row of enlarged injector orifices, rather than the double row of smaller orifices called for in the original design.

(2) Full Diameter Vortex Injector – In this case, the fuel injector inner diameter is the same as the inner diameter of the chamber barrel (Figure 25). This design was also a propellant-cooled scale-up of the heat sink hardware used earlier. The design concepts of the mid- and full diameter vortex injectors are similar.

TABLE IX

TASK II - INJECTOR CONFIGURATIONS

Injector Designation	S/N	Combustion - Side Materials	Method of Assembly	Run No.	Accumulated Run Time (sec)
Mid-Diameter Vortex, Fuel	1	Cr-Cu	Mechanical Seal, Teflon O-rings	6CX1445	0.35
				6CX1446	0.60
				6CX1450	2.75
				6CX1451	2.77
				6CX1452	2.75
				6CX1453	10.10
				6CX1455	1.74
				6CX1456	19.30
					40.36
Mid-Diameter Vortex, Fuel	2	"A" Nickel	Welded	6CX1447	0.80
				6CX1448	2.28
				6CX1449	2.53
					5.61
Mid-Diameter Vortex, Oxidizer	1	"A" Nickel	Welded	6CX1445	0.35
				6CX1446	0.60
					0.95
Mid-Diameter Vortex, Oxidizer	2	"A" Nickel	Welded	6CX1447	0.80
				6CX1448	2.28
				6CX1449	2.53
					5.61
Mid-Diameter Vortex, Oxidizer	3	"A" Nickel	Welded	6CX1450	2.75
Mid-Diameter Vortex, Oxidizer	4	"A" Nickel	Welded	6CX1451	2.77
				6CX1452	2.75
				6CX1453	10.10
					15.62
Mid-Diameter Vortex, Oxidizer	5	Cr-Cu	Lithobraze 925	6CX1455	1.74
				6CX1456	19.30
					21.04
Full Diameter Vortex, Fuel	1	"A" Nickel	Welded	6CX1454	1.08
				6CX1464	1.68
				6CX1465	1.65
				6CX1466	1.67
				6CX1467	2.12
					8.20
Full Diameter Vortex, Oxidizer	1	"A" Nickel	Welded	6CX1454	1.08
Full Diameter Vortex, Oxidizer	2	Cr-Cu	Lithobraze 925	6CX1464	1.68
				6CX1465	1.65
				6CX1466	1.67
				6CX1467	2.12
					7.12
Coaxial Showerhead, Oxidizer	1	Cr-Cu, Zirconia coated face	Mechanical, Al gasket	6CX1457	1.78
				6CX1458	1.74
				6CX1459	1.78
	1	(Dual Inlet)	Mechanical, Al gasket	6CX1468	1.90
				6CX1469	2.65
				6CX1470	2.61
					12.46
Coaxial Showerhead, Fuel	1	321 SS	Mechanical, Al gasket	6CX1457	1.78
				6CX1458	1.74
	2	321 SS	Mechanical, Al gasket	6CX1459	1.78
Installed New Fuel Pin on S/N 1 and Modification for Dual Ox Inlet	2	321 SS	Mechanical, Al gasket	6CX1468	1.90
				6CX1469	2.65
				6CX1470	2.61
					12.46
Multiple Doublet, Fuel and Oxidizer	1	"A" Nickel Zirconia coated face	Welded	6CX1461	1.75
				6CX1462	1.72
				6CX1463	1.71
					5.18

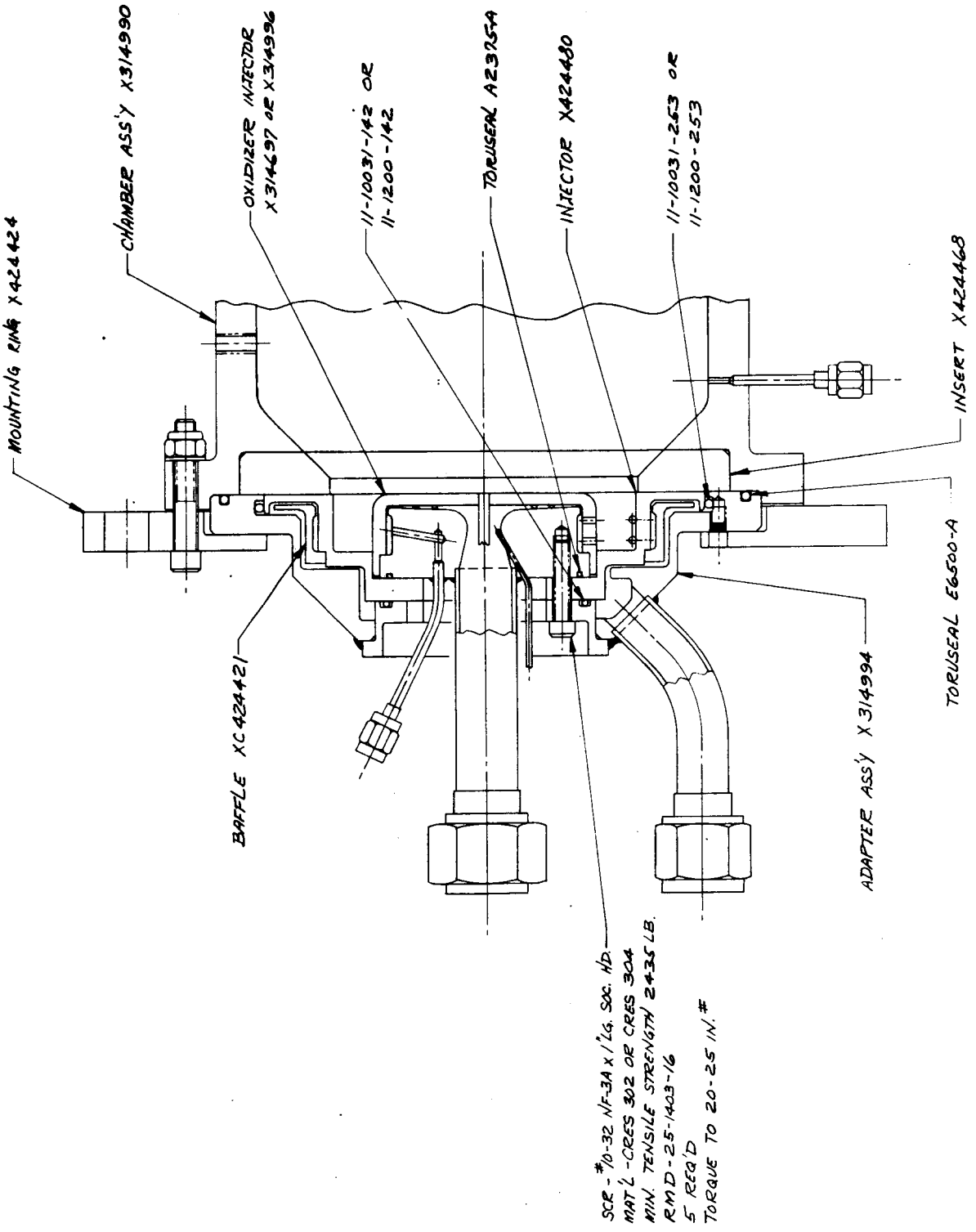

Dwg X315005

Figure 23. Mid-Diameter Vortex Injector Assembly

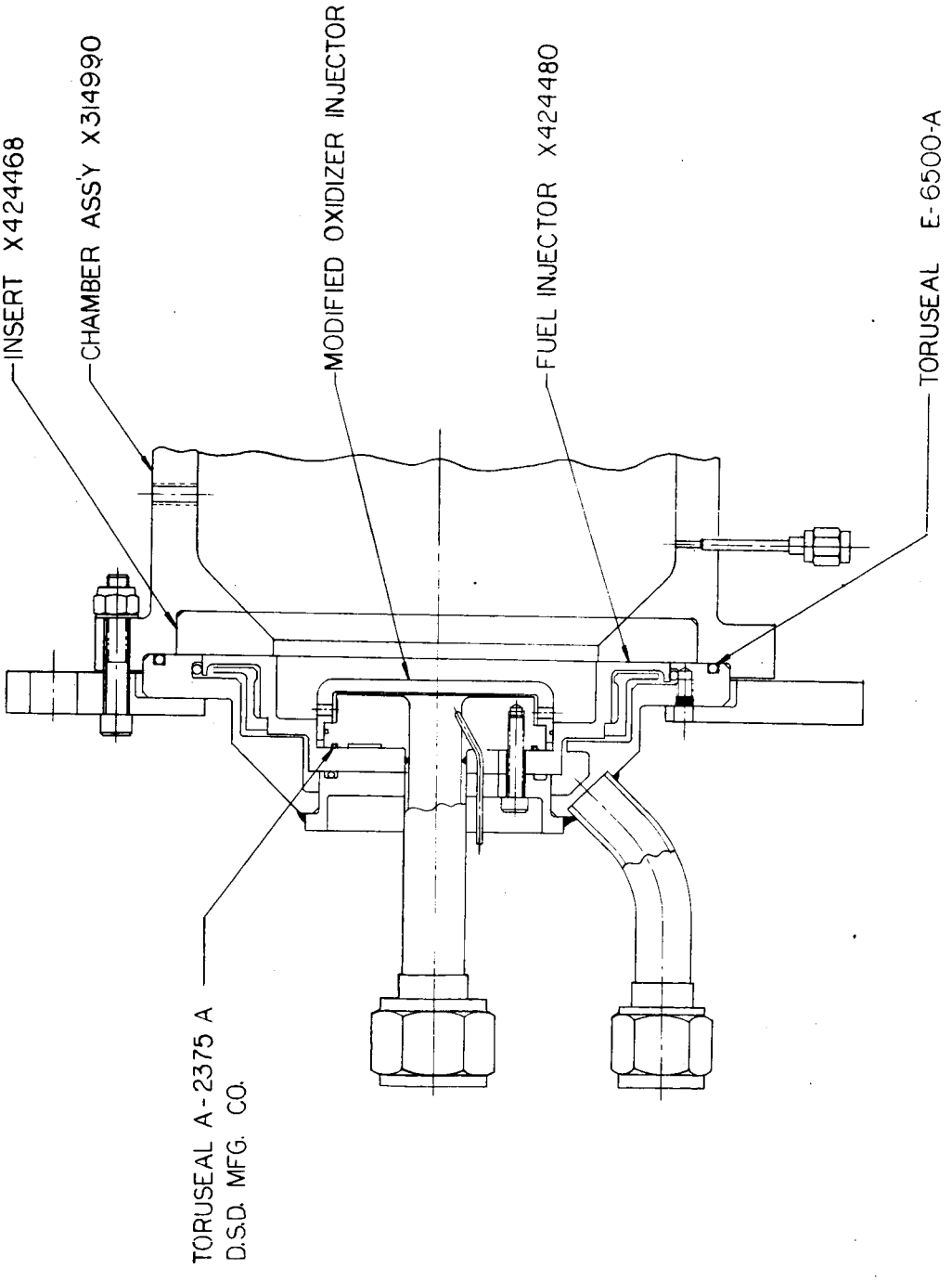

Figure 24. Modified Mid-Diameter Vortex 2K Injector Dwg 53978

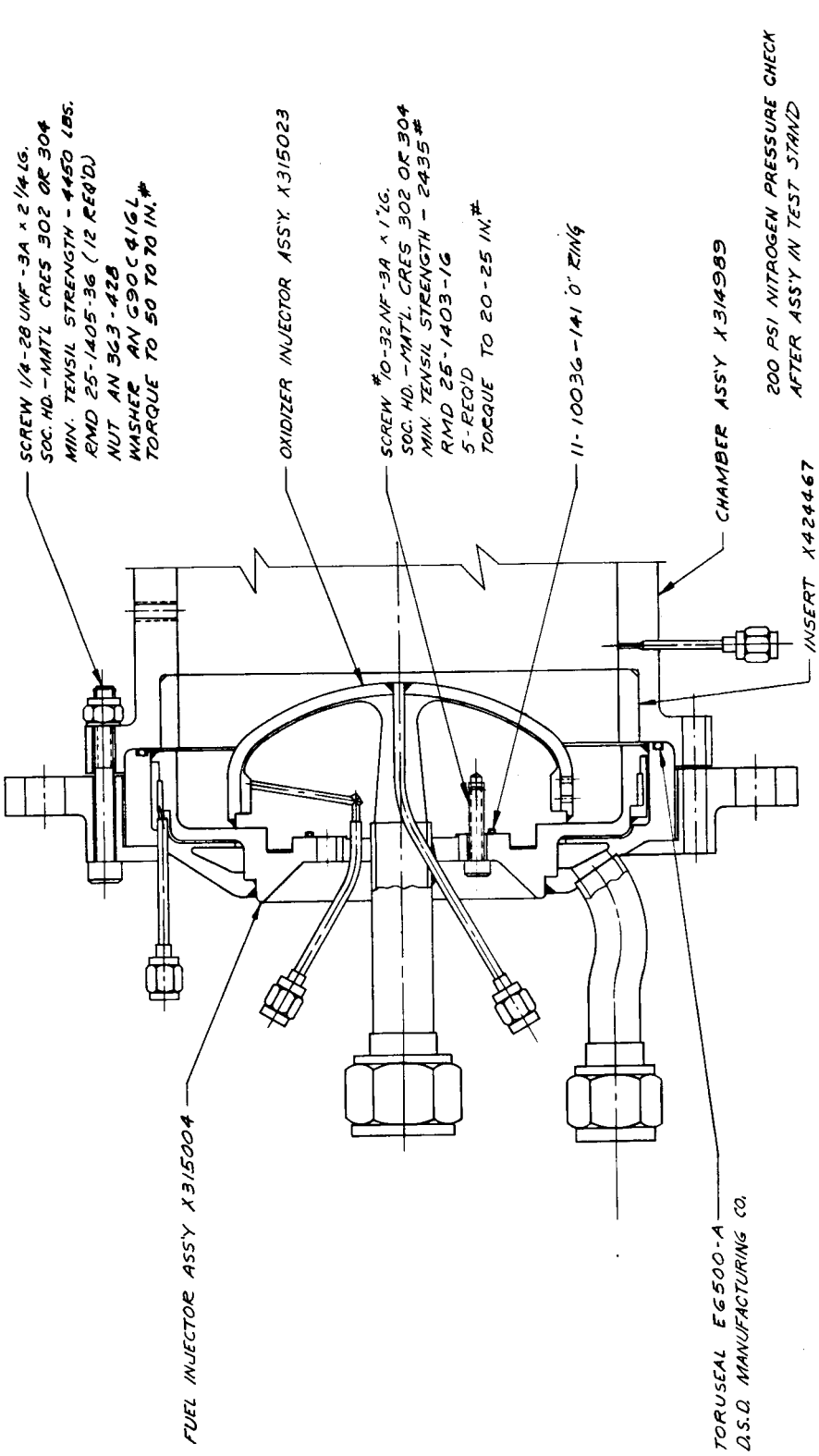

Figure 25. Full Diameter Vortex Injector Assembly

Dwg X315363

During the course of the program, the original oxidizer spud design was changed to incorporate a flat plate chromium-copper face (Figure 26) as a substitute for the original elliptical "A" nickel face to improve injector durability. The injection pattern, however, remained unchanged.

(3) Doublet Injector – The multiple-doublet impinging stream injector (Figure 27) consists of 32 doublet pairs arranged circumferentially at diameters of 2.500 inches (fuel) and 2.925 inches (oxidizer). The fuel is injected axially and the oxidizer streams intersect the fuel streams at an angle of 45 degrees. The orifices were sized to produce an oxidizer velocity of 50 feet per second and a fuel velocity of 65 feet per second.

This injector design is a propellant-cooled scaleup of the heat sink doublet used in the feasibility demonstration conducted under Contract NAS-w-449.

(4) Coaxial Showerhead – The coaxial showerhead injector is shown in Figure 28. This injector type was chosen because NASA-Lewis RC test experience indicated that high performance could be attained over a wide O/F range with such high temperature, high performance propellant combinations as F_2/H_2.

The injector has 27 injection elements. Each element consists of a central 0.064 in. fuel orifice and a concentric annular oxidizer orifice (0.013 in. annular gap). Experience with this type of injector with hydrogen fuel has shown that a large number of elements (approximately 6/in.^{2}) is necessary to obtain maximum performance (NASA Report TMX-485). However, the number of elements was minimized in this case (1.1/in.^{2}) to reduce the critical fabrication tolerance problems inherent in the smaller orifices associated with the comparatively (compared to liquid H_2) high density fuel.

The injector face is OF_2 cooled; diborane cooling did not appear feasible. To facilitate design evaluation by minimization of fabrication problems, cooling passage gaps of 0.018 in. - 0.020 in. were employed. Since this gap results in oxidizer velocities insufficient for cooling during steady-state operation, the injector face was coated with zirconia and protected with a graphite cloth-phenolic ablative cap.

During the course of the program, the original design was changed to incorporate a dual oxidizer inlet manifold in place of a single inlet to increase injector durability.

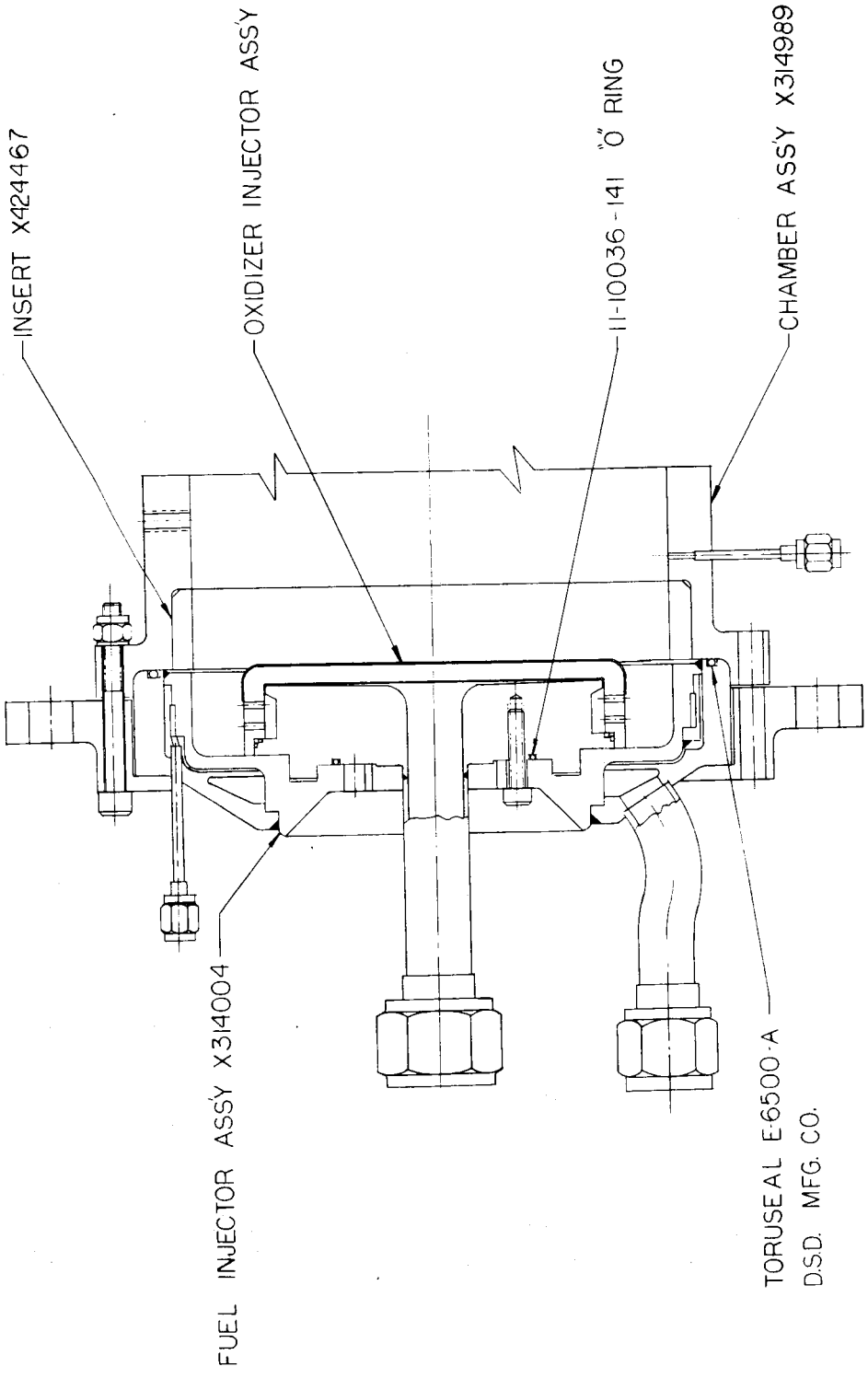

Figure 26. Modified Full Diameter Vortex 2K Injector Dwg 53979

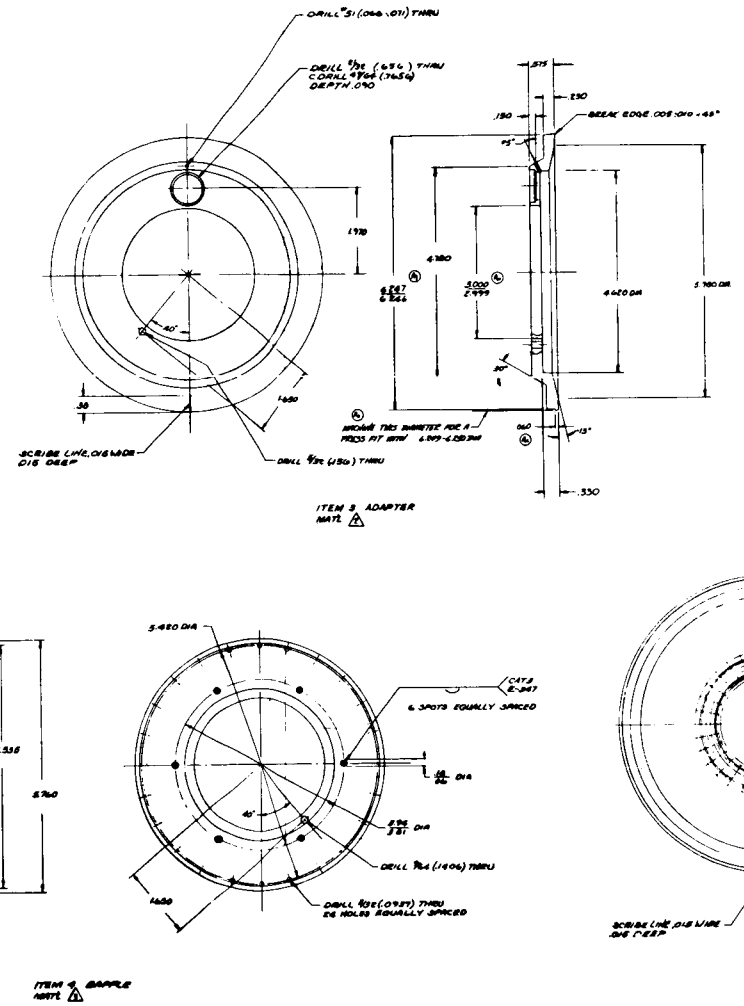

Figure 27. Impinging Stream Doublet Injector Dwg 53006

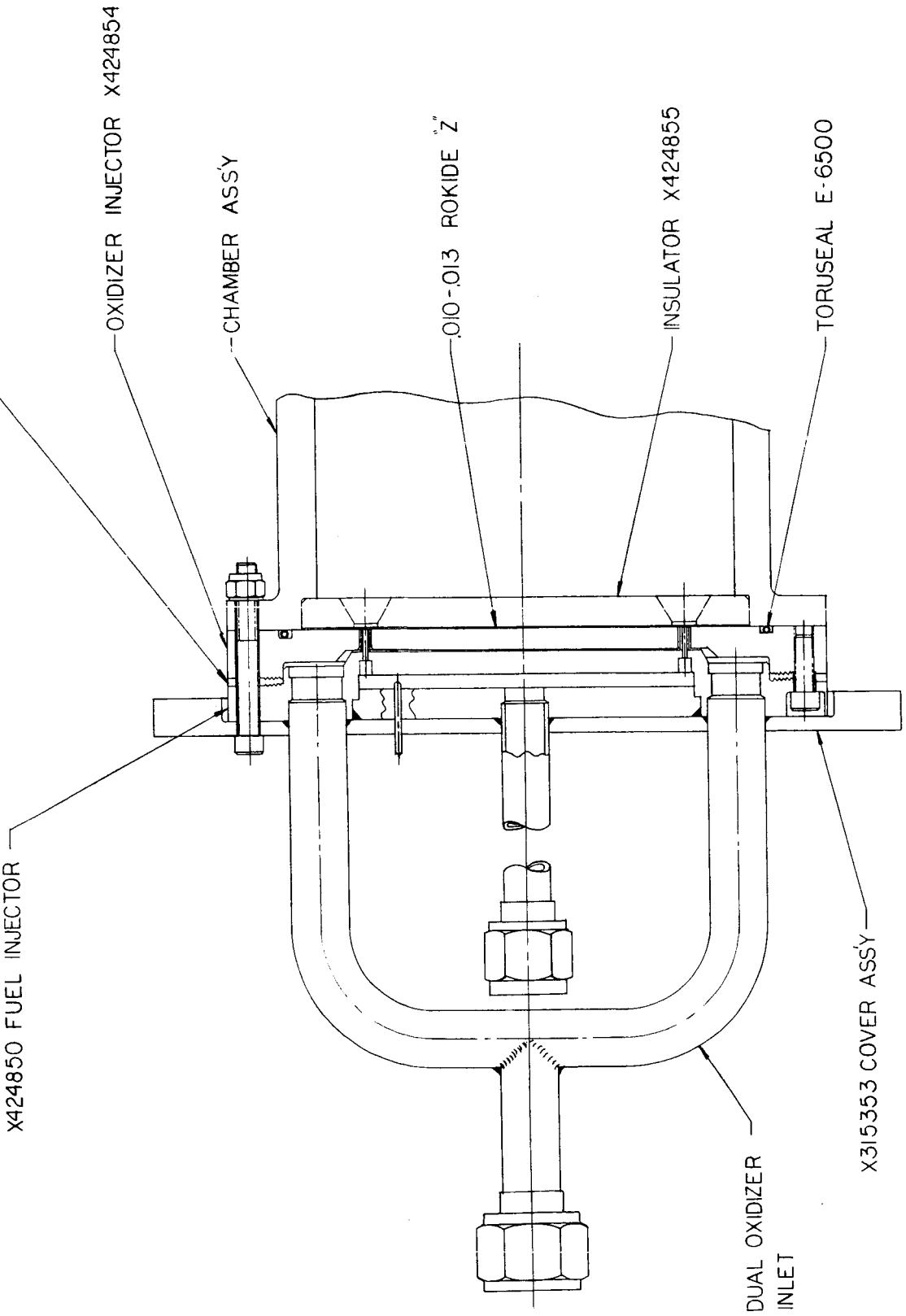

Dwg 53977

Figure 28. Coaxial Showerhead 2K Injector

b. Thrust Chambers

Two types of thrust chamber assemblies were used in the injector test program. A copper heat-sink type chamber and nozzle assembly was used for injector performance and streaking evaluations, while an instrumented water-cooled chamber and nozzle assembly was used for heat transfer evaluation tests. The chamber assemblies were designed to operate at 150 psia at sea level. Significant chamber parameters were $L^* = 30$, $A_c/A_t = 2.75$, and $\varepsilon = 2.17$.

(1) Uncooled Heat-Sink Thrust Chamber - The uncooled heat-sink chamber and nozzle are shown in Figure 29. The design accommodated ablative inserts at both the injector end of the chamber and at the entrance to the nozzle. Sacrificial ablative inserts were used to determine the streaking characteristics of each injector during the short duration performance tests.

(2) Water-Cooled Thrust Chamber - The water-cooled thrust chamber assembly is shown in Figure 30. The combustion chamber barrel (Figure 31) consisted of 54 flattened 1/4 inch stainless steel tubes welded together to form the gas side wall of the combustion chamber as well as the chamber coolant passages. Water entered at the injector end of the chamber and exited at the nozzle end at a design flowrate of 10 pounds per second. The water-cooled nozzle (Figure 32) was a single-pass, mechanically sealed assembly with dual inlets and outlets. An average coolant velocity of 45 feet per second was provided at the throat plane.

Water temperatures were measured at the outlet of each cooled section. Inlet temperatures were measured at the common manifold from which each inlet was fed. Water flowrates for each section were controlled by orifices and cavitating venturis in the water lines.

4. Test Results

a. Performance and Streaking

Twenty-one tests were conducted with the 2000 lb space thrust uncooled hardware to evaluate injector performance and streaking characteristics. Performance data were also obtained from four heat transfer tests conducted with the water-cooled thrust chamber assembly. The nominal chamber pressure level was 110 psia. Tests were conducted over a mixture ratio range of 3.0 to 4.16. Sacrificial paper-phenolic inserts in the combustion chamber were used to assess injector streaking.

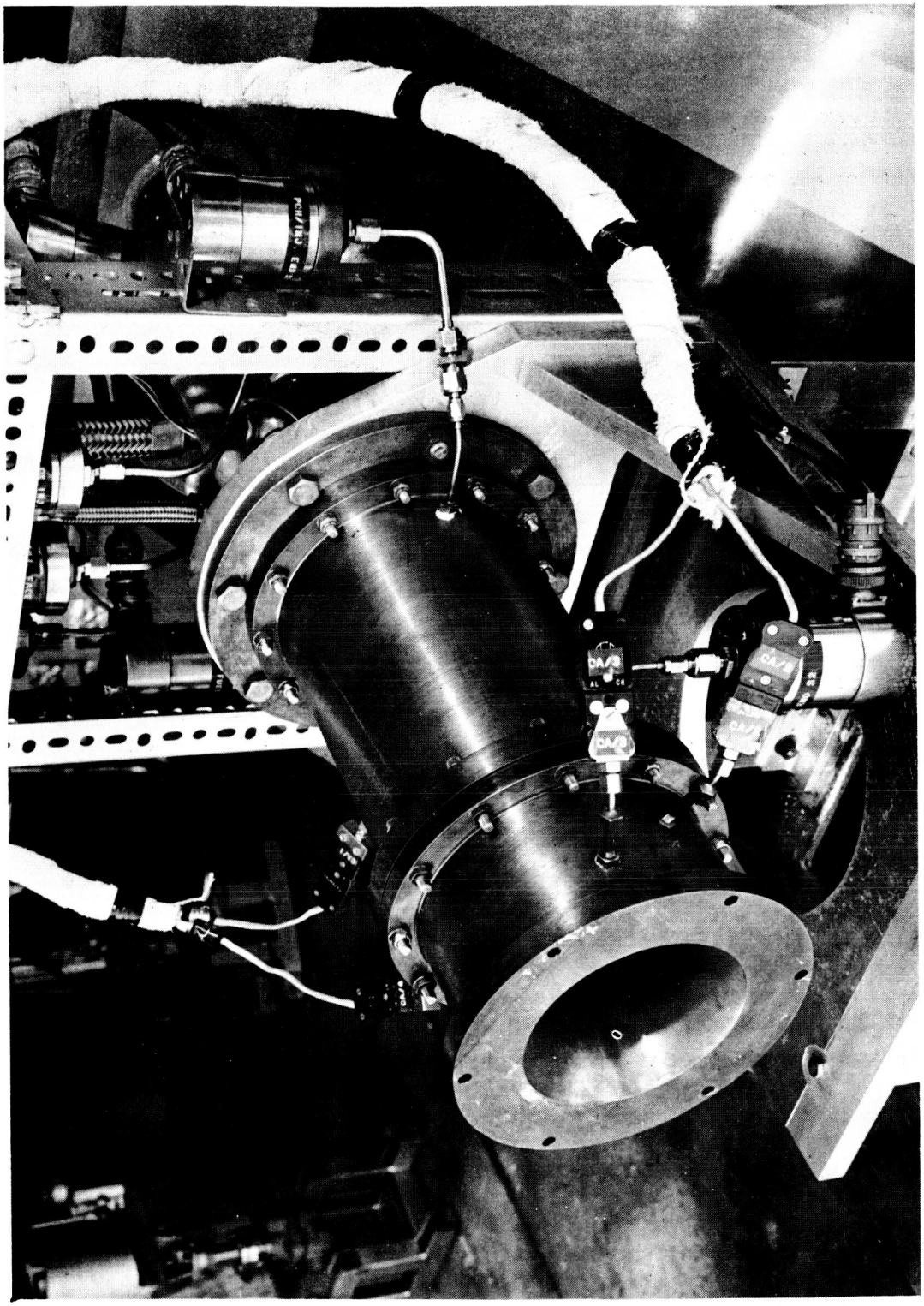

6028-122

Figure 29. 2K Thrust Chamber Assembly, X315005

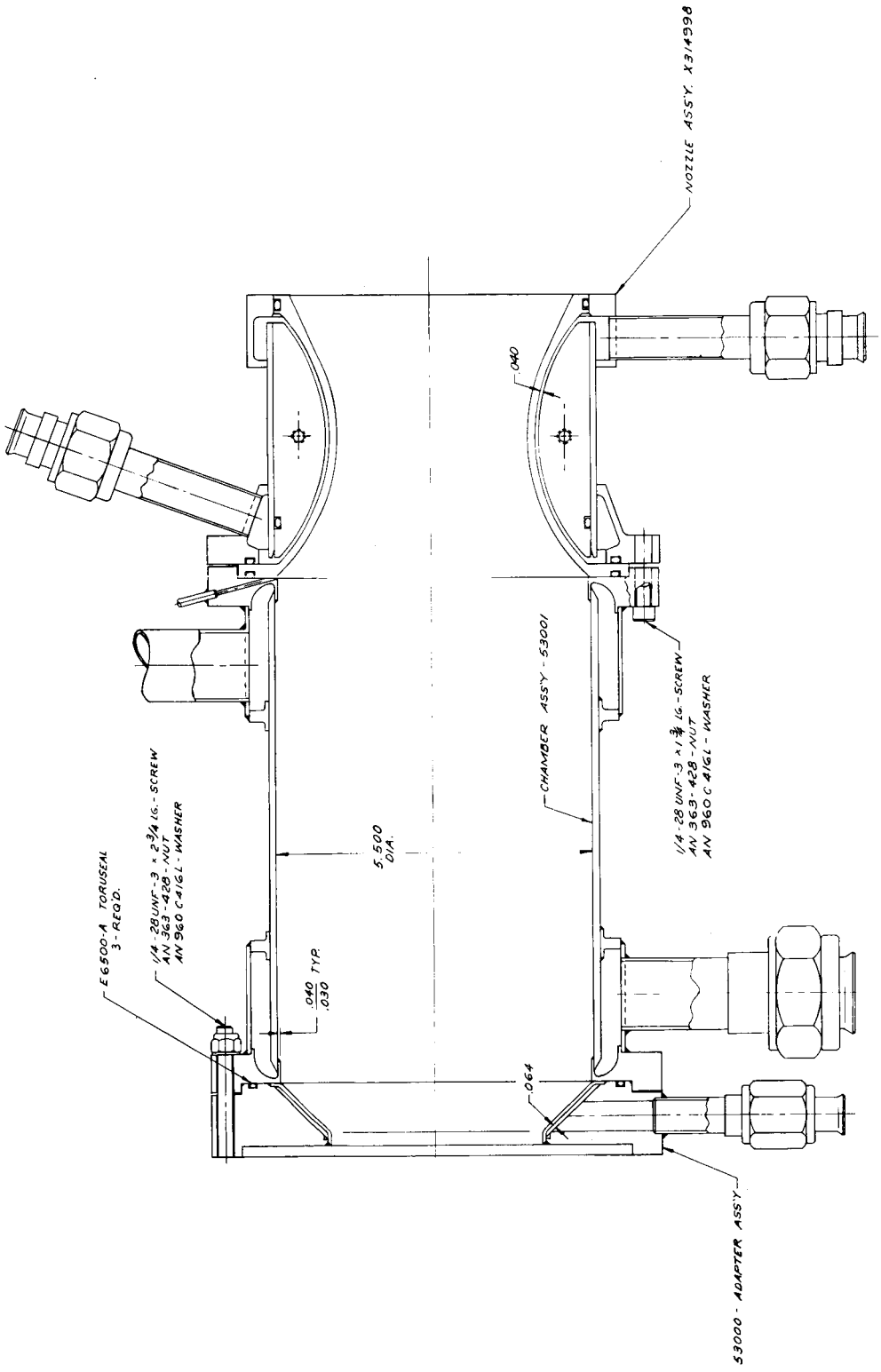

Dwg X315003

Figure 30. Water Cooled Chamber Layout

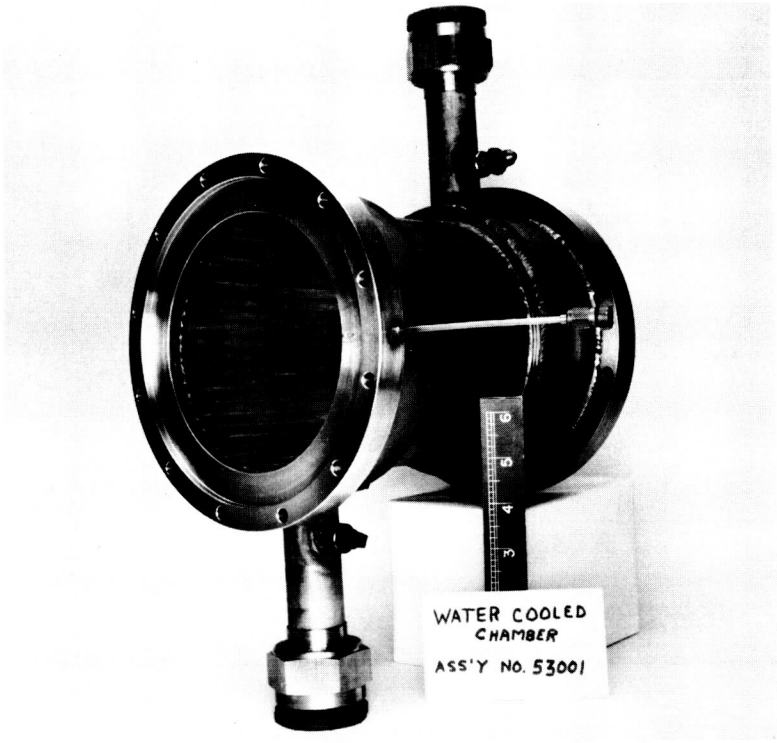

6028-219

Figure 31. Water-Cooled Chamber Assembly, 53001

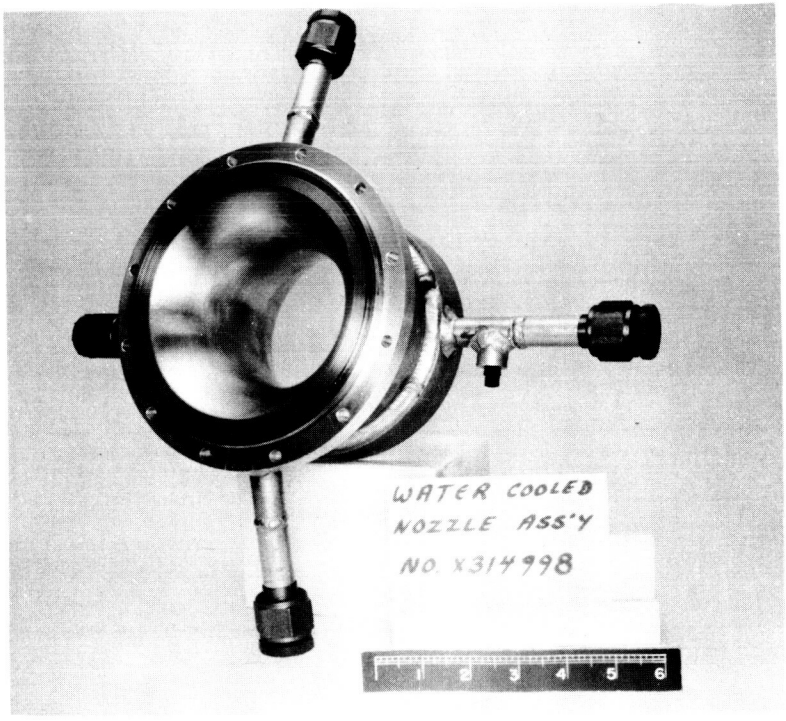

6028-222

Figure 32. Water-Cooled Nozzle Assembly, X314998

The Task II test data are summarized in Table X. The performance data presented were obtained at 0.5 to 1.0 seconds after attainment of 100% chamber pressure. The vortex injectors gave the highest performance (92.5-100% c*), the coaxial injector gave moderately high performance (93-94.5% c*) and the multiple-doublet gave very poor performance (78-80.9% c*). Injector streaking was not evident in any of these tests. Since streaking is a strong function of the combustion performance level (c*),it is especially significant that none occurred in the high performance runs made with the vortex injectors. Photographs of the injector streaking evaluation sacrificial inserts are presented in Appendix A.

The injector performance ratings are based on characteristic velocity and sea level thrust coefficient and specific impulse. The theoretical characteristic velocity is based on shifting equilibrium (Appendix C). The specific impulse and thrust coefficient data presented in the summary plot are interpreted in terms of the maximum achievable sea level performance ($I_{sp\,map}$ and $C_{F\,map}$) for the nozzle geometry used and the recorded test conditions. The equations used for these performance calculations are presented in detail in Appendix C.

Since the nozzle exit divergence angle for the water-cooled thrust chamber assembly (25^{o}) was less than that of the uncooled heat-sink thrust chamber (38^{o}) due to design considerations, slightly higher (6%) predicted maximum achievable thrust coefficient and specific impulse were attainable with the water-cooled chamber. The performance data (c* and I_{sp}) from the tests conducted with the water-cooled thrust chamber assembly were corrected for heat losses (Appendix C).

The OF_2/B_2H_6 propellant combination has consistently delivered high percentages of maximum achievable equilibrium sea level specific impulse. Allowing for the divergence losses (11%) of the sharply truncated test nozzles, approximately 99% of equilibrium impulse was obtained. The test nozzle design was based on a 40:1 contoured nozzle, truncated at an ξ of 2.17 to produce optimum sea level expansion. This provided a nozzle divergence angle of 38^{o} with the heat-sink nozzle and 25^{o} with the water-cooled nozzle.

A statistical data analysis of the experimental performance data (c* and I_{sp}) was performed for each injector. A summary of the statistical analysis is presented in Table XI, giving the standard deviation from the mean value for a 68% confidence level ($\pm\ 1\sigma$), a 95% confidence level ($\pm\ 2\sigma$), and a 99.7% confidence level ($\pm\ 3\sigma$). The agreement of standard deviations between the c* and I_{sp} data is very good. The 3σ standard deviation for each injector is also

ON

TABLE X

TASK II - TEST DATA SUMMARY

Run No.	Chamber Configuration	Injector	P_{ch} (psia)	Thrust (lb)	$\dot{w}_t$ (lb/sec)	Mixture Ratio	Duration[1] (sec)	c* (fps)	% c*	C_F test	$\%C_F$ map	S.L.[5] I_{sp} (sec)	Remarks
6CX1445	Heat Sink Copper	X315005 mid-dia vortex; S/N 1 Cr-Cu fuel spud, "A" Ni ox spud (S/N 1)	---	---	---	---	0.35	---	---	---	---	---	Shutdown during start transient delayed oxidizer entry due to large manifold volume.
6CX1446	Heat Sink Copper	(same as above)	---	---	---	---	0.60	---	---	---	---	---	Ox prop leak overboard led to series of explosions which damaged ox system.
6CX1447	Heat Sink Copper	X315358 mid-dia vortex; "A" Ni spuds	---	---	---	---	0.80	---	---	---	---	---	Increased run timer. Shutdown during start transient; delayed ox entry due to large manifold volume. Reduced ox manifold volume.
6CX1448	Heat Sink Copper	(same as above)	109.7	1010	4.59	3.78	2.28	6600	95.5	1.07	101	220	Good run - slight erosion on fuel and ox spuds.
6CX1449	Heat Sink Copper	(same as above)	114.3	1125	4.652	3.58	2.53	6800	98.2	(2)	(2)	---[2]	Ox and fuel spuds eroded.
6CX1450	Heat Sink Copper	X315005 mid-dia vortex; S/N 1 Cr-Cu fuel spud, S/N 3 "A" Ni ox spud	111[4]	985	4.434	3.54	2.75	6930	100.0	1.033	97.5	222.5	Centerline P_{ch} tube failure at 1.3 secs. - data taken just prior to tube failure.
6CX1451	Heat Sink Copper	mid-dia vortex; S/N 1 Cru-cu fuel spud, mod. "A" Ni ox spud (one row of orifices)	107	1073	4.545	3.11	2.77	6530	94.2	(2)	(2)	---[2]	Good run - slight localized erosion on corner of ox spud at 1:30 - rest of hardware in excellent condition.
6CX1452	Heat Sink Copper	(same as above)	107.7	1000	4.599	3.22	2.75	6490	93.7	1.08	102.2	217.5	Good run - no further ox spud erosion - hardware in excellent condition.

(1) From light off
(2) Pre-run and post-run thrust cal zero shift
(3) Corrected for heat losses
(4) ℄ P_{ch} tap
(5) ζ = 2.17

TABLE X

TASK II - TEST DATA SUMMARY (cont)

Run No.	Chamber Configuration	Injector	P_{ch} (psia)	Thrust (lb)	$\dot{w}_t$ (lb/sec)	Mixture Ratio	Duration[1] (sec)	c* (fps)	% c*	C_F test	%C_F map	S.L.[5] I_{sp} (sec)	Remarks
6CX1453	X315003 H_2O cooled TC Assy.	(same as above)	102.6	990	4.347	3.51	10.10	6730[3]	97.2	1.113	100.5	233[3]	Heat transfer evaluation; ox spud eroded at corner and face at 12:00 to 3:00 - failure occurred at 4 secs.
6CX1454	(same as above)	X315363 full-dia vortex; "A" Ni spuds	113.7	1102	4.723	3.07	1.08	6710[3]	97.0	1.124	98.8	234.5[3]	Programmed for 2 sec run - ox spud explosion at 1.08 - ox spud cap & inlet line blown off - H_2O cooled tube bundle damaged.
6CX1455	Heat Sink Copper	mid-dia vortex; S/N 1 Cr-Cu fuel spud, mod. Cr-Cu ox spud (one row of orifices)	108.5	1001	4.593	3.09	1.74	6545	94.5	1.073	101.9	218	Good run - hardware in excellent condition.
6CX1456	X315003 H_2O Cooled TC Assy.	Mod. mid-dia vortex with Cr-Cu ox & fuel spuds	107.9	990	4.706	3.12	19.3	6400[3]	92.5	1.069	95.0	213[3]	The ox inj cup was ejected at 19 secs. The remainder of the hardware was in good condition.
6CX1457	Heat Sink Copper	53011 coaxial shower head	108.9	1031	4.619	3.04	1.78	6510	94.0	(2)	---	---[2]	Rough start - hardware in good condition - 600 cps P_{ch} oscillation through run.
6CX1458	Heat Sink Copper	(same as above)	111.9	1100	4.740	3.60	1.74	6520	94.2	(2)	---	---[2]	Rough start - fuel pin burned off 180° from ox inlet - 600 cps P_{ch} oscillation through run.
6CX1459	Heat Sink Copper	(same as above)	113.8	1122	4.864	3.52	1.78	6460	93.4	(2)	---	---[2]	Rough start - fuel pin burned off 180° from ox inlet
6CX1461	Heat Sink Copper	X315006 mult. doub.	93.4[4]	800	4.635	3.01	1.75	5600	80.9	0.998	99.4	173	Good run - hdw in good condition
6CX1462	Heat Sink Copper	(same as above)	92.0[4]	772	4.736	3.57	1.72	5390	78.0	0.976	97.6	163.5	(same as above)
6CX1463	Heat Sink Copper	(same as above)	96.6[4]	842	4.81	3.91	1.71	5380	78.0	1.014	99.8	175	(same as above)
6CX1464	Heat Sink Copper	X315363A full-dia vortex Cr-Cu spuds	115.4	1085	4.715	3.05	1.68	6750	97.5	1.095	101.8	230	Good run - hdw in good condition
6CX1465	Heat Sink Copper	(same as above)	115.8	1090	4.611	4.06	1.65	6930	100.5	1.098	102.0	236	(same as above)
6CX1466	Heat Sink Copper	(same as above)	111.9	1028	4.63	3.03	1.67	6690	96.5	1.070	100.4	221.9	(same as above)
6CX1467	X315003 H_2O cooled TC Assy.	(same as above)	108.4	1052	4.68	3.09	2.12	6520[3]	94.3	1.13	100.4	228.5[3]	Chamber barrel burnout at injector flange to tube bundle joint at 1.9 sec - ox cup separated from ox body.
6CX1468	Heat Sink Copper	Mod 53011 coaxial showerhead (dual ox inlet)	107.4	995	4.62	3.07	1.90	6440	93	1.081	102.7	215.5	Rough run - hdw in good condition 600 cps P_{ch} oscillation through run
6CX1469	Heat Sink Copper	(same as above)	115.4	1062	4.898	4.16	2.65	6520	94.6	1.071	99.7	217	(same as above)
6CX1470	Heat Sink Copper	(same as above)	108.5	1002	4.645	3.65	2.61	6460	93.4	1.073	101.9	215.9	(same as above)

(1) From light off
(2) Pre-run and post-run thrust cal zero shift
(3) Corrected for heat losses
(4) ℄ P_{ch} tap
(5) ξ = 2.17

TABLE XI

SUMMARY OF STATISTICAL DATA ANALYSIS

Injector Description	Confidence Level					
	99.7% (3σ)		95.0% (2σ)		68.0% (1σ)	
	I_{sp} (sec)	c* (fps)	I_{sp}	c*	I_{sp}	c*
Mid-Diameter Vortex	nil	±141.6	nil	±94.4	nil	±47.2
Full Diameter Vortex	±6.9	±171.6	±4.6	±114.4	±2.3	±57.2
Coaxial Showerhead	±17.1 (1)	±84.6	±11.4 (1)	±56.4	±5.7 (1)	±28.2
Multiple Doublet	nil	nil	---	---	---	---

(1) Thrust measurement errors due to pre-run and post-run zero shifts for three runs.

shown in the performance plots by means of shaded bars (where large enough to be seen). Detailed discussions of the data acquisition and performance calculations are presented in Appendixes B and C.

(1) Mid-Diameter Vortex Injector – This was the first injector fired in this program. Eleven tests were conducted with the mid-diameter vortex injector. The performance data are shown on Figure 33. The first three tests were terminated during the start transient before rated oxidizer flow to the injector was achieved. The oxidizer manifold volume was reduced and rated oxidizer flow to the injector was attained without difficulty for the remainder of the program.

Three performance tests with the original mid-diameter vortex injector design (two rows of fuel and two rows of oxidizer orifices) yielded high performance (95%, 98.2% and 100% of theoretical c*). Five tests, including two heat transfer tests, were conducted with the modified mid-diameter vortex injector (Figure 24). The performance level of the modified injector averaged 94.4% of theoretical c* over a mixture ratio range of 3.09 to 3.51. The lower performance level with the modified injector is attributed to the fact that one row of oxidizer orifices was employed with two rows of fuel orifices. However, the high performance level demonstrated by the modified mid-diameter vortex injector is encouraging, especially in view of the fact that no attempt was made to redesign the injection pattern.

It is significant to note that no attempt was made to optimize the injection parameters during the program in either case. Past experience has shown that relatively simple design refinements can produce an additional 2-3% increase in performance for this type of injector. The performance levels obtained with the mid-diameter vortex injector corroborated the higher performance levels obtained on the prior contract (NAS-w-449).

The test data also yielded good corroboration between the predicted and experimental C_F. Thus, a high level of confidence in the validity of the performance data was established.

(2) Full Diameter Vortex Injector – Five tests, including two with water-cooled chambers, were conducted with the full diameter vortex injector. The performance data are shown on Figure 34. The performance level of this injector was consistently high (averaging 97.1% of theoretical c*) over a mixture ratio range of 3.03 to 4.06. Again, no attempt was made to optimize

Original Design 6028-226

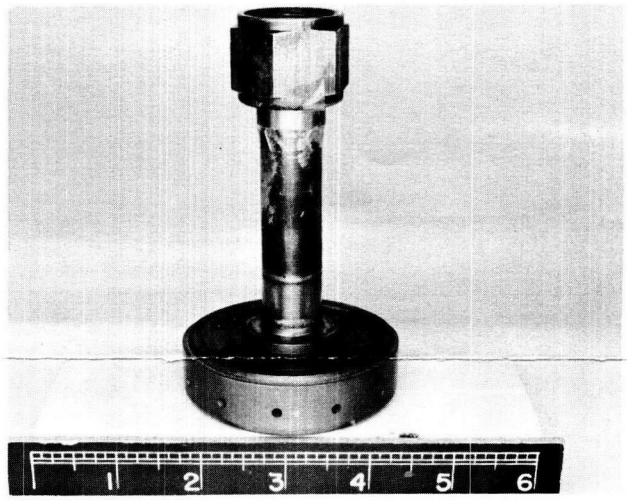

Modified Oxidizer Injector 6028-330

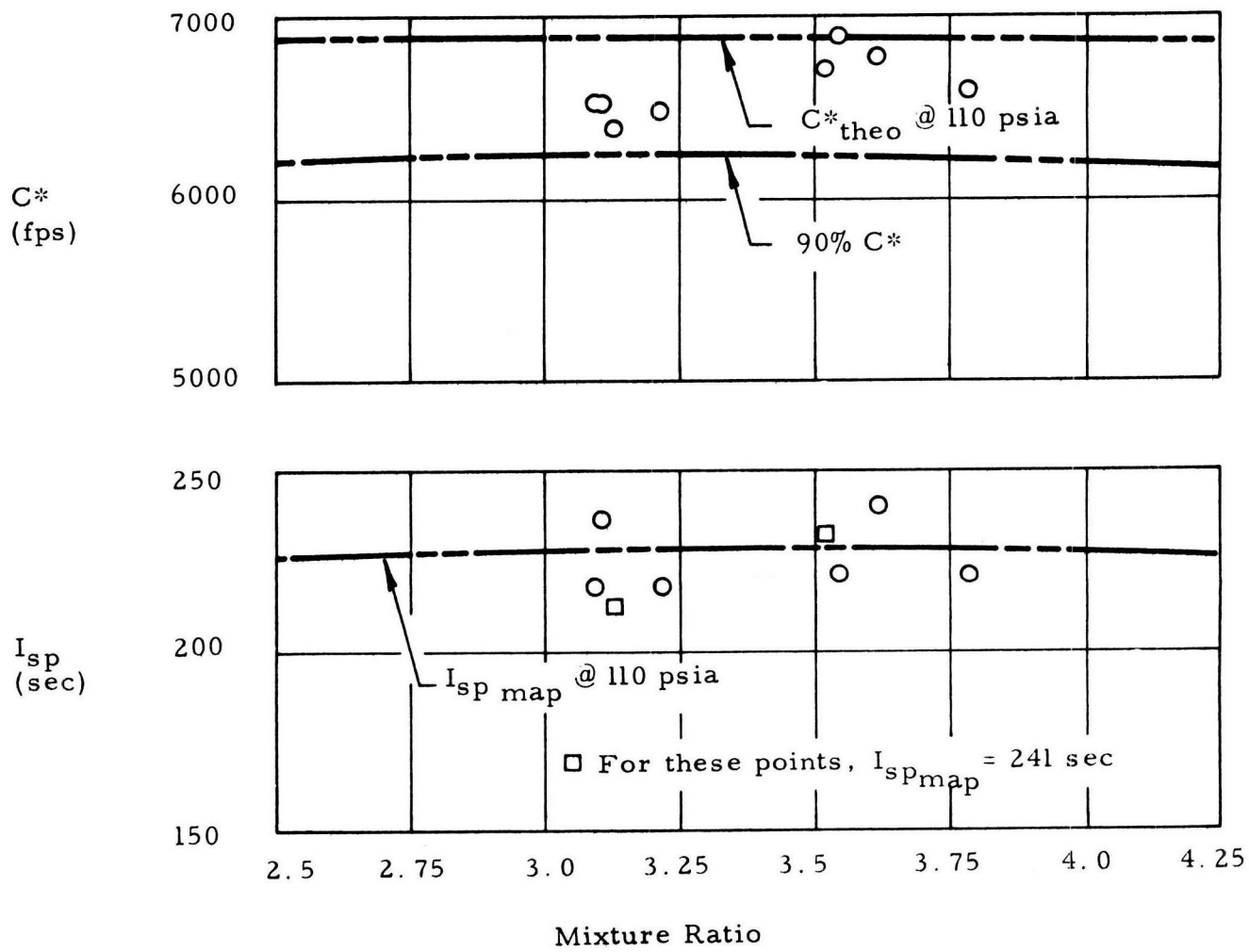

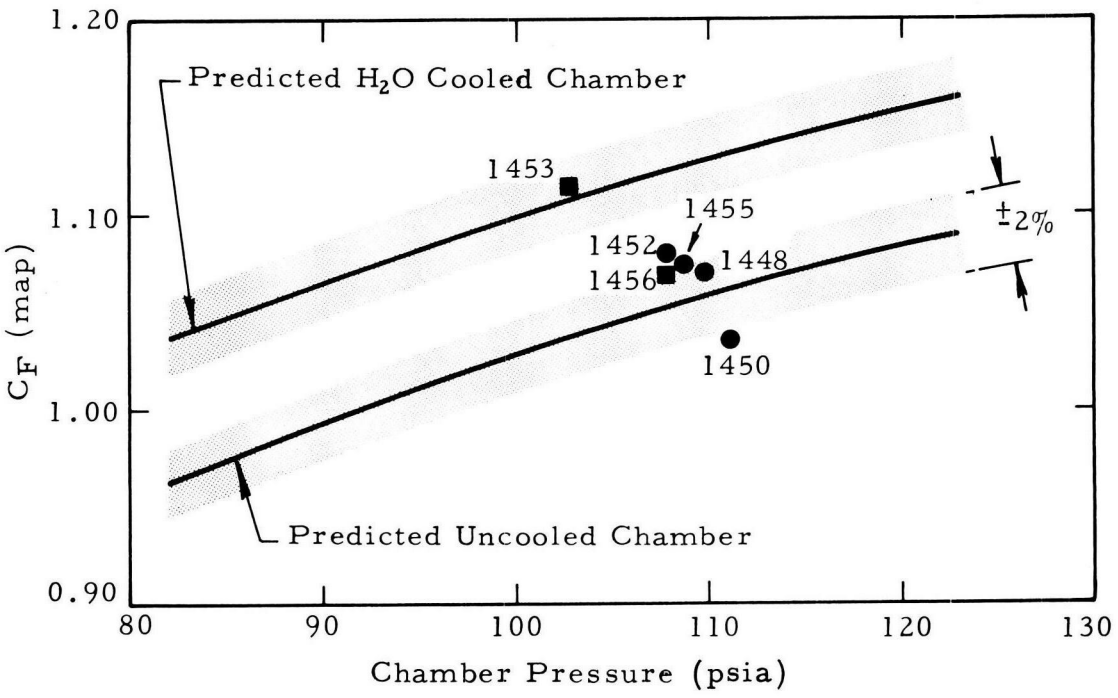

Figure 33. Mid-Diameter Vortex Injector Performance

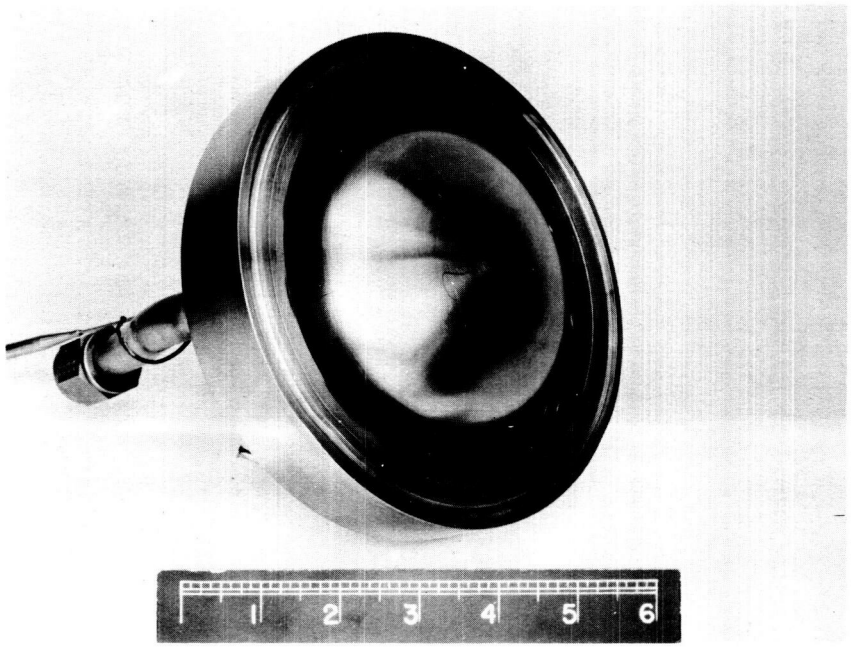

6028-326

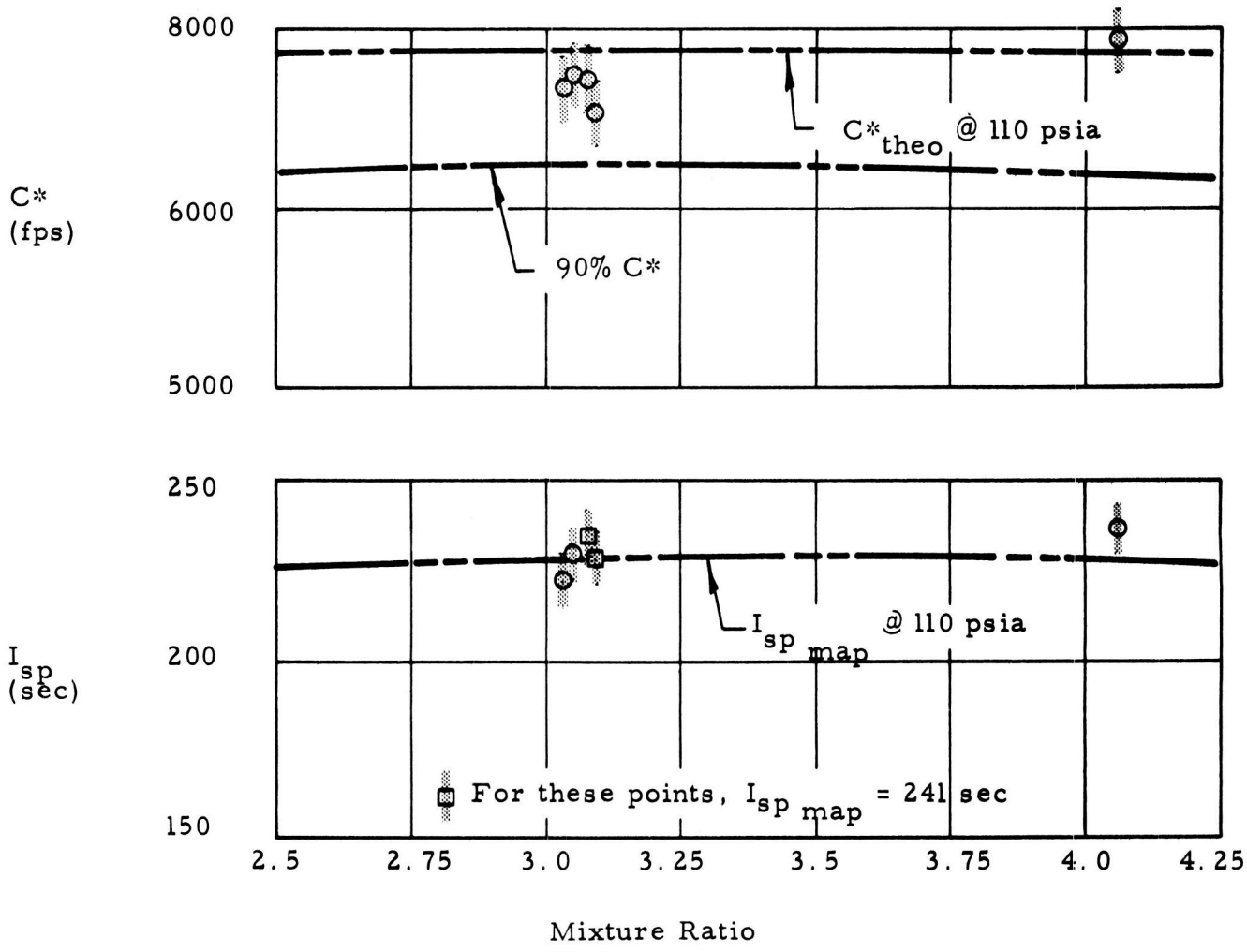

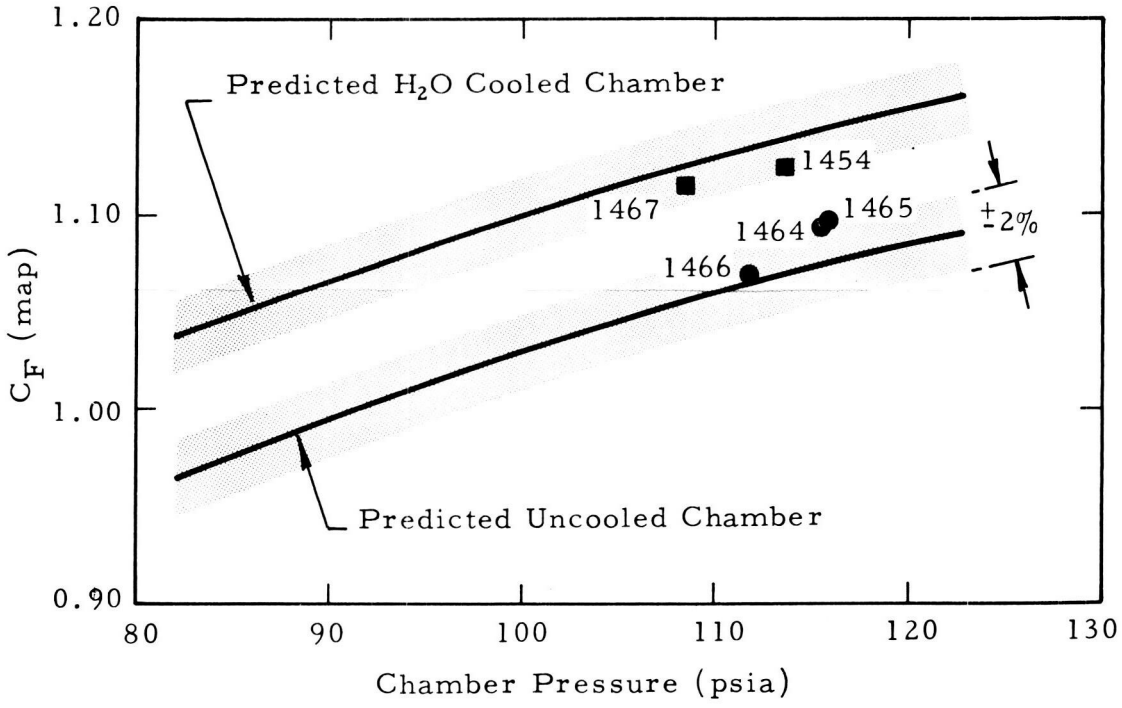

Figure 34. Full Diameter Vortex Injector Performance

performance. One test was conducted with the original full diameter vortex injector design and four tests were conducted with the modified (chromium-copper oxidizer face) injector. The injection pattern in the modified version was the same as in the original version.

The experimental performance data obtained with the full diameter vortex yielded excellent corroboration between the predicted and experimental C_F. The performance levels obtained with this injector duplicate the high performance levels obtained during the Task I portion of this program (150 lb thrust materials evaluation) and the prior feasibility program (NAS-w-449).

(3) Multiple-Doublet Injector - Three tests were conducted with the multiple-doublet impinging stream injector. The performance data are presented in Figure 35. The performance level of this injector was consistently very low ($\leq$81% of theoretical c*) over a mixture ratio range of 3.01 to 3.91. Excellent agreement between the predicted and experimental C_F confirms the validity of these data. The performance of this injector was much lower than the performance level obtained with the 150 lb thrust doublet injector evaluated in the feasibility program (NAS-w-449), possibly because of changes in state of injected propellants and changes in injection momentum ratios as a result of propellant cooling of the injector, in contrast to the prior heat-sink model tests.

(4) Coaxial Showerhead Injector - Six tests were conducted with the coaxial showerhead injector. The performance data are presented in Figure 36. The performance level of this injector averaged 93.8% of theoretical c* over a mixture ratio range of 3.04 to 4.16. The performance level attained was considered good in view of the fact that the optimum number of injection elements were not incorporated in the design (to avoid fabrication problems). The larger standard deviations in the I_{sp} data, as compared to the c* data in Figure 36, are attributed to thrust measurement errors due to pre-run and post-run zero shifts for three runs. The performance of this injector was virtually constant over the mixture ratio range evaluated. The showerhead injector evidenced a cyclic variation in chamber pressure of approximately $\pm$ 12 psi at approximately 600 cps. This was the only injector exhibiting this behavior.

b. Heat Transfer

Four tests were conducted with the water-cooled thrust chamber assembly, of which only three were scheduled as heat transfer firings. The remaining

6028-217

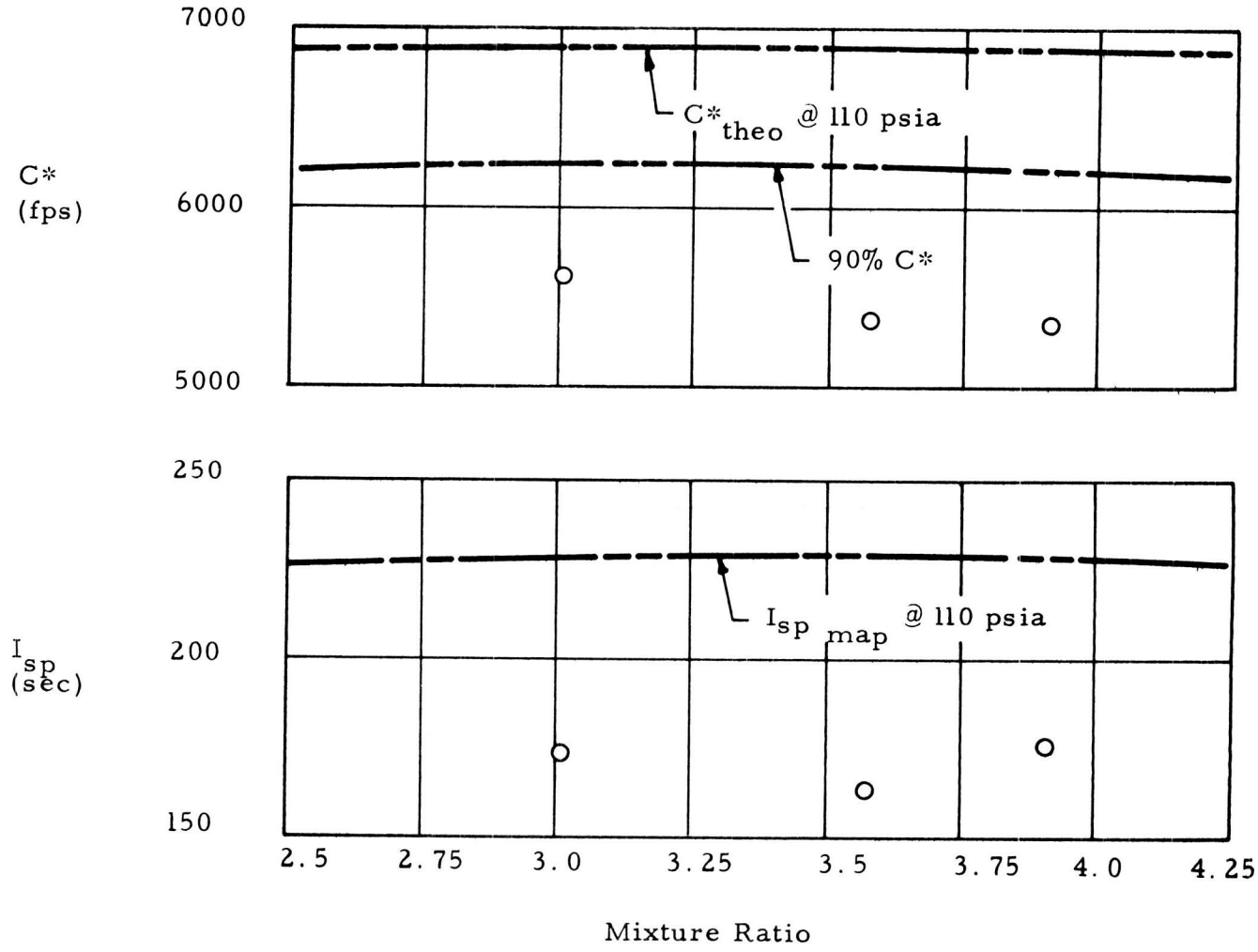

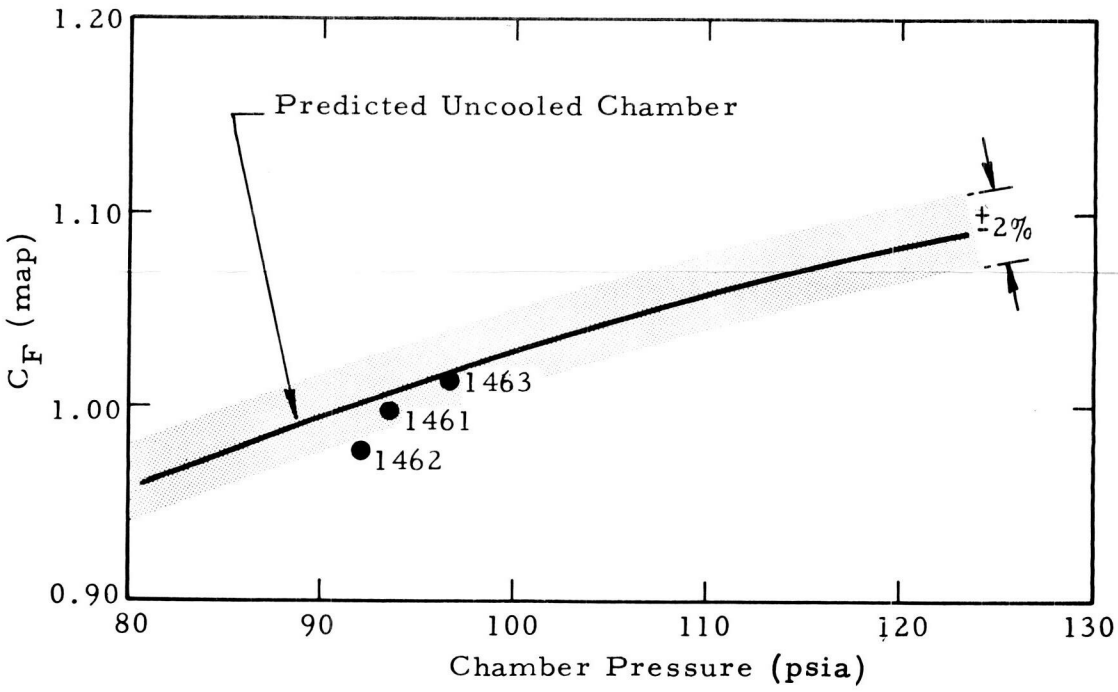

Figure 35. Multiple Doublet Injector Performance

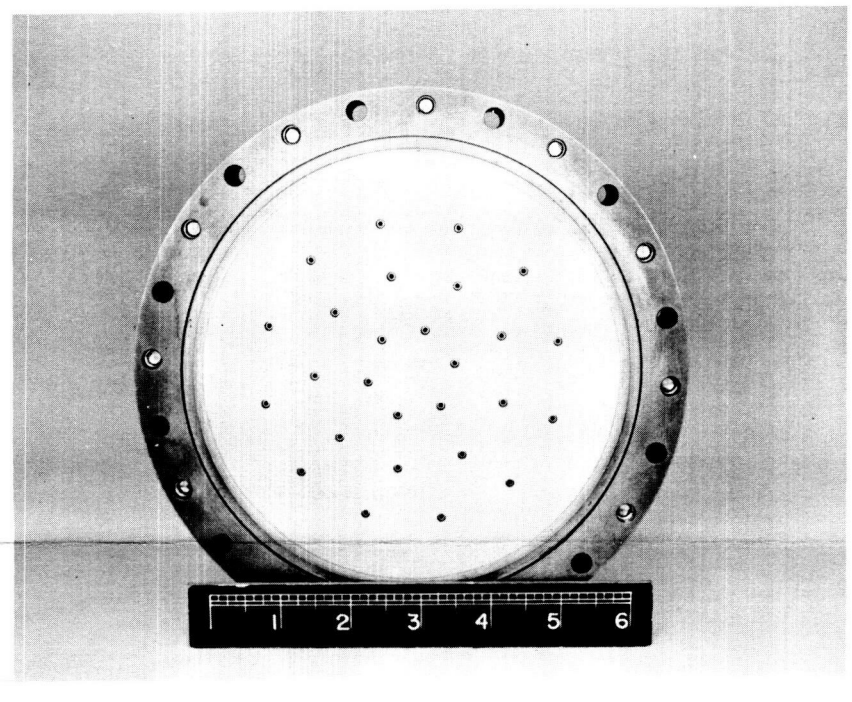

6028-329

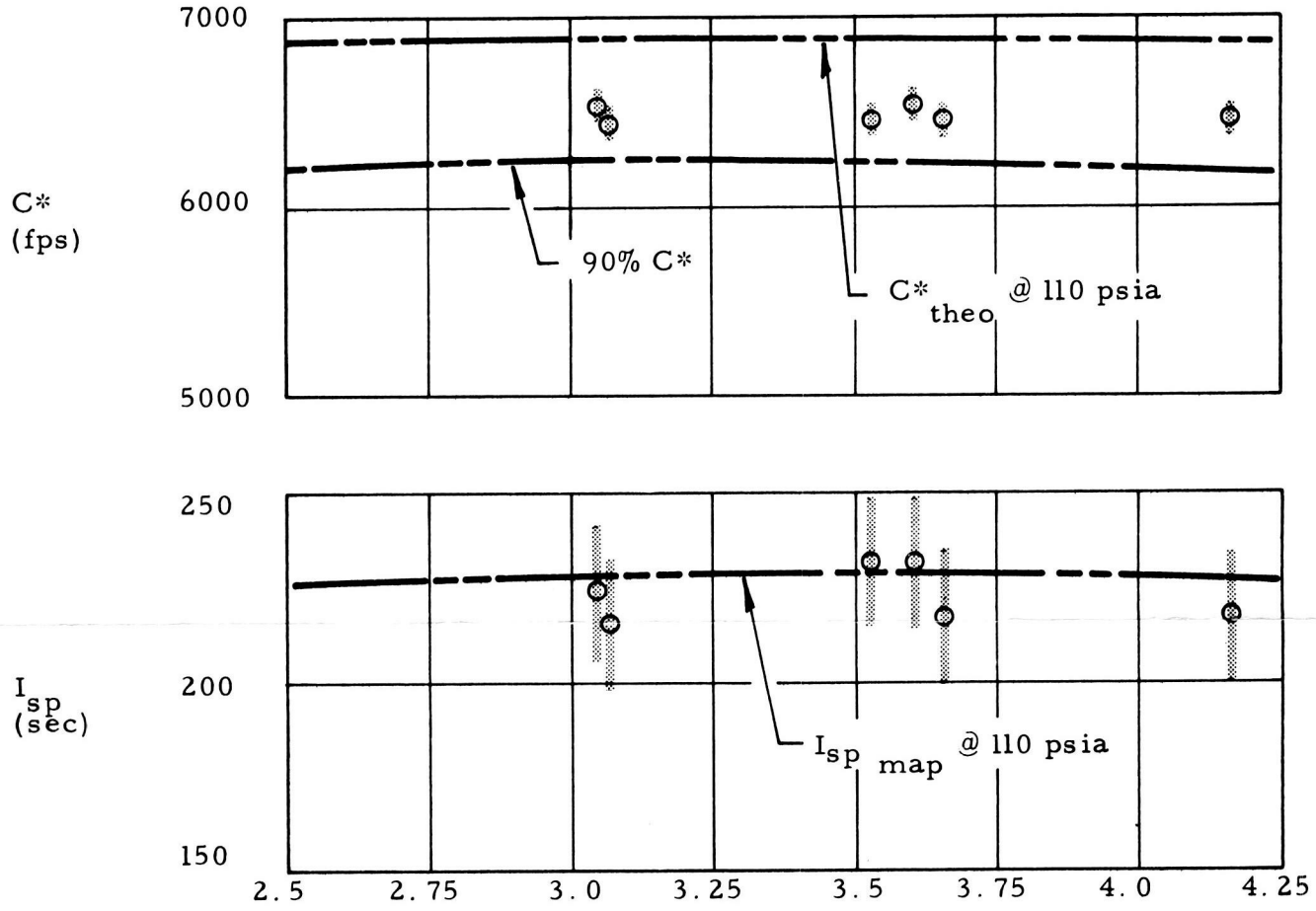

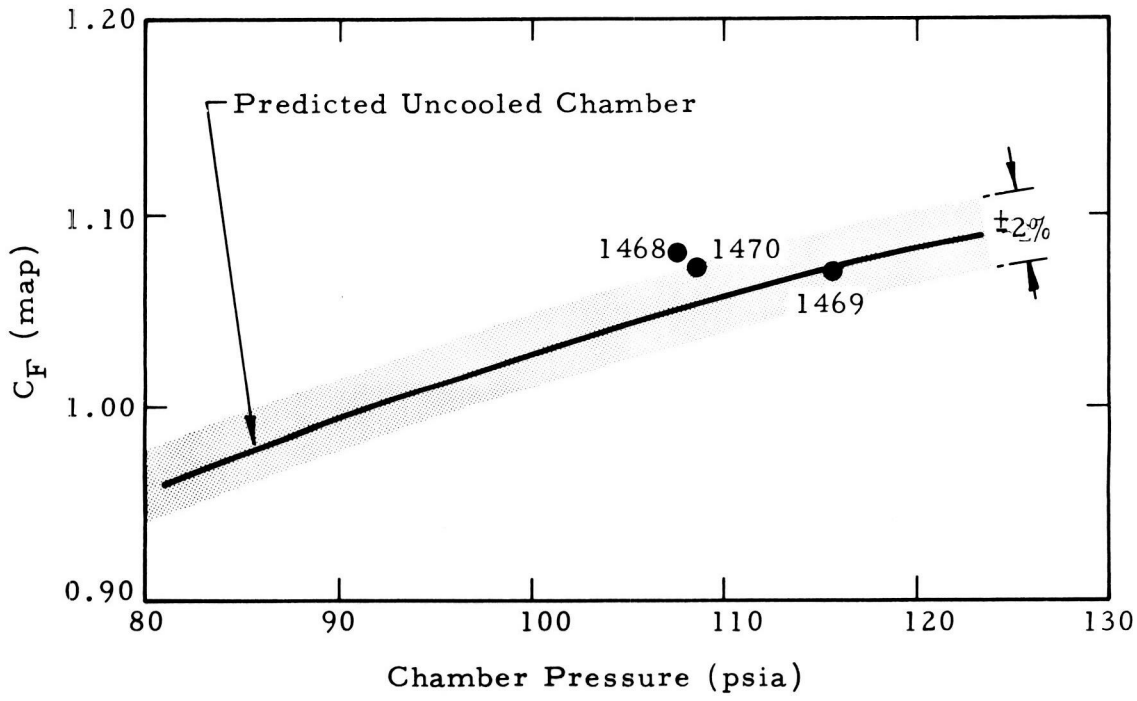

Figure 36. Coaxial Showerhead Injector Performance

test, conducted with the full diameter vortex injector, was programmed as a 2-second performance firing. Two heat transfer tests were conducted with the mid-diameter vortex injector and one with the full diameter vortex injector. No heat transfer firings were attempted with the doublet injector due to the low performance level ($\leq$80% c*) of this configuration. A modification to incorporate a dual oxidizer inlet manifold on the coaxial showerhead injector was not completed in time to enable a heat transfer firing to be made.

The heat transfer data acquired with the water-cooled thrust chamber assembly are shown in Figure 37, as are the theoretical heat fluxes for the chamber barrel and nozzle sections. The data for the nozzle section are based on overall heat fluxes since a single pass nozzle assembly was employed. Theoretical heat fluxes were predicted using the heat transfer data acquired on the previous program (NAS-w-449) adjusted for the 2000 lb space-thrust chamber geometry and the operating chamber pressure level experienced during this program. The predicted heat flux levels are based on a combustion efficiency of 100% (i.e., T_{gas} actual = T_{gas} theoretical).

Heat transfer tests of 10.1 seconds duration (6CX1453) and 19.3 seconds duration (6CX1456) were made with the modified mid-diameter vortex injector. An oxidizer injector ("A" nickel material) burnout occurred at about four seconds during the 10.1 second test. The heat transfer data for the nozzle section were taken just prior to the failure. An open thermocouple lead prevented useful data acquisition from the chamber barrel section. The 19.3 second test, which was programmed for 20 seconds duration, was terminated when the oxidizer injector spud was ejected from the thrust chamber as a result of a braze joint failure; however, useful data were acquired up to the time of the failure. The heat transfer data for both of these tests is in approximate agreement with the predicted heat flux levels.

One heat transfer test (6CX1467) was conducted with the full diameter vortex injector and water-cooled thrust chamber assembly. This run was terminated at 2.12 seconds when the oxidizer injector cup separated from the injector body, also as a result of a braze joint failure. No useful heat transfer data were acquired in this short duration test.

5. Injector Durability

The initial injector designs utilized heat treatable chromium-copper material for the combustion side components. This alloy will operate appreciably cooler than stainless steel, or even nickel, and is capable of being heat

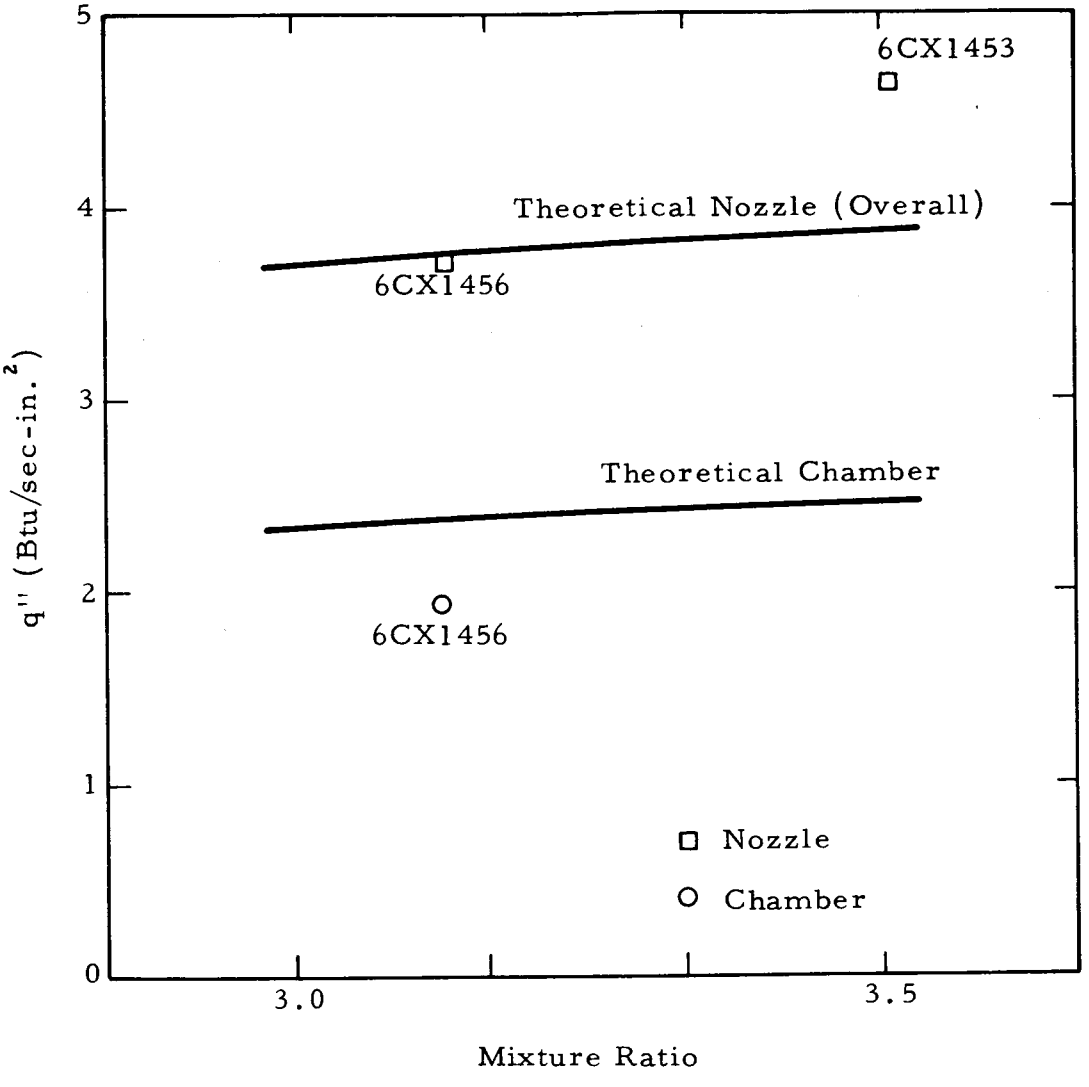

Figure 37. Water Cooled Chamber Heat Flux vs O/F

treated to a minimum of 38,000 psi. A design study indicated that this material was also suitable for flight-type injectors.

After brazing of the first injector, a mid-diameter vortex, it was discovered that the braze alloy attacked the chromium-copper base metal, resulting in base metal flow which completely plugged the injector flow passages. In order to meet program schedules, a review of the injector designs was undertaken to find a substitute for the chromium-copper braze joint design approach with minimum modification of the initial design configurations.

Design and heat transfer analyses indicated that "A" nickel was the most suitable substitute for chromium-copper and the vortex and doublet injector designs were modified to permit utilization of "A" nickel injection spuds. The coaxial showerhead design retained its chromium-copper face since it did not require a braze joint.

Continuing braze investigations did result in a successful chromium-copper braze joint technique in test samples. However, since fabrication of the welded "A" nickel injector designs was well underway, reversion to the original design was held in abeyance pending the test evaluation of the "A" nickel injector designs.

Test experience with the first injector configuration, the mid-diameter vortex, revealed two problem areas: the occurrence in several tests of severe pressure surges in the oxidizer injector manifold during the start transient, which led to injector damage in three tests and localized erosion of the "A" nickel oxidizer spud. Metallurgical analyses of the eroded spuds and examination of the oxidizer manifold designs were undertaken.

The pressure surges were suspected to be reactions of OF_2 with either weldments, gaps, or protuberances in the flow passages which may not have been completely passivated. The amount of internal welding in the injectors was reduced, a lap weld joint was changed to a butt-welded joint and the centerline chamber pressure tube and orifice inlet pressure tube were eliminated. Subsequent testing revealed that the pressure surges in the oxidizer system had been eliminated.

Metallurgical analyses of the eroded nickel oxidizer injector spud indicated that extensive boron diffusion and the formation of nickel-boride led to rapid deterioration of the "A" nickel exposed to the combustion gases. As a result

of this discovery, a decision was made not to test injectors with combustion-side components of "A" nickel. The "A" nickel injector designs (except the doublet) were modified to accept the substitution of chromium-copper material as necessary.

A long duration (19.3 sec) test was accomplished with the modified chromium-copper mid-diameter vortex injector. This test was programmed for 20 seconds and was terminated when the oxidizer injector cup was ejected from the thrust chamber as a result of a mechanical braze joint failure. The remainder of the oxidizer injector, however, was in excellent condition. The 19.3 second test was the longest in the injector evaluation program and demonstrated the promising durability of the chromium-copper design approach.

Eight test firings were conducted with the mechanically sealed, chromium-copper fuel spud of the mid-diameter vortex injector for a total duration of 40.36 seconds. The fuel spud was in excellent condition.

Four tests were conducted with the modified full diameter vortex injector (chromium-copper oxidizer spud face). The chromium-copper oxidizer cup separated from the oxidizer body on the last run as a result of incomplete wetting in the braze joint. Examination of the injector prior to the last run revealed that it was in good condition.

The first series of tests with the coaxial showerhead injector resulted in erosion of a fuel injection pin on two injectors. In each case, the location of the pin was identical (180 degrees from the oxidizer inlet manifold). The injector was modified to incorporate a dual oxidizer inlet manifold to improve the original, volute-controlled, flow distribution across the oxidizer injector plate. Three tests were made with the modified configuration with no evidence of fuel pin erosion. The coaxial showerhead was less stable than the vortex or doublet injectors. The test runs with the coaxial showerhead consistently exhibited chamber pressure oscillations on the order of $\pm$ 10%, compared to $\pm$ 3% for the vortex injectors and $\pm$ 2% for the doublet.

No durability problems were experienced with the multiple-doublet injector, obviously as a result of the poor performance level experienced with this injector.

6. Thrust Chamber Design Study

A study has been conducted to develop a design for a 2000 pound space thrust chamber using the results of the Task I and Task II investigations as design inputs. The chamber design conditions were 400 seconds of continuous operation with OF_2/B_2H_6 at a chamber pressure of 120 psia, a mixture ratio of 3.0, a combustion efficiency of 96% corresponding to a theoretical combustion temperature of 6030F and a maximum external structural shell temperature of 400F.

Two design concepts evolved: the first an all-ablative (graphite phenolic) chamber and the second an ablative chamber with a propellant cooled nonablating throat.

a. All-Ablative Design

Figure 38 depicts the design of the graphite cloth-phenolic resin ablative chamber. The graphite-phenolic material combination was chosen on the basis of the Task I screening tests in which Fiberite's MX4500 displayed outstanding performance. The backup insulation, RMD's Type 1A Ablatalite, was chosen on the basis of prior Thiokol-RMD experience and also on the basis of Task I performance.

The material thicknesses were sized by RMD's proprietary analytical ablative prediction program. This program, made available for use in this study, predicts erosion, char depths, and temperature profiles for an ablative chamber design operating under any given set of conditions. Conversely, the prediction program also permits determination of the required material properties to maintain a predetermined level of performance for a given set of operating conditions. The design criteria (erosion, char, temperature gradients) were confirmed by the Task I test results.

The design uses a 15 degree wrap angle in the barrel graduating to a 60 degree angle in the throat since Thiokol-RMD experience in this and other programs has shown that this combination of angles results in maximum durability.

The structural shell, 7178 aluminum alloy, has mounting flanges for both the injector and nozzle extension, besides furnishing support for the ablative liner and backup insulation. The Ablatalitc insulation is cast and cured in place

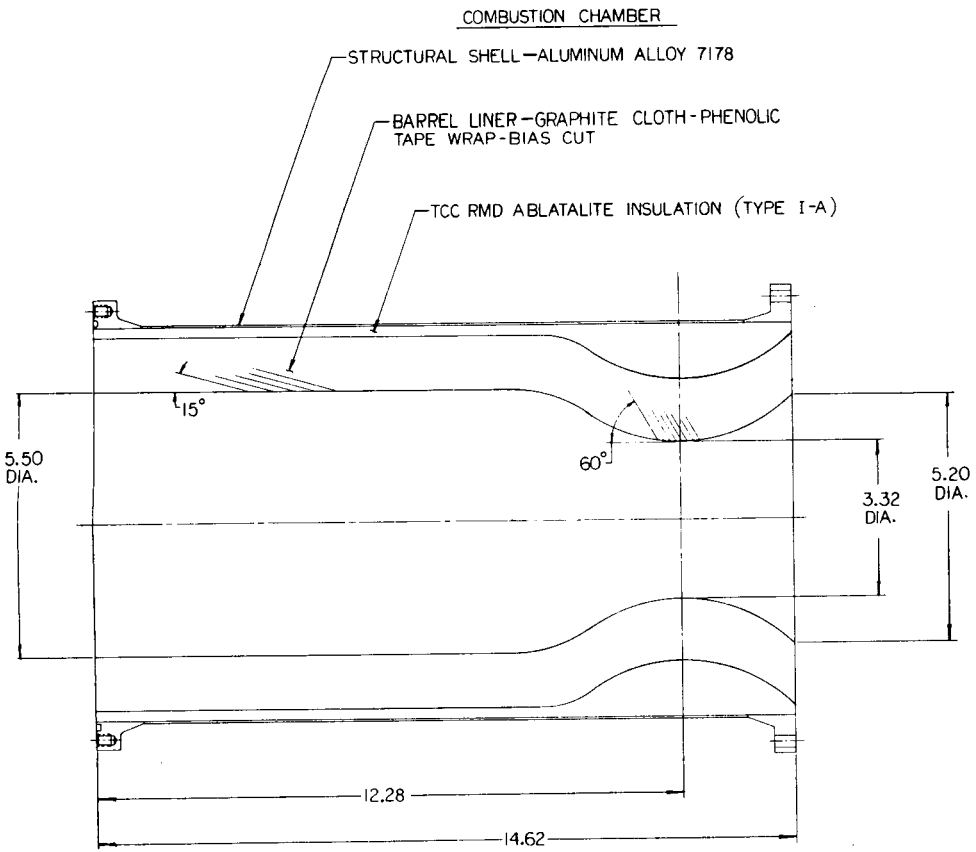

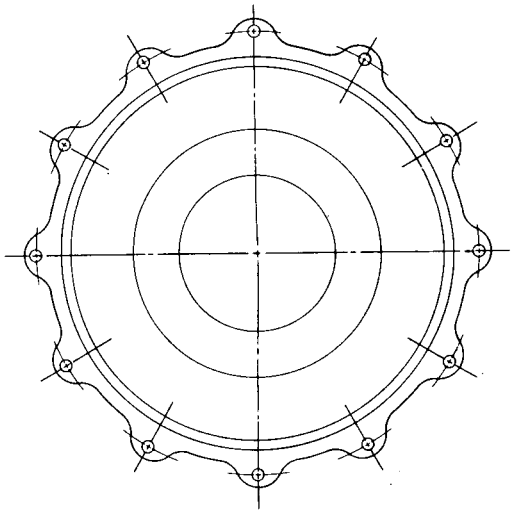

Figure 38. Ablative Thrust Chamber

Dwg 53786

between the jig-aligned aluminum shell and ablative liner. The design of this chamber is similar to RMD's highly successful TD-321 10,000 lb space thrust engine.

The Task I test data were utilized to predict the analytical behavior of graphite phenolic ablative thrust chambers up to the 15,000 lb space thrust level. The chamber design conditions were 400 seconds of continuous operation with OF_2/B_2H_6 at a chamber pressure of 120 psia, a mixture ratio of 3.0, and a combustion efficiency of 96%. Figure 39 shows the predicted chamber pressure decay due to throat erosion of a 150 lb, 2000 lb and 15,000 lb space thrust chamber. The significant influence of thrust chamber size on ablative performance is readily apparent from comparisons of the performance plots for the three thrust levels (150 lb, 2000 lb and 15,000 lb).

Based on Thiokol-RMD experience, the performance of graphite phenolic with OF_2/B_2H_6 is equivalent to that of silica phenolic with N_2O_4/50-50 (Figure 39). The significance of this equivalence in ablative performance indicates that propulsion performance upgrading can be achieved within acceptable throat erosion limits with present state of the art ablative materials.

b. Noneroding Throat

Since there are some mission profiles in which erosion is intolerable, a nonablating throat configuration was also designed. Figure 40 illustrates the Torox concept in which a propellant cooled tube is imbedded in the chamber throat. The entire throat substrate is metal loaded, conducting heat from the general area of the throat to the cooled tube where conductive-convective heat transfer to the propellant takes place.

The geometry of this chamber is identical with that of the all-ablative chamber and the materials of construction are the same (graphite cloth phenolic chamber liner, Ablatalite insulation, and aluminum structural shell).

c. Other Cooling Approaches

Film, transpiration, and regenerative cooling techniques were also investigated but were considered to be unreliable due to the limited knowledge available concerning the cooling properties of the propellants; heat-sink cooling was simply not feasible for this propellant combination and duration.

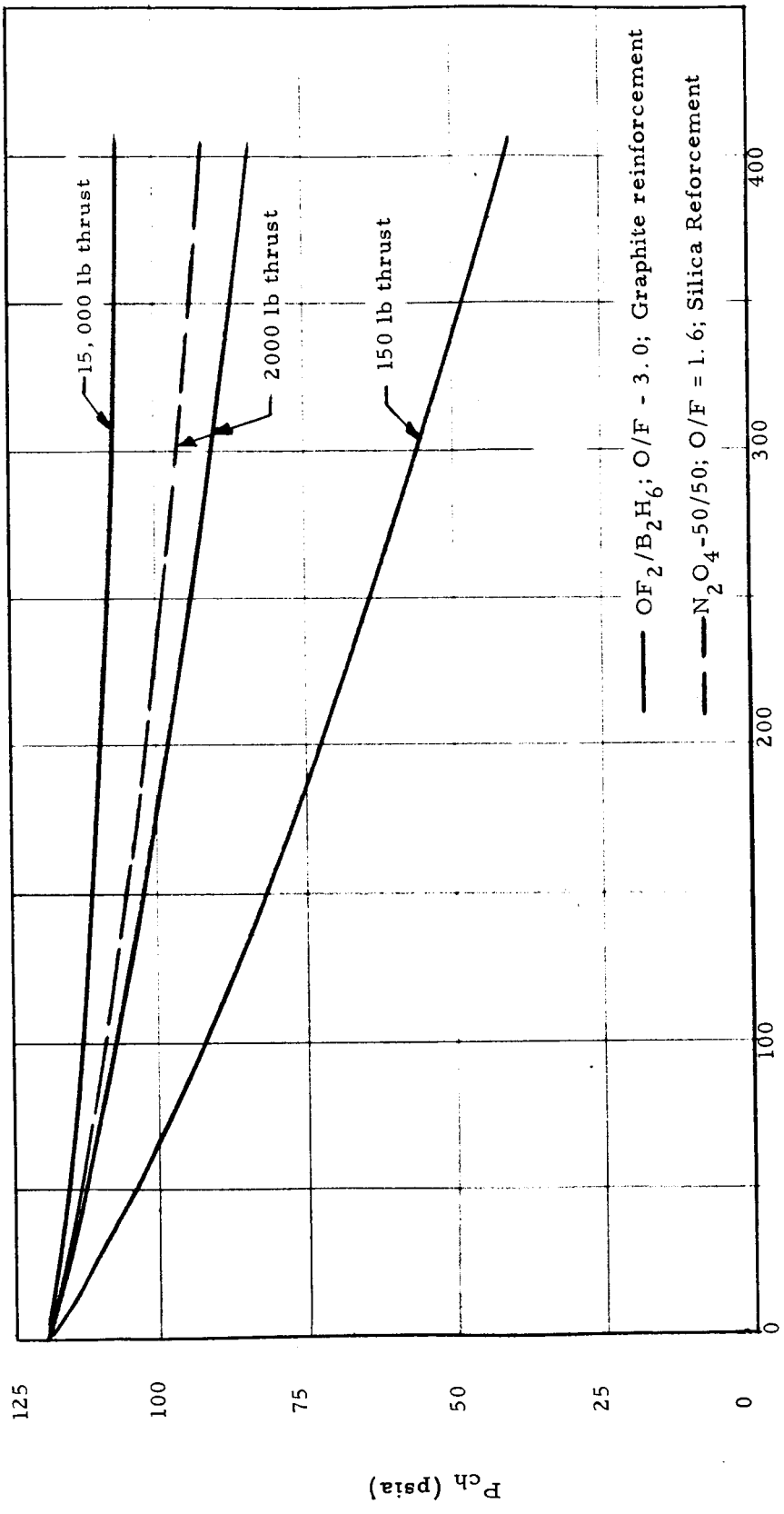

Figure 39. Predicted Ablative Behavior OF_2/B_2H_6, N_2O_4/50-50

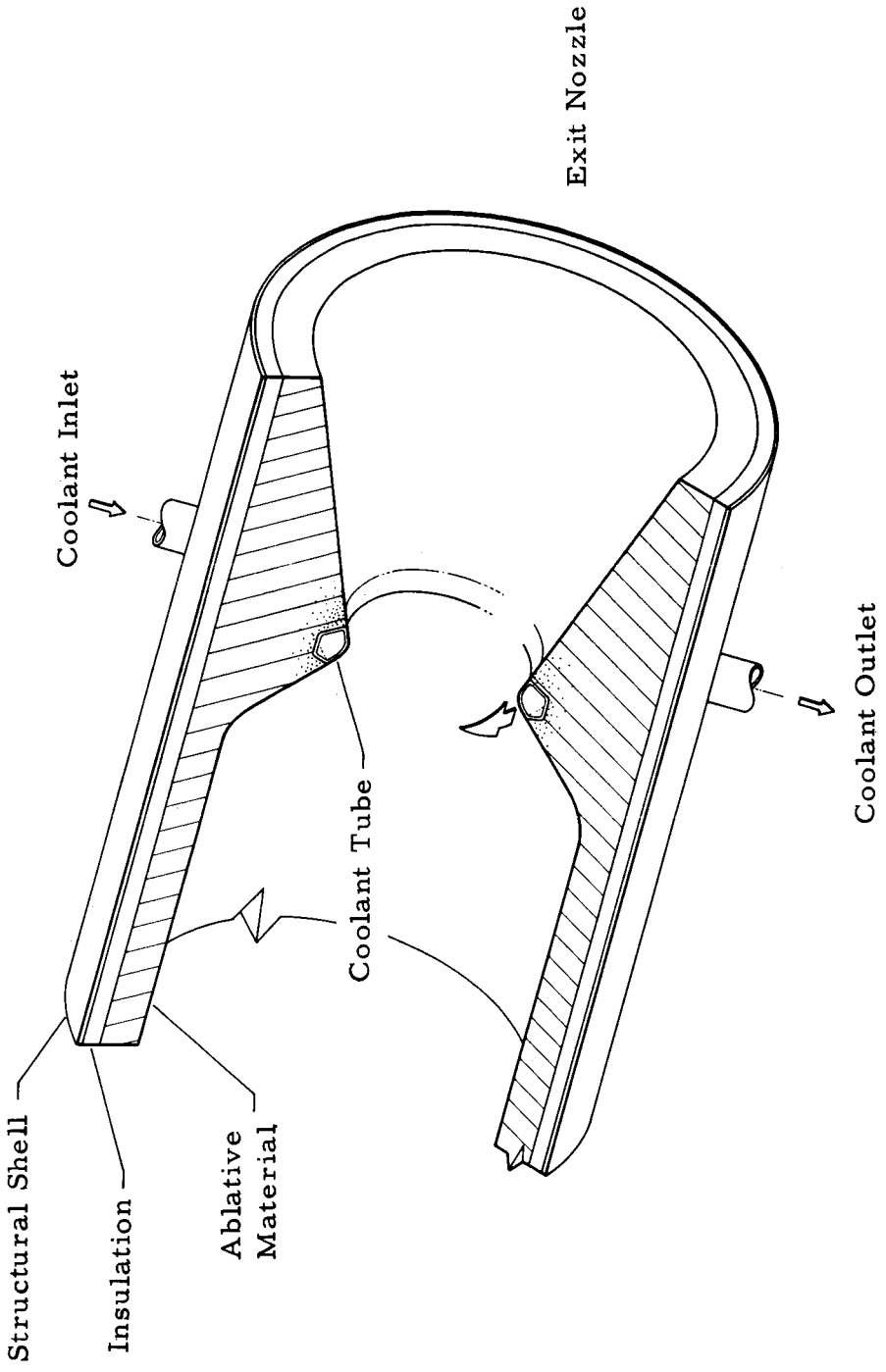

Figure 40. Torox Thrust Chamber

Cooling approaches other than ablative and Torox may be feasible with OF_2/B_2H_6 but further work is required to provide data on propellant cooling properties and transpiration materials. In addition, heat-sink cooling is feasible for limited duty cycles.

Although the design study was limited to the OF_2/B_2H_6 propellant combination, there are other coolant fuels which, in combination with OF_2, can provide essentially equivalent performance and offer the additional capability as regenerative coolants. Among these promising fuels for use with OF_2 are the light fraction hydrocarbons and hydrazine and amine blends. The majority of these fuels have a broader range of coolant capabilities than that of diborane. Thiokol-RMD has successfully demonstrated OF_2/MMH test firings at the 150 lb thrust and 10,000 lb space thrust level utilizing MMH as a regenerative coolant.

7. Task II - Conclusions

On the basis of the results of the 2000 pound space thrust injector evaluation program, the following conclusions are made:

- The OF_2/B_2H_6 propellant combination can provide high performance over a mixture ratio range of 3.0 to 4.16.
- Successful scaleup of injector performance to the 2000 pound space thrust level with OF_2/B_2H_6 propellants was demonstrated.
- Consistently high performance (in excess of 94% c* theo) over a wide mixture ratio range was obtained with vortex injectors, even without attempts to optimize performance through design refinements.
- Uniform combustion (as determined by streaking tests) at high performance levels was demonstrated with several vortex injectors.
- Performance optimization and cooling of the coaxial showerhead injector using OF_2/B_2H_6 propellants require more development effort.

- Low performance ($\leq$81% c* theo) was obtained with the multiple doublet injector. No attempt at optimization was made. Because of the large number of critical parameters inherent in impinging stream designs, the amount of design refinement and tailoring necessary to obtain high performance is unpredictable.

- On the basis of the measured heat flux levels, injector propellant cooling is feasible.

III. PROGRAM CONCLUSIONS

The following conclusions are drawn from the results of experimental investigations conducted under Contract NAS-3-2553:

1. Based on the analytical predictions and the subsequent test data obtained in this program, present state of the art ablative materials were found to behave in a predictable manner with OF_2/B_2H_6. On the basis of four tests, the durability (erosion rate) of graphite cloth reinforcement materials with these propellants is approximately equivalent to that experienced previously at Thiokol-RMD with state of the art silica-phenolic materials and the N_2O_4/50-50 propellant combination.

2. Ignition tests conducted at a nominal chamber pressure level of 150 psia indicate that OF_2/B_2H_6 is reliably hypergolic over extreme ranges of environmental and operating conditions and propellant states.

3. OF_2/B_2H_6 delivers high sea level specific impulse (99% of predicted shifting equilibrium). The specific impulse is insensitive to wide variations in mixture ratio.

4. High performance 150 pound thrust injector designs can be scaled up to deliver high performance at the 2000 pound space thrust level.

5. Based on Thiokol-RMD experience, utilizing two stands simultaneously during the program, OF_2 and B_2H_6 can be handled safely with normal precautions. With proper selection and adequate cleanliness and passivation, materials compatibility poses no significant problems.

6. Additional investigations are required to determine the most desirable thrust chamber design for very long duration, multiple restart applications.

7. Injector designs utilizing combustion side components fabricated from chromium-copper have demonstrated promising durability. With the development of the chromium-copper braze joint, it is believed that good injector durability can be demonstrated.

IV. RECOMMENDATIONS

In view of the promising results obtained during this program, it is recommended that the following investigations of the OF_2/B_2H_6 propellant combination be continued at the 2000 pound space thrust level:

1. The test evaluation of the vortex injector should be continued to provide a reliable high performance design that can be applied to flight configurations. Based on test evaluations, this injector offers the highest confidence level in meeting the requirements for a reliable high performance injector.

2. Evaluation of an ablative thrust chamber configuration to demonstrate scalability of the successful 150 pound thrust configuration evaluated in this program should be undertaken. This evaluation would provide design criteria for the containment of high flame temperature propellants and would be applicable to flight configurations.

3. High area ratio nozzles should be designed, fabricated, and test evaluated to determine the space performance capabilities of OF_2/B_2H_6 propellants. Space performance data must be acquired in order to accurately assess the space vehicle potential of this propellant combination. Two types of nozzle configurations, a 15 degree conical nozzle and a contoured nozzle design, should be evaluated at simulated altitude (100,000 ft) to provide space nozzle design criteria.

4. Definition of the cooling properties of OF_2 and B_2H_6 is required to provide more rational design criteria for component designs (i.e., injectors, thrust chamber cooling, throat cooling). Basic heat capacity and upper limit of nucleate boiling data will be required for flight hardware optimization and should be acquired now.

5. Analytical studies based upon the methods employed in this program should be pursued to define the requirements for more durable and efficient containment materials (i.e., ablative, refractory composites), thus providing performance growth potential for high flame temperature propellants. Consideration of the combination of these methods with other cooling modes, such as transpiration, film cooling, etc., should also be initiated.

APPENDIX A

STREAKING TEST RESULTS

STREAKING TEST RESULTS

Sacrificial ablative inserts were placed in the test motors of Tasks I and II to evaluate the uniformity of combustion produced by the test injectors. Thiokol-RMD has successfully demonstrated the utility of this technique in assessing injector streaking characteristics.

In all cases, combustion was uniform, with no evidence of streaking or uneven erosion of the inserts.

The photographs, Figures 1, 2, 3 and 4, in this appendix show the Task II nozzle inserts in their post firing condition with no attempt made to remove combustion deposits. The reference mark which appears at the top of many of the inserts indicates the uppermost or "12 o'clock" point of the injector. Slight eccentricities of camera position have produced foreshortening in some cases, resulting in an erroneous impression of uneven erosion. As mentioned previously, however, ablation was both even and uniform in all cases.

6028-301

Figure 1. Mid-Diameter Vortex Injector Streaking Insert

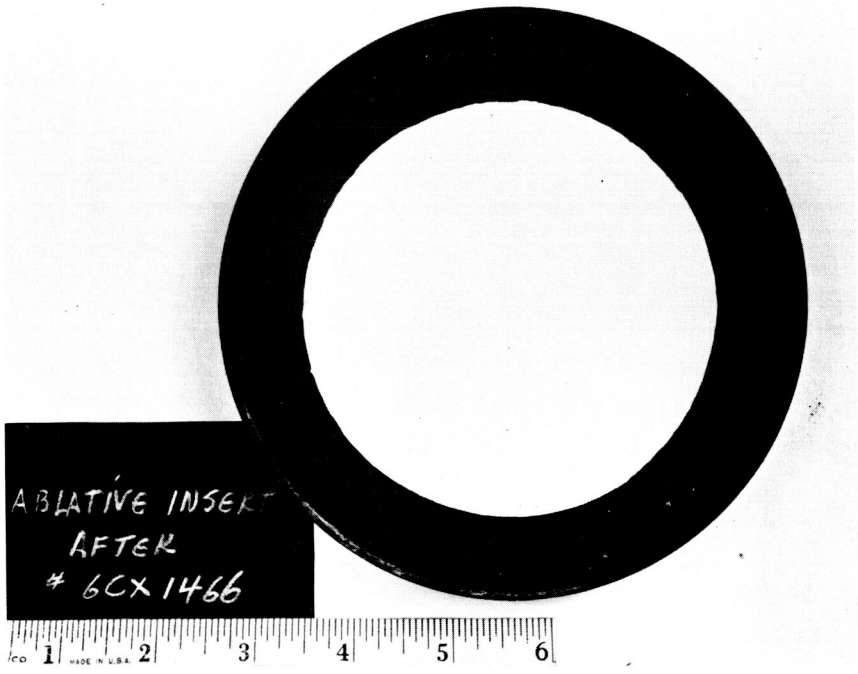

6028-523

Figure 2. Full Diameter Vortex Injector Streaking Insert

6028-383

Figure 3. Multiple Doublet Injector Streaking Insert

6028-390

Figure 4. Coaxial Showerhead Injector Streaking Insert

APPENDIX B

INSTRUMENTATION AND DATA ACQUISITION

FOREWORD

The value of any experimental investigation is a function of the quality of its acquired test data. Measurement of the parameters of interest in rocket engine performance tests is particularly difficult because of the magnitudes involved and the destructive environments in which the measuring equipment must operate. The following pages outline the methods used by the Reaction Motors Division of Thiokol Chemical Corporation to acquire meaningful data and to verify its accuracy.

INSTRUMENTATION AND DATA ACQUISITION

The measurement of physical phenomena necessarily begins with a verification of the accuracy of the measuring instruments relative to standards of length, mass, time and temperature. Thiokol measurement accuracy is directly traceable to the standards maintained by the National Bureau of Standards, Washington, D.C. This documented calibration program (available as TER 64C) is accomplished at Thiokol-RMD for three distinct categories of measuring equipment:

1. Primary Standards
2. Laboratory Standards
3. Working Standards

1. Primary Standards

Primary standards are used exclusively as master references for the other two categories of standards. They are maintained (where necessary) in controlled environments, and are never removed from the Instrument Laboratory. Primary standards are calibrated by the Bureau of Standards whenever possible; alternatively, calibration is accomplished by certified commercial laboratories such as United States Testing Co., and Precision Resistor Co., Inc., or by the State of New Jersey, Bureau of Weights and Measures. Such organizations must furnish written confirmation that their reference standards have current certification with the National Bureau of Standards.

2. Laboratory Standards

Laboratory standards are used to transfer values from the primary to the working standards, thus preserving the life and accuracy of the primary standards. Laboratory standards are also confined to the Instrument Laboratory, and may be used only for the calibration of working standards, or in connection with experimental instrumentation activities.

3. Working Standards

Working standards are instruments of high accuracy and rugged design, suitable for transportation to test areas, control rooms, etc., for the calibration of operational instrumentation.

A tabulation of RMD standards, showing their derivation from NBS standards, is given in Figure 1. The acceptable accuracies and calibration schedules for all three types of standards are specified in RMD Report TER 64-C; the calibration procedures are set forth in RMD TER 85-B.

a. Test Measurements

The measurement of rocket engine performance is predicated upon these precisely calibrated standards. Descriptions of the measurement process for temperature, pressure, and thrust are given in Figures 2, 3 and 4. In general, the procedure is the same for each variable: a transducer generates an electrical signal proportional to the magnitude of the variable to be measured; the signal is then transmitted to a strip recorder which plots signal magnitude as a function of time. The data acquisition channel (transducer, transmission, and recorder equipment) is calibrated against the appropriate working standard, providing exact knowledge of the numerical relationship between the magnitudes of the measured variable and plotted data. Channel calibration is checked both before and after each test run.

The determination of propellant flow by the cavitating venturi method (Figure 5) requires two separate measurements: the first is a pressure measurement required to obtain flow through the measuring device (venturi) from a pressure vs flow calibration curve; the second is a temperature measurement, required to determine the specific gravity of the propellant from a temperature — SG curve. This is necessary since flowmeters are calibrated in terms of water flow; propellant flow, therefore, must be calculated from the relationship

$$\dot{W}_{prop} = \dot{W}_{H_2O}\sqrt{SG\ prop}\ .$$

If the propellant possesses a substantial vapor pressure, as in the case of diborane, for example, it is necessary to subtract this vapor pressure (obtained from a temperature - vapor pressure curve) from the observed pressure, before using the pressure vs flow calibration curve.

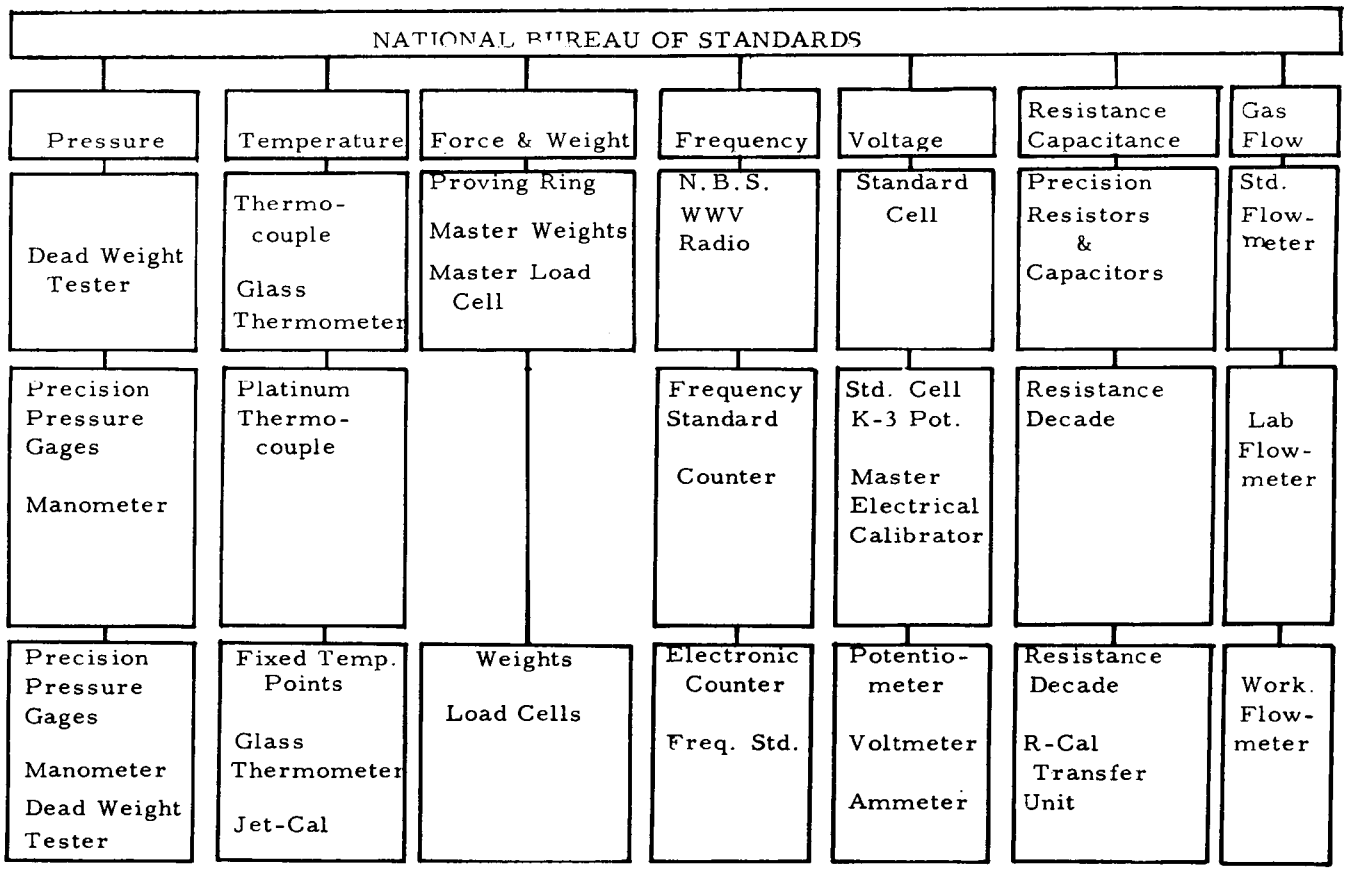

Figure 1. Tabulation of RMD Standards for Instrument Calibration

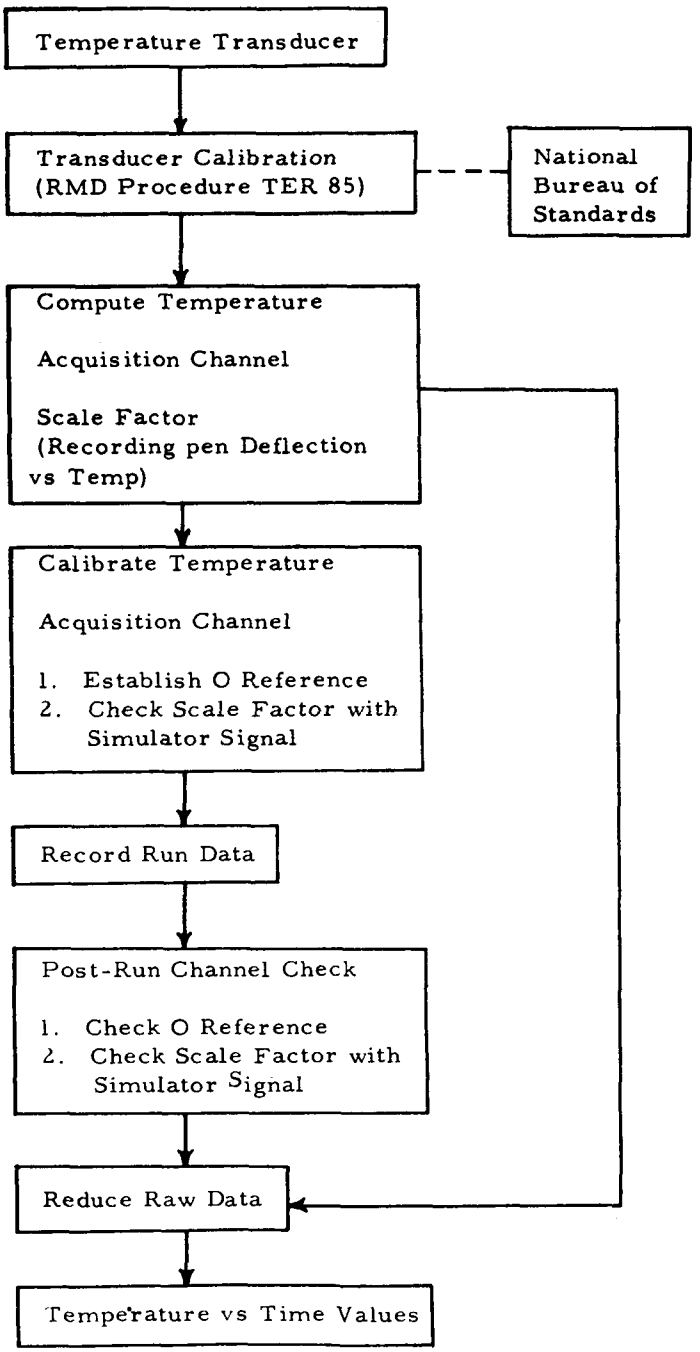

Figure 2. Data Acquisition, Temperature

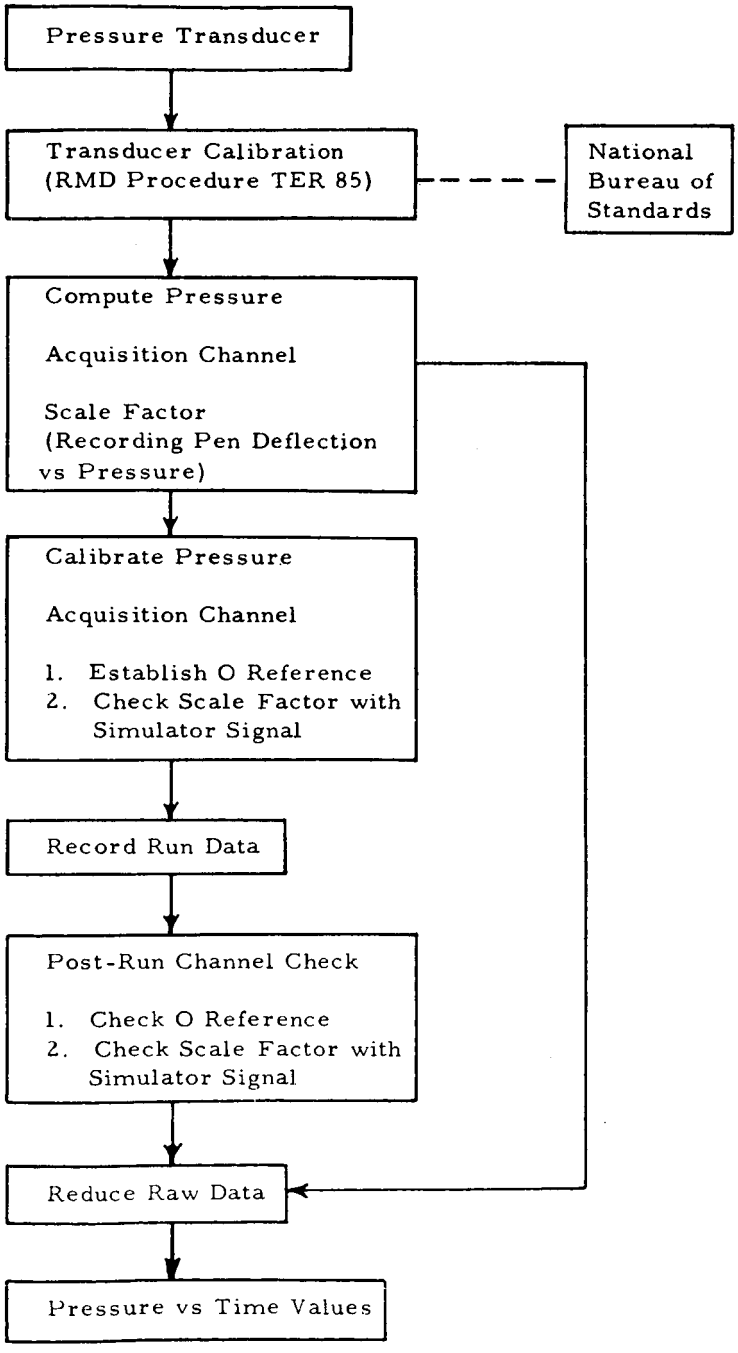

Figure 3. Data Acquisition, Pressure

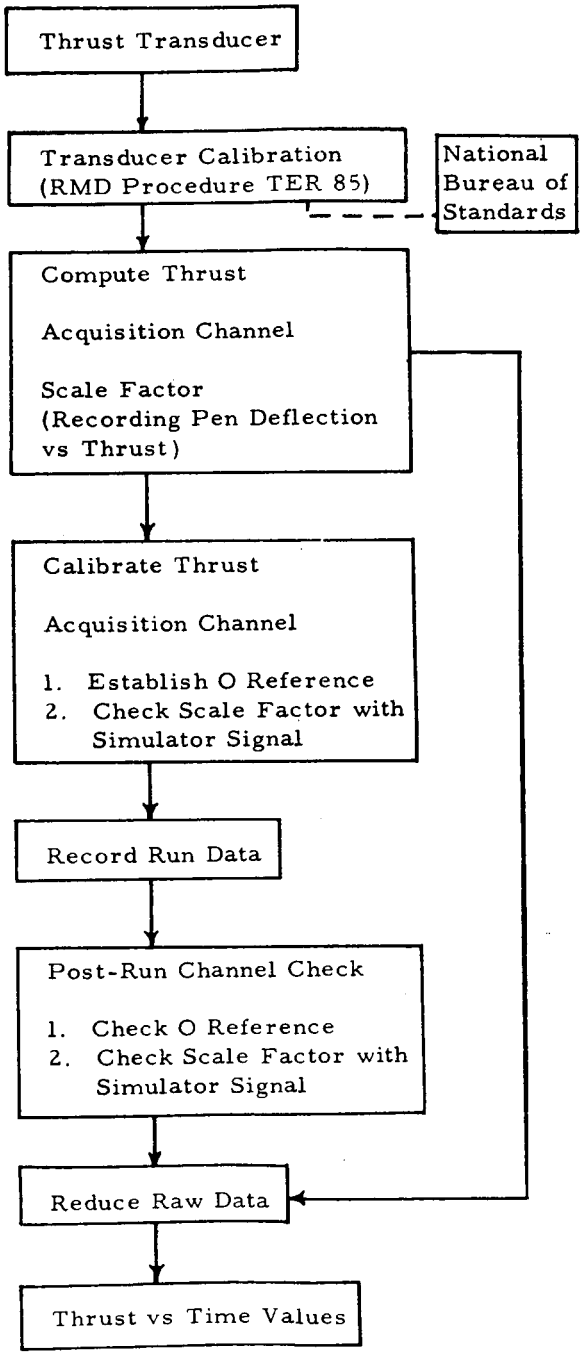

Figure 4. Data Acquisition, Thrust

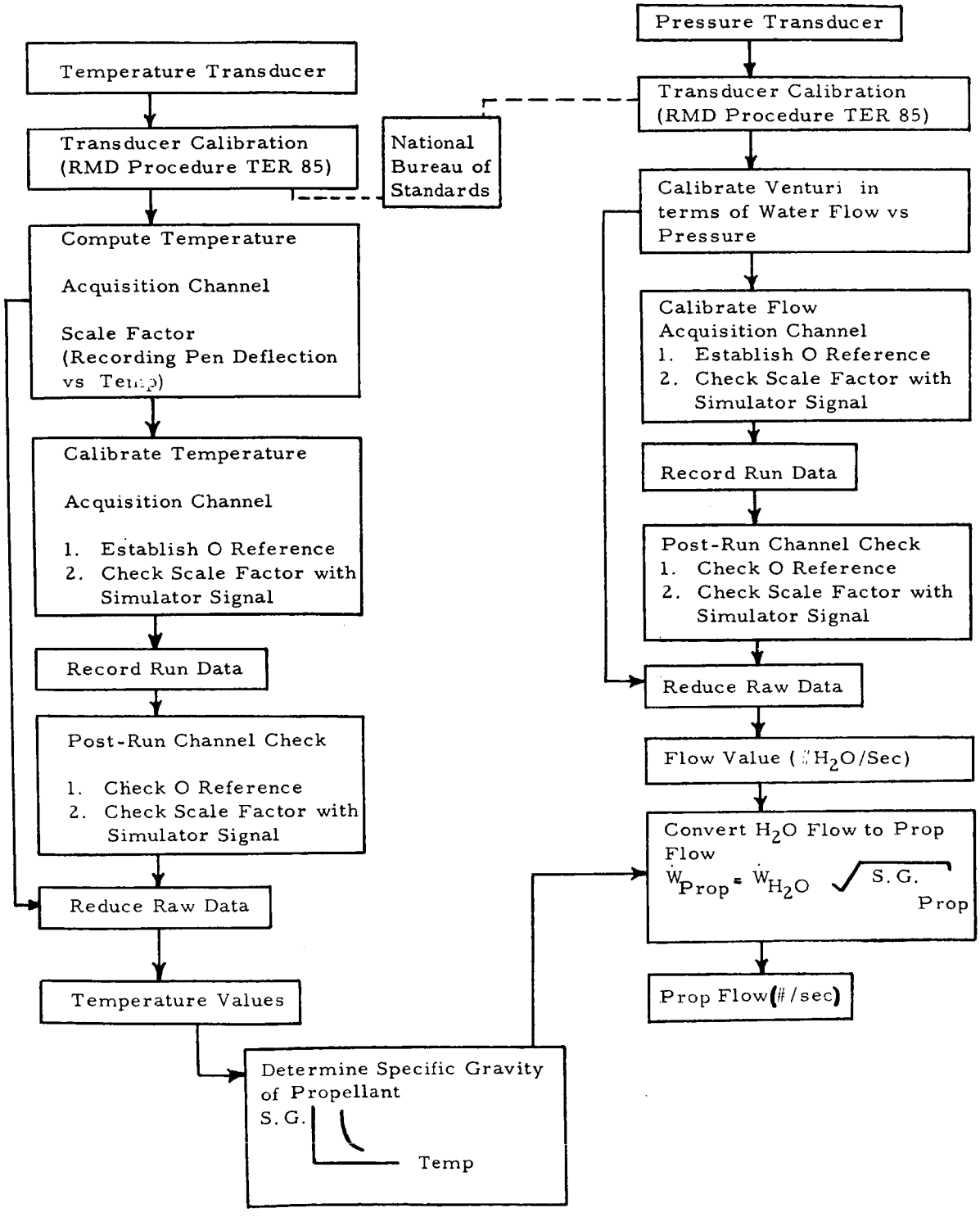

Figure 5. Data Acquisition, Propellant Flow (Venturi Method)

An alternate procedure for measuring propellant flows uses the turbine-type flowmeter (Figure 6). This instrument generates sinusoidal electric signals proportional (in frequency) to the volume of propellant flow. An electronic counter measures the number of cycles generated by the flowmeter; dividing the recorded number of cycles by the elapsed time results in the number of cycles per second. It is then possible to multiply the number of cycles per second by the calibration factor, (pounds of water flow/cycle), to obtain the water flowrate, in pounds per second.

A temperature measurement and temperature-specific gravity curve for the propellant is used to obtain the specific gravity of the propellant, permitting conversion of water flow to propellant flow, by the same relation used for venturi flowmeter measurements.

b. Accuracy

The accuracy of the measured data is assured both by the use of precision instruments, carefully calibrated and maintained, and by test procedures which provide for checking and rechecking, (as in the case of the pre- and post-run channel calibration check).

Furthermore, provision is often made for redundant measurements of critical variables (i. e., the use of two separate devices to measure the same parameter).

Descriptions of typical operational instrumentation, including accuracies, are given in Table I.

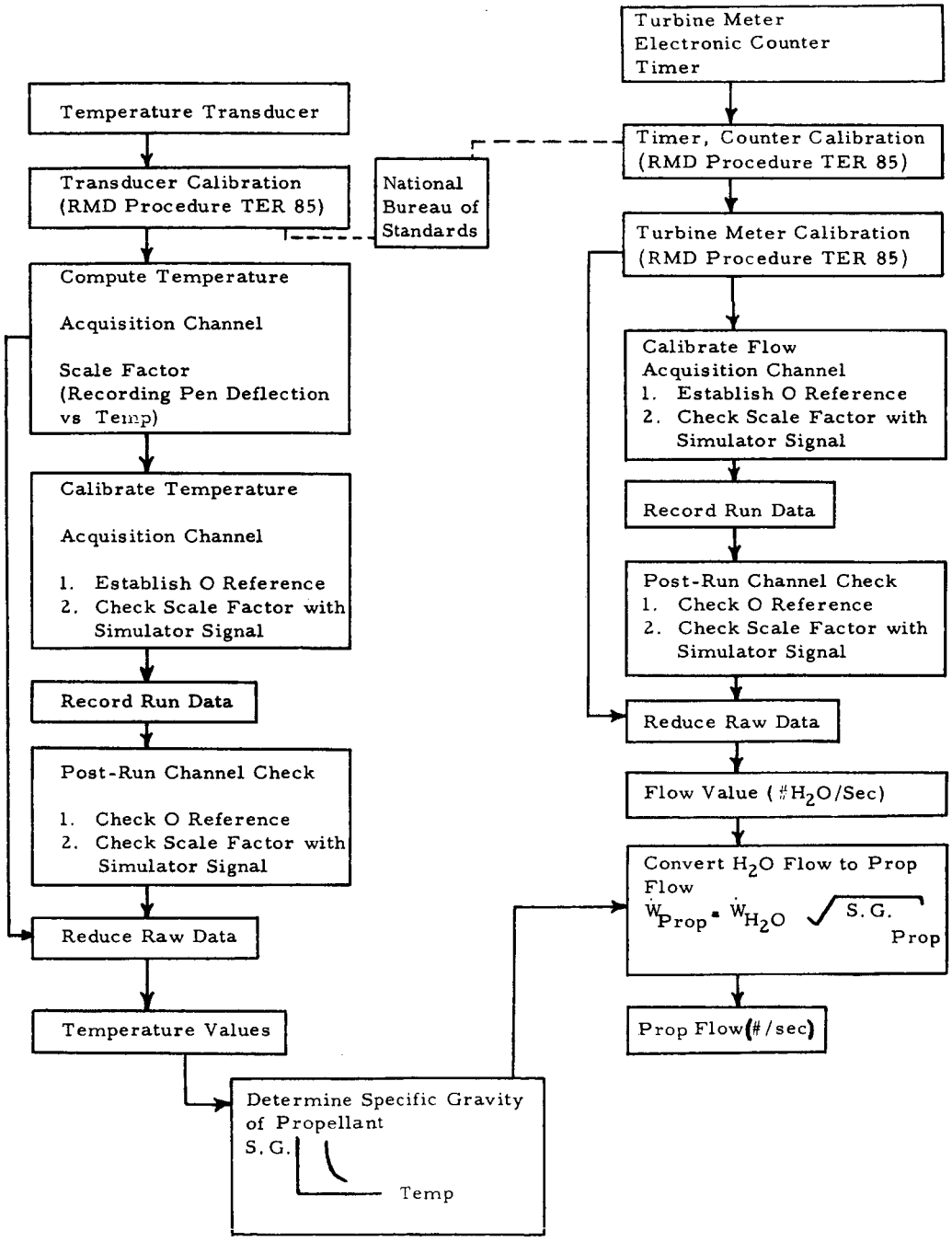

Figure 6. Data Acquisition, Propellant Flow (Turbine Meter Method)

TABLE I

ACCURACY ANALYSIS

I. Serially Connected Components

(a) Transducers

Transducer	Type & Capacity	Environment	T_a Nonlinearity & Hysteresis	T_b Repeatability	T_c Temperature Effect	Total Tolerance $T_x = \sqrt{T_a^2 + T_b^2 + T_c^2}$
Thrust	Baldwin-Lima-Hamilton Type U3XX, 5000 lb & 10,000 lb	15 to 115F	±.10% of full scale	±.05% of full scale	±.04% of load	±.12% at full scale ±.26% at 50% FS ±1.14% at 10% FS
Pressure	Teledyne Model 176 0-1000 psig	-65 to +250F	±.26% of full scale	±.05% of full scale	±.25% of full scale	±.36% at full scale ±.73% at 50% FS ±3.64% at 10% FS
Flow	Potter Aeronautical Series 5000 - 1 in. & 2 in. size	-65 to +250F	±.25% of flow	±.25% of flow	±.05% of flow	±.36% of flow
Temperature	Thermoelectric Cooper Constantan Thermo-couple, -65 to +250F	-65 to +250F	Correctable	±.35% of Temperature	See: Reference Junction	±.35% of reading
Vibration	Endevco Model 2211, 200 g, 40 - 8000 cps	-65 to 250F	±2% of point	Included in Temperature Effect	±5% of point	±5.4% of reading
Position	Bournes Align-O-Pot Model 140 0-2.25 in.	-65 to 220F	±.5% of reading	±.1% of reading	±.5%	±.75% of reading

(b) Signal Conditioning Equipment

Equipment	Manufacturer & Type	Environment	T_a Nonlinearity of Reading	T_b Repeatability of Reading	Total Variation of Reading $T_x = \sqrt{T_a^2 + T_b^2}$
Temperature Reference Junction	Thermo Electric Co. -65 to +250F range 150F Reference	Control Room	--	±.2%	±.2%
Cathode Follower Amplifier	Endevco Model No. 2608	0 to 100F	±1.0%	±.25%	±1.03%
Strain Gage Module	Video Instruments Type SR200	Control Room	±.05%	±.10%	±.11%
Attenuator	International Resistor Corp.	Control Room	±.05%	±.05%	±.07%
DC Amplifier	Kintel Type III	Control Room	±.05%	±.10%	±.11%
Flow Integrator	Potter Aeronautical Model 3C	Control Room	±.10%	±.25%	±.27%
Voltage Power Supply	Kepco	--	--	±.10%	±.10%
(c) Transmission and Terminations					
Cable, Connectors Patchcords DC to 10 KC	--	0 - 100F	--	±.10%	±.10%
(d) Recorders					
Strip Chart	Minneapolis Honeywell	Control Room	±.25% of reading	±.50% at FS ±1.00% at 50% FS ±5.00% at 10% FS	±.56% at FS ±1.03% at 50% FS ±5.00% at 10% FS
Oscillograph	Consolidated Electro-Dynamics Corporation	Control Room	±1.0% of reading	±.50% at FS ±1.00% at 50% FS ±5.00% at 10% FS	±1.12% at FS ±1.41% at 50% FS ±5.10% at 10% FS
FM Magnetic Tape	Ampex	Control Room	±.50% of reading	±.25% at FS ±.25% at FS ±2.5% at FS	±.56% at FS ±.71% at 50% FS ±2.55% at 10% FS

II. Total Accumulative Variation for Individual Measurements, from Initial Calibration to Final Readout

Total Variation $\pm 3\sigma$

Measurement	Strip Chart	Oscillograph	FM Tape/Oscillograph
Thrust	± 0.68% at FS ± 1.21% at 50% FS ± 5.71% at 10% FS	± 1.23% at FS ± 1.76% at 50% FS ± 7.25% at 10% FS	± 1.38% at FS ± 1.91% at 50% FS ± 7.66% at 10% FS
Pressure	± 0.75% at FS ± 1.30% at 50% FS ± 6.18% at 10% FS	± 1.22% at FS ± 1.62% at 50% FS ± 6.27% at 10% FS	± 1.41% at FS ± 2.02% at 50% FS ± 8.40% at 10% FS
		Cycle Count	Cycle Count
Flow	± 0.81% at FS ± 1.26% at 50% FS ± 5.63% at 10% FS	± 0.94% of Reading	± 0.94% of Reading
Temperature	± 0.80% at FS ± 1.25% at 50% FS ± 5.62% at 10% FS	± 1.33% at FS ± 1.80% at 50% FS ± 7.16% at 10% FS	± 1.44% at FS ± 1.94% at 50% FS ± 7.60% at 10% FS
Vibration	---	---	± 5.78% at FS ± 5.91% at 50% FS ± 9.42% at 10% FS
Position	± 0.99% at FS ± 1.38% at 50% FS ± 5.65% at 10% FS	± 1.45% at FS ± 1.89% at 50% FS ± 7.18% at 10% FS	± 1.56% at FS ± 2.02% at 50% FS ± 7.62% at 10% FS

III. Performance Parameter Variation

Total Variation $\pm 3\sigma$

Performance Parameter	Strip Chart	Oscillograph	Tape
$I_{sp} = \frac{Fg}{\dot{W}}$	± 1.29% at FS ± 2.12% at 50% FS ± 9.78% at 10% FS	± 1.55% at FS ± 2.00% at 50% FS ± 7.30% at 10% FS	± 1.95% at FS ± 2.13% at 50% FS ± 7.73% at 10% FS
$c^* = \frac{P_c A_t g}{\dot{W}}$	± 1.33% at FS ± 2.18% at 50% FS ± 10.00% at 10% FS	± 1.55% at FS ± 1.87% at 50% FS ± 6.35% at 10% FS	± 1.70% at FS ± 2.22% at 50% FS ± 8.42% at 10% FS

The above calculations are based on the differential equation for a quotation; since

$$I_{sp} = k\frac{F}{\dot{W}} \quad \pm 3\sigma I_{sp} = \frac{\sqrt{\dot{W}^2\sigma F^2 + F^2\sigma\dot{W}^2}}{\dot{W}^+}$$

Note: When σF and $\sigma\dot{W}$ are expressed in percent,

$$\pm 3\sigma I_{sp} \text{ becomes } = \sqrt{\sigma F^2 + \sigma\dot{W}^2}$$

APPENDIX C

PERFORMANCE CALCULATIONS

APPENDIX C

PERFORMANCE CALCULATIONS

Theoretical

As a result of revisions in the heat of formation data for OF_2, the theoretical performance (c* shifting) for oxygen difluoride and diborane has been recalculated and used for performance evaluation in this program. The revised performance is based on the following inputs:

Heat of Formation $(\Delta H)\ OF_2$ = classified

Heat of Formation $(\Delta H)\ B_2H_6$ = 3.2 kcal/mole at $-70^{\circ}F$

Chamber Pressure = 110 psia

The revised theoretical performance data are presented in Figure 1, along with the theoretical data calculated on the prior program (NAS-w-449). The earlier theoretical data were based on an OF_2 heat of formation value of +3.9 kcal/mole. The effect of the more recent heat of formation data on previous performance evaluations is small, amounting to approximately 1.4%.

Experimental

The experimental results designated as "maximum achievable (sea level) specific impulse" were calculated according to the procedure outlined below. Corrections for nonaxial (divergent) flow losses were included in the calculations for maximum achievable specific impulse. Also, corrections for heat losses were made for the test runs conducted with the water cooled thrust chamber assembly. No corrections were made for the heat losses to the heat sink chamber walls.

Chamber Pressure - Chamber pressure was measured at the injector end of the chamber, at the entrance to the nozzle, and in several runs at the centerline of the chamber axis. The chamber pressure measurements in

the chamber barrel (i.e., injector and nozzle entrance) were consistently within 1.8% of one another, in close agreement with the theoretical pressure profile for this chamber geometry (i.e., A_{ch}/A_t and Mach No.). Chamber pressures measured at the centerline of the chamber axis for four runs gave consistent c* and C_F results. Except for these four runs, the chamber pressure data acquired at the nozzle entrance were used in the performance calculations.

Characteristic Velocity - The experimental characteristic velocity was calculated by the following equation:

$$c^*_{test} = \frac{P_{ch}\,(\text{nozzle})\,A_t\,g}{\dot{w}}$$

Maximum Achievable Thrust Coefficient - Performance comparisons of thrust coefficient are gased on the maximum achievable performance, $C_{F\,(map)}$, for the test nozzle geometry used and the recorded test conditions and are obtained by using the following equation:

$$C_{F\,(map)} = C_V \cdot C_D \cdot \lambda \cdot C_{F\,opt} + \left[\frac{P_e - P_a}{P_{ch}}\right] \xi_1$$

where:

$C_D \cdot C_V$ = nozzle discharge and velocity coefficients (0.98 used);

α = divergence half angle, 38^o for heat sink nozzle, 25^o for water cooled nozzle;

λ = divergence correction (nonaxial exhaust gas losses), .894 for heat sink nozzle and .953 for the water cooled nozzle;

$$C_{F\,opt} = \sqrt{\left(\frac{2\bar{\gamma}^2}{\bar{\gamma}-1}\right)\left(\frac{2}{\bar{\gamma}+1}\right)^{\frac{\bar{\gamma}+1}{\bar{\gamma}-1}}\left[1-\left(\frac{P_e}{P_{ch}}\right)^{\frac{\bar{\gamma}-1}{\bar{\gamma}}}\right]};$$

$\bar{\gamma}$ = ratio of specific heats (C_p/C_v) of combustion products during the combustion and expansion process;

ξ_1 = 2.17;

P_e = nozzle exhaust pressure, (calculated from one dimensional, isentropic expansion);

P_a = 14.4 psia, and

P_{ch} = chamber pressure.

The experimental thrust coefficient was calculated from the equation:

$$C_{F\,test} = \frac{F}{P_c A_t} .$$

The test nozzle design was based on a 40:1 contoured nozzle, truncated at an ε of 2.17 (without contour modification) to produce sea level expansion. This provided a nozzle divergence angle of 38° for the heat sink nozzle and 25° for the water cooled nozzle. Allowing for the large divergence losses (11%) of the sharply truncated test nozzles, approximately 99% of predicted equilibrium impulse was obtained.

Maximum Achievable Specific Impulse - Performance comparisons of specific impulse are based on the maximum achievable performance, $I_{sp\,(map)}$, and are obtained by using the following equation:

$$I_{sp\,(map)} = \frac{c^*\,theo \cdot x\, C_{F\,(map)}}{g}$$

The experimental specific impulse was calculated by using measured thrust and total propellant weight flow with the equation:

$$I_{sp\,(test)} = F/W$$

Heat Loss Corrections - The test data for firings conducted with the water cooled thrust chamber assembly were corrected for heat losses to the coolant water by using the following relation:

$$I_{sp\,(corr)} = 6.9544 \sqrt{0.0207\, I_{sp\,(test)}^2 + \frac{T_c - T_e}{T_c}\left(\Delta H_{ch} + \frac{\bar{\gamma}+1}{2}\Delta H\ nozzle\right)}$$

where:

T_c = theoretical combustion temperature,

T_e = theoretical exhaust temperature,

ΔH_{ch} = enthalpy rejected to chamber cooling water (Btu/lb propellant),

ΔH Nozzle = enthalpy rejected to nozzle cooling water (Btu/lb propellant),

$\bar{\gamma}$ = isentropic expansion coefficient, and

6.9544 and 0.0207 = unit conversion factor.

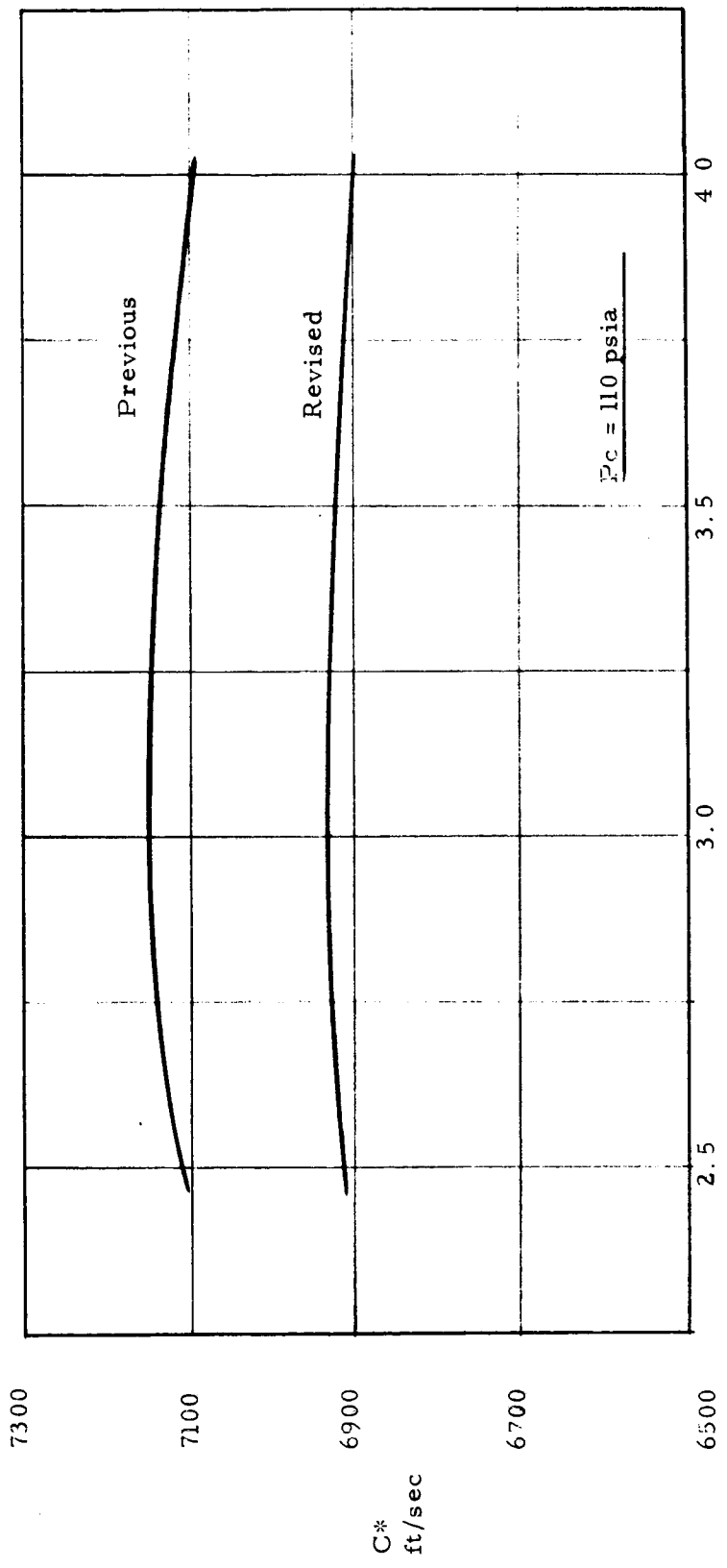

Figure 1. Theoretical Characteristic Velocity vs Mixture Ratio